IMT School for Advanced Studies, Lucca

Lucca, Italy

Neural plasticity induced by different degrees of perturbation in auditory and visual sensory systems

PhD Program Cognitive and Cultural Systems

Curriculum in Cognitive, Computational and Social Neurosciences

XXXIII Cycle

By

Alessandra Enrica Chiara Federici

2023

The dissertation of Alessandra Enrica Chiara Federici is approved.

PhD Program Coordinator: Prof. Maria Luisa Catoni, IMT School for Advanced Studies Lucca

Advisor: Dr. Davide Bottari, IMT School for Advanced Studies Lucca

Co-Advisor: Prof. Emiliano Ricciardi, IMT School for Advanced Studies Lucca

The dissertation of Alessandra Enrica Chiara Federici has been reviewed by:

Prof. Vincenzo Romei, University of Bologna

Dr. Striem-Amit, Georgetown University.

IMT School for Advanced Studies, Lucca

2023

To my mom Rosetta

Contents

Acknowledgements

The studies collected in this dissertation are based on co-authored pre-print or co-authored papers in progress.

Chapter 2 is a pre-print paper under submission:
Federici, A., Bernardi, G., Senna, I., Fantoni, M., Ernst, M. O., Ricciardi, E., & Bottari, D. (2022). "Short-term monocular deprivation boosts neural responsiveness to audio-visual events for the undeprived eye". bioRxiv.

Chapter 3 is a paper in progress with the following list of authors: Federici A., Fantoni M., Bednaya E., Pavani F., Martinelli A., Ricciardi E., Nava E., Orzan E., Bianchi B., Bottari D.
Note that the employed methods are based on a previous work in pre-print of which I am a coauthor:
Bednaya, E., Mirkovic, B., Berto, M., Ricciardi, E., Martinelli, A., Federici, A., ... & Bottari, D. (2022). "Early visual cortex tracks speech envelope in the absence of visual input". bioRxiv.

Chapter 4 is a pre-print paper under submission: **Federici A., Bennett C.R., Bauer C.M., Manley, C.E., Ricciardi E., Bottari D., Merabet L.B. (2022) "Altered Neural Oscillations Underlying Visuospatial Processing in Cerebral Visual Impairment (CVI)." medRxiv.**
Note that some parts of the methods are based on previous works of Lotfi Merabet (the senior author with whom I collaborated for this project):
Bennett, C. R., Bauer, C. M., Bex, P. J., Bottari, D., & Merabet, L. B. (2021). "Visual search performance in cerebral visual impairment is associated with altered alpha band oscillations". Neuropsychologia, 161, 108011;
Manley, C. E., Bennett, C. R., & Merabet, L. B. (2022). "Assessing Higher-Order Visual Processing in Cerebral Visual Impairment Using Naturalistic Virtual-Reality-Based Visual Search Tasks". Children, 9(8), 1114;
Pamir, Z., Bauer, C. M., Bailin, E. S., Bex, P. J., Somers, D. C., & Merabet, L. B. (2021). "Neural correlates associated with impaired global motion perception in cerebral visual impairment (CVI)". NeuroImage: Clinical, 32, 102821.

To acknowledge the contribution of everyone, the term "we" is used in these chapters.

First of all, I would like to thank Vincenzo Romei and Ella Striem-Amit for reviewing my thesis and for their inspiring feedback.

Starting from Giulio Bernardi, Irene Senna, and Marc Ernst, my gratitude goes to every person I could work with and from whom I had the pleasure of learning. Thanks to my SEED colleagues, especially Marta Fantoni, tireless acquisitions-mate. And thanks to every interesting mind with whom I could exchange ideas and thoughts in these PhD years.

An essential thank goes to Luca Casartelli and Luca Ronconi, your passion for doing research switched on the spark in me. Thanks to Emiliano Ricciardi for always supporting me and allowing me to follow my way. And definitely, thanks to Davide Bottari. Thank you for being my mentor, spurring and supporting me throughout this twisting journey. Thank you for all the chances you have offered me and for keeping me from losing enthusiasm in the most arduous moments. You have shown me the most beautiful research side, never neglecting the human one.

Thanks to all friends with whom I shared this PhD life. Especially to Tatiana, Demetrio, and Alice, you have been my home. And to Alice Martinelli for being my benchmark in Lucca. Last but not least, thanks to my lifetime friends far away but always close, to my Family for letting me get here, and thank you, Valerio, for being there and firmly believing in me.

Vita

March 12, 1990	Born, Milan, Italy
01/11/2017 – Current	PhD student in Cognitive, Computational and Social Neurosciences (CCSN) IMT School for Advanced Studies Lucca Lucca, Italy
12/2019 – 06/2020	Visiting (supported by Erasmus+ Grant) Department of Applied Cognitive Psychology, Ulm University Ulm, Germany
2016 – 2017	Research Assistant Child Psychopathology Unit, Scientific Institute IRCCS "Medea" Bosisio Parini, Italy
03/2017 – 04/2017	Research fellowship SISSA Scuola Internazionale Superiore di Studi Avanzati Trieste, Italy
29/02/2016	Psychologist, Ordine degli Psicologi della Lombardia (Italy) n 18376
10/2014 – 10/2015	Post-graduate internship Child Psychopathology Unit, Scientific Institute IRCCS "Medea" Bosisio Parini, Italy

10/2012 – 09/2014	Master of Science in Psychology, curriculum Cognitive Neuroscience Vita-Salute San Raffaele University Milano, Iltay
02/2014 – 06/2014	Erasmus Master Neurosciences Plurifacultaires, Université de Genève Genève, Switzerland
09/2009 – 07/2012	Bachelor in Psychology University of Milano-Bicocca Milano, Italy

Publications

Peer-reviewed original articles (published during the PhD)

Ronconi, L., Gori, S., Federici, A., Devita, M., Carna, S., Sali, M. E., ... & Facoetti, A. (2018). Weak surround suppression of the attentional focus characterizes visual selection in the ventral stream in autism. NeuroImage: Clinical, 18, 912-922.

Federici, A.*, Parma, V.*, Vicovaro, M., Radassao, L., Casartelli, L., & Ronconi, L. (2020). Anomalous Perception of Biological Motion in Autism: A Conceptual Review and Meta-Analysis. Scientific Reports, 10(1), 1-19.

Casartelli, L., Federici, A., Fumagalli, L., Cesareo, A., Nicoli, M., Ronconi, L., ... & Sinigaglia, C. (2020). Neurotypical individuals fail to understand action vitality form in children with autism spectrum disorder. Proceedings of the National Academy of Sciences, 117(44), 27712-27718.

Ronconi, L., Vitale, A., Federici, A., Pini, E., Molteni, M., & Casartelli, L. (2020). Altered neural oscillations and connectivity in the beta band underlie detail-oriented visual processing in autism. NeuroImage: Clinical, 102484.

Betta, M.*, Handjaras, G.*, Leo, A., Federici, A., Farinelli, V., Ricciardi, E... & Bernardi, G. (2021). Cortical and subcortical hemodynamic changes during human sleep slow waves in human light sleep. NeuroImage 236, 118117.

Ronconi, L., Vitale, A., Federici, A., Mazzoni, N., Battaglini, L., Molteni, M., & Casartelli, L. (2022). Neural dynamics driving audio-visual integration in autism. Cerebral Cortex.

Pre-print

Federici, A., Bernardi, G., Senna, I., Fantoni, M., Ernst, M. O., Ricciardi, E., & Bottari, D. (2022). Short-term monocular deprivation boosts neural responsiveness to audio-visual events for the undeprived eye. bioRxiv.

Bednaya, E., Mirkovic, B., Berto, M., Ricciardi, E., Martinelli, A., Federici, A., ... & Bottari, D. (2022). Early visual cortex tracks speech envelope in the absence of visual input. bioRxiv.

Federici A., Bennett C.R., Bauer C.M., Manley, C.E., Ricciardi E., Bottari D., Merabet L.B. (2022) "Altered Neural Oscillations Underlying Visuospatial Processing in Cerebral Visual Impairment (CVI)." medRxiv.

Presentations (during the PhD)

The Effects of Temporary Monocular Deprivation in a Multisensory Context, SIPF - Società Italiana di Psicofisiologia e Neuroscienze Cognitive virtual edition, 21/11/2020 – 22/11/2020.

Temporary monocular deprivation elicits distinct effects on visual and audio-visual neural oscillations, OHBM - Organization for Human Brain Mapping virtual edition, 30/05/2021 – 04/06/2021.

Induced oscillatory activity is affected by temporary monocular deprivation: distinct effects for visual and audio-visual processing, CuttingEEG - Cutting-edge methods for EEG research. Aix-Marseille University, Aix-en-Provence, France, 04/10/2021 – 07/10/2021.

Induced oscillatory activity is affected by temporary monocular deprivation: distinct effects for visual and audio visual processing. NeuroCog, UCLouvain, Louvain-la-Neuve, Belgium, 23/11/2021 - 24/11/2021.

Induced oscillatory activity is affected by temporary monocular deprivation: distinct effects for visual and audio-visual processing. ICON - International conference of cognitive neuroscience, University of Helsinki, Finland, 18/05/2022 – 22/05/2022.

Impaired evoked and induced neural oscillations during visual search in cerebral visual impairment. ICON - International conference of cognitive neuroscience, University of Helsinki, Finland, 18/05/2022 – 22/05/2022.

Brief monocular deprivation alters induced neural activity of visual and audio-visual processing OHBM Organization for Human Brain Mapping virtual edition 07/06/2022 – 08/06/2022.

Impaired evoked and induced neural oscillations during visual search in cerebral visual impairment OHBM Organization for Human Brain Mapping virtual edition 07/06/2022 – 08/06/2022.

Short term monocular deprivation boosts neural responsiveness to audio visual events for the undeprived eye. IMRF - International Multisensory Research Forum, Ulm University, Germany, 04/07/2022 – 07/07/2022.

Impaired evoked and induced neural oscillations during visual search in cerebral visual impairment SIPF - Società Italiana di Psicofisiologia e Neuroscienze Cognitive 15/09/2022 – 17/09/2022.

Neural tracking of speech envelope is delayed in cochlear implanted children SIPF - Società Italiana di Psicofisiologia e Neuroscienze Cognitive 15/09/2022 – 17/09/2022.

Abstract

Visual or auditory sensory deprivation represents a key model for studying experience-dependent plasticity. Different types of deprivations (congenital-late, temporary-permanent, peripheral-central) are characterized by a certain degree of perturbation of the typical sensory experience and can be represented in a three-dimensional space showing the distance from the typical experience. The dimensions are: (i) when the deprivation occurs, (ii) how long the deprivation lasts, and (iii) where is the barrier that causes the deprivation. Each dimension can be responsible for a low, medium, or high degree of perturbation. In this dissertation, visual and auditory deprivation models are employed to investigate unisensory and multisensory neural plasticity. The first study (low degree of perturbation) aimed to unveil whether short-term monocular deprivation in the adult brain can induce neural plasticity beyond the visual system. The second study (medium degree of perturbation), using the model of temporary deprivation, assessed whether neural tracking of speech envelope could develop even in the absence of auditory stimulation from birth. Finally, the third study (high degree of perturbation) investigated how cerebral visual impairment affects visuospatial processing. Neural oscillations were used as windows to investigate plasticity mechanisms; time-frequency analysis was employed when short stimuli were presented, and neural tracking when the stimuli were continuous. Results revealed that even a low degree of sensory perturbation induces plasticity that extends beyond the deprived modality (study 1); altered neural tracking develops following a medium degree perturbation (study 2); a high degree of perturbation has a widespread impact on neural activity (study 3). These results strengthen evidence of the pivotal role of sensory experience revealing multifaced aspects of experience-dependent plasticity. Modeling the degree of perturbation could be a helpful perspective for a deeper understanding of how neural dynamics are affected by different types of deprivation and for shedding light on ranges of flexibility in neural processing with potential clinical implications.

Abbreviations

A audio

V visual

CI Cochlear Implant

CVI Cerebral Visual Impairment

CD Congenital Deaf

DD Delayed Deaf

HC Hearing Control

MD Monocular Deprivation

TRF Temporal Response Function

List of Figures

List of Tables

Chapter 1

Introduction

During my PhD I have been working in the research field of the experience-dependent plasticity to explore the impact of atypical auditory and visual experience on sensory processing of simple and more complex ecological stimuli. With three studies, I have explored either unisensory and multisensory processing (audio, visual, or audio-visual). In particular, I used three different deprivation models to assess the impact of different degrees of sensory perturbation on neural processing compared to typical sensory processing.

1.1. Experience-dependent plasticity

Neuroplasticity is the intrinsic brain ability to functionally adapt to different contexts, creating new connections and resulting in a different organization (Pascual-Leone et al., 2005). Particularly, experience-dependent plasticity is a crucial mechanism for which structural and functional brain organization are shaped by experience (Nelson, 1999). Sensory information processing represents individual's connections with the external world, and for humans specifically, most of our everyday interactions with the environment are characterized by visual and auditory information. Visual and auditory experiences are, thus, crucial building-blocks for typical human development.

Experience-dependent plasticity allows the typical development of sensory and cognitive functions thanks to proper environmental input (Knudsen, 2004). All along the development, the brain is extremely plastic, and sensory stimulations are fundamental. Environment statistics tunes neural circuits to process information in an adaptive way to quickly discriminate external information. Experience-dependent plasticity brings clear evolutionary advantages, allowing certain degrees of developmental variability. For example, infants are predisposed to learn any language according to the environment in which they grow up and, thus, the language to which they are exposed. This fascinating relationship between our neural response and experience changes

during life (Bavelier and Neville, 2002; Takesian and Hensch, 2013; Reh et al., 2022).

Experience shapes brain development according to genetically predetermined developmental constraints. The correct development of sensory processes and cognitive functions results from the proper environmental stimulations at precise developmental stages known as critical and sensitive periods (Hensch, 2004; Levelt and Ḧubener, 2012; Werker and Hensh, 2015; Kral et al., 2019). Critical periods are time windows during the development in which the correct sensory stimulation is mandatory to achieve typical development. Changes occurring within critical periods are considered immutable (Hubel and Wiesel 1970). Sensitive periods are phases during development in which the brain circuits are particularly receptive to external information, and thus, the impact of experience on brain development is particularly strong. These mechanisms explain why human infants are predisposed to learn languages so easily while adults are not (Kuhl, 2004). Within the first phases of development, infants are able to discriminate any phonemes of any language, then their neural response specializes according to their experience, and thus, they become able to discriminate only meaningful phonemes in the natal language (Maurer and Werker, 2014). Complex cognitive functions, such as language, need multiple subsequent critical and sensitive periods starting from the more low-level functions (Werker and Hensh, 2015); when all critical and sensitive periods are closed, the brain becomes more stable.

In adulthood, neural circuits stability dominates, and the brain is less plastic. However, some residual experience-dependent plasticity was demonstrated to be maintained in adulthood even for sensory functions previously considered immutable (Castaldi et al., 2020; Merabet et al., 2008; Karmarkar and Dan, 2006; Spolidoro et al., 2009; Espinosa and Stryker, 2012; Hensch and Quinlan, 2018). Nevertheless, brain plasticity that can occur after the closure of sensitive periods is constrained within the connection established during development. In case typical sensory information is absent during development, atypical connections stabilize, and sensory and cognitive functions development follow different trajectories (Knudsen, 2004). In order to understand different trajectories that the brain can follow in the absence of the typical sensory

experience, a key model is represented by the study of the effects induced by sensory deprivation.

1.2. Visual or auditory deprivation as key model to study experience-dependent plasticity

To understand experience-dependent plasticity, a crucial model is the study of situations in which a sensory modality was deprived (Ricciardi et al., 2020; Cardin et al., 2020). The study of blindness and deafness consents to understand how the brain is reorganized in the absence of vision or audition. Striking plasticity effects have been found in congenital blind and congenital deaf individuals. Many studies have consistently shown that some brain areas traditionally considered dedicated to a specific sensory modality can instead be involved in processing other sensory modalities (e.g., Benetti et al., 2017; Bottari et al., 2020; Vetter et al., 2020). This phenomenon, known as crossmodal plasticity, demonstrated that plasticity could establish new connections but also unmask existing ones. Spared modalities can also be enhanced in late blind or deaf individuals (e.g., Fieger et al., 2006). However, congenital or late deprivations do not lead to the same plastic effects, revealing differences in being deprived during development or later in life (Röder et al., 2004; Berto et al., 2021).

Assessing the neural plasticity of the modality that was deprived is possible only when the deprivation is temporary. Studying brain activity after a period of deprivation is crucial to understanding the existence of critical/sensitive periods for a specific function. The pioneers of the research line investigating the existence of critical periods using temporary deprivation are Hubel and Wiesel (Wiesel and Hubel, 1963; Hubel and Wiesel, 1970); they explored the plasticity of the visual system of cats when normal sight was restored after a period of deprivation. They demonstrated that if the cat is monocularly deprived during the first months after birth, it is enough to permanently change the typical arrangement of the ocular dominance in the visual system, affecting binocular representation. Even if the binocular vision was restored, the columns of ocular dominance could not be modified by the correct visual experience, and the same effect was not evident whether deprivation occurred in adulthood, suggesting the existence of a critical period for ocular dominance. Moreover, it is important to highlight that epigenetics

can also trigger critical periods. That is, specific sensory experiences could be needed to open a specific critical period; if the stimulation is absent for a certain period during development, this can lead to an extension or a delay of the critical period. For example, whether animals are kept in total darkness for the first weeks, the critical periods for ocular dominance open only when they are exposed to light, and thus, they begin to receive visual input (Mower, 1991). A similar effect can be seen in auditory modality when animals are reared in a noisy environment, a form of pattern deprivation (Chang and Merzenich, 2003).

In humans, natural models of temporary deprivation are rare situations in which a deprived modality can be restored. In the visual domain, sight restoration can be studied in individuals who had been born or developed cataracts and then were treated with surgery to remove them (Röder and Kekunnaya, 2021). In the auditory domain, the ability to experience sound in deaf individuals can be restored thanks to cochlear implants (CIs, Kral and O'Donoghue, 2010). These cases represent critical models for studying the impact of a period of atypical sensory experience on sensory processing. Fundamental neurophysiological mechanisms of sensory processing, such as alpha desynchronization in visual processing, were reported to be permanently impaired after a deprivation period (Bottari et al., 2016), as well as some other high-level visual functions (e.g., face perception, Röder et al., 2013). Similarly, congenital deaf individuals who received cochlear implants late in life can perceive sound but might display difficulties in processing language (Kral and Sharma, 2012).

Temporary deprivation, as well as permanent deprivation, was demonstrated to impact also beyond the deprived modality. A brief period of early postnatal visual deprivation can cause long-lasting crossmodal plasticity effects (Bottari et al., 2018; Collignon et al., 2015; de Heering et al., 2016), as well as atypical multisensory processing (Guerreiro et al., 2015; Putzar et al., 2007). Crossmodal plasticity was also demonstrated in deaf CI individuals showing a higher response to visual stimuli in auditory areas (Sandmann et al., 2012; Stropahl et al., 2015). Moreover, there is also evidence of functions that can be acquired at any age when the deprived modality is restored, even after a long period of deprivation, both unisensory (e.g., biological motion perception, Bottari

et al., 2015; Hadad et al., 2012), but also multisensory processing (Senna et al., 2021).

What emerges in this complex context of studies employing sensory deprivation as a model to study plasticity is that different types of deprivation specifically affect sensory experiences and thus reveal different plastic changes in the brain (Bavelier and Neville, 2002; Röder et al., 2021). The main factors that characterize a deprivation model are (i) when sensory deprivation occurs during individual life (e.g., during development or in adulthood), (ii) how long lasts the deprivation (e.g., temporary or permanent), and finally, (iii) where the deprivation occurs in the sensory processing (e.g., peripherally or centrally).

1.3 Different deprivation models with different degrees of sensory perturbation

This dissertation explores neural plasticity induced by different deprivation models compared to a typical non-deprived experience. Deprivation models can be organized according to three dimensions having a gradient of how much the sensory experience is distant from the typical one. This distance reflects the *degree of perturbation* of the typical sensory experience.

(i) **When** dimension:
- low degree of perturbation: deprivation after typical development
- high degree of perturbation: deprivation since birth

(ii) **Duration** dimension:
- low degree of perturbation: short deprivation
- high degree of perturbation: permanent deprivation

(iii) **Where** dimension:
- low degree of perturbation: peripheral deprivation
- high-degree of perturbation: deprivation induced by a central lesion

In this three-dimensional perturbation space, the typical experience in healthy adults corresponds to the origin of the cartesian plane. The more distance from the typical experience, the higher the degree of sensory perturbation.

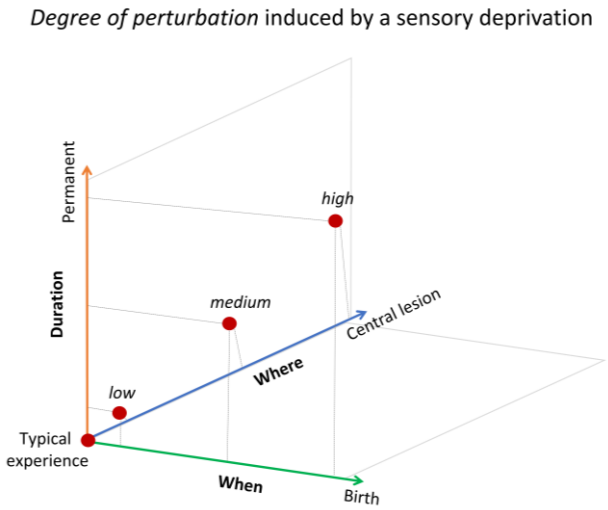

Figure 1. Three-dimensional space showing the degree of perturbation induced by sensory deprivation.

The three studies in this dissertation are characterized by the analyses of different degrees of perturbation: low, medium, and high, according to the three mentioned dimensions. Here are summarized for each dimension the degree of perturbation that characterized the deprivation model employed in each study:

First study:

(i) **when** the deprivation occurs: in adulthood after typical development (low degree of perturbation);
(ii) **duration** of the deprivation: minutes-hours (low degree of perturbation);
(iii) **where** is the barrier causing the deprivation: peripheral occlusion of the sensory system (low degree of perturbation).

Second study:

(i) **when** the deprivation occurs: during development (medium-high degree of perturbation);
(ii) **duration** of the deprivation: months-years (medium degree of perturbation);
(iii) **where** is the barrier causing the deprivation: peripheric lesion of the sensory system (medium degree of perturbation).

Third study:

(i) **when** the deprivation occurs: since birth (high degree of perturbation);
(ii) **duration** of the deprivation: permanent (high degree of perturbation);
(iii) **where** is the barrier causing the deprivation: central lesion in the sensory system (high degree of perturbation).

Using these three different deprivation models, we aimed to answer specific open questions in the field of experience-dependent plasticity.

In the first study, we measured the neural changes during sensory processing due to a low degree of sensory perturbation, a short-term monocular deprivation in the typically developed adult brain. While short-term monocular deprivation (150 minutes) in the adult brain was demonstrated to induce plasticity within the visual system (Lunghi et al., 2011), whether the effect of this deprivation extends beyond visual processing is still unclear. Studies conducted in individuals with permanent or temporary visual deprivation reported that sensory deprivation in one modality affects the processing of stimuli in spared modalities (e.g., Fieger et al., 2006) and multisensory stimulation (e.g., Guerreiro et al., 2015). Here, we wanted to explore whether plasticity extending beyond the deprived modality can be seen even in the typically developed brain of sighted individuals exposed to an atypical visual experience for a brief period.

> Research question 1: ***Does short-term monocular deprivation in the adult brain induce neural changes in audio-visual multisensory and auditory unisensory processing?***

The second study investigated the effect of a medium degree of sensory perturbation: a temporary deprivation caused by a deficit in the periphery of the auditory system occurring during early development. Deprivation during early phases of development was demonstrated to prevent the correct development of the deprived sensory modality that could have cascade effects on more complex functions (e.g., Röder et al., 2013), while some other functions could be spared (e.g., Bottari et al., 2015). Deaf children, if early implanted, are able to learn and understand language (Osberger et al., 2002; Kral and O'Donoghue, 2010). However, to which degree the auditory cortices in CI individuals develops the ability to track and synchronize their activity with continuous speech is yet unknown. This neural function was recently found to be tracked at the neural level already by 4 months old infants, revealing an early development. Here, we assessed whether auditory deprivation experienced early in life could affect the neural tracking of the envelope of natural speech, a simple feature known to carry crucial information for language comprehension. Moreover, studying early deaf CI children with different deafness onsets allowed the investigation of the presence of sensitive periods for the development of auditory tracking.

> Research question 2: ***Is the neural tracking of continuous speech affected by a period of auditory deprivation during development? Is there a perinatal sensitive period for the emergence of this type of neural response?***

The third study investigated the impact of a high degree of sensory perturbation: a permanent perinatal lesion that causes visual impairment. Most studies have focused on plasticity induced by sensory deprivation due to ocular blindness, while very little is known about neural plasticity in the case of visual impairments due to cerebral lesions from birth (Bennet et al., 2020). Cerebral visual impairment (CVI) is a brain-based neurological condition in which ocular deficits cannot explain visual impairments. CVI individuals develop with damages to central visual retrochiasmatic pathways that pervasively affect the typical developmental trajectory affecting high-level visual functions. Here, we aimed to unveil the neurophysiological basis of CVI visuospatial impairment.

Research question 3: ***Which are the neurophysiological bases of CVI impairment during ecological visual search? Does the CVI mainly affect feedforward or feedback neural activity?***

In these three studies, we aimed to unveil the neural changes associated with a specific deprivation that otherwise can be hidden by testing only behavioral performance. Electrophysiological (EEG) activity during visual and/or auditory processing was measured to highlight differences in brain oscillations. Two main methods were employed: time-frequency decomposition and neural tracking. Time-frequency decomposition analyses were employed with short stimulation to explore fingerprints of the plasticity induced by sensory perturbation. Moreover, induced and evoked oscillatory components were assessed to unveil whether feedback or feedforward connections were mainly affected (Klimesch et al., 1998; Tallon-Baudry and Bertrand, 1999; Chen et al., 2012). When continuous stimuli were used, we employed a new method to reveal how oscillations in the brain are synchronized with external stimulation (Lakatos et al., 2019; Crosse et al., 2016; Lalor et al., 2009).

1.4 Dissertation outline

In the second Chapter, we explored whether a brief period of monocular deprivation MD elicits neural changes beyond visual processing. Behavioral data suggested that MD can affect the interplay between sensory modalities. Thus, we measured neural oscillations associated with visual and audio-visual processing for both the deprived and the undeprived eye before and after a period of MD. Results revealed that MD changed neural activity associated with unimodal and multisensory processes in an eye-specific manner. Selectively for the deprived eye, after MD alpha activity was reduced within the first 150 ms of visual processing. Conversely, gamma activity was enhanced in response to audio-visual events only for the undeprived eye within 100-300 ms after stimulus onset. The analysis of gamma responses to unimodal auditory events revealed that MD elicited a crossmodal upweighting for the undeprived eye. Distributed source modeling suggested that the right parietal cortex played a major role in all neural effects induced by MD. Finally, visual and audio-visual processing alterations emerged

selectively for the induced (but not the evoked) component of the neural oscillations, indicating a major role of feedback connectivity. These findings support a model in which MD increases excitability to visual events for the deprived eye and to audio-visual and auditory events for the undeprived eye. On the one hand, these results reveal the causal impact of MD on both unisensory and multisensory processes but with distinct frequency-specific profiles. On the other hand, they highlight the feedback nature of short-term neural plasticity. Overall, this study shed light on the high flexibility and interdependence of unimodal and multisensory functions.

In the third Chapter, we investigated to what extent the development of neural synchronization with continuous speech envelope requires early experience with acoustic information. The envelope of speech was recently found to be tracked at the neural level already by 4 months old infants. Using a natural model of temporary auditory deprivation, we investigated the neural tracking of the speech envelope in children who were born or developed - at some later point - profound bilateral deafness and whose hearing was partially restored with cochlear implants (CIs). Thus, we assessed whether CIs allow these children to develop hearing-like neural tracking of continuous speech and whether a temporary auditory deprivation starting at birth alters the development of this neural activity. We employed temporal response function (TRF) to measure the synchronization between brain activity and speech envelope in CI children who were profoundly congenital deaf (CD) or who became deaf on average 36 months later (i.e. delayed deaf, DD) as well as in hearing controls (HC). Results unveiled a clearly defined auditory response function in CI children, both CD and DD. However, while in HC, auditory response function was characterized by early activity occurring at~60 ms and by a subsequent phase at~250 ms, in CI children, early tracking was substantially delayed (~120 ms), and the subsequent activity was not detectable. Notably, while CD and DD groups' auditory response functions substantially overlapped, the earliest response latency depended on the age at which children received the implant and children's experience with CIs. In conclusion, data revealed that, even if altered, neural tracking of speech envelope emerged in CI children independently by deafness onset and thus, regardless of whether they experienced deprivation from auditory

deprivation since birth or not, ultimately revealing the absence of a perinatal sensitive period for the emergence of this type of neural response. Moreover, results highlighted that early implantation (i.e., hearing restoration) and long-term implant use are critical factors for reducing the lag of hearing system development in CI users.

In the fourth Chapter, we assessed the neurophysiological changes underlying higher-order perceptual impairments in Cerebral visual impairment (CVI). Visuospatial processing deficits are commonly observed in individuals with CVI, even in cases where visual acuity and visual field functions are intact. However, their neurophysiological bases are unexplored. Here, we measured eye movements and electroencephalography (EEG) in a group of CVI individuals with "functionally useful vision" and neurotypical age-matched controls while they performed a virtual-reality-based visual search task. We investigated ocular behavior and neural oscillations associated with the visual search task in CVI and controls. Analyzing evoked and induced components of EEG activity, we aimed to shed light on neural computations with different degrees of time and phase anchoring to visual events, that is, with prevalent feedforward or feedback profiles. We found that visual search performance in CVI was impaired, as indexed by ocular behavioral outcomes of success rate, reaction time, and gaze error. Analysis of EEG oscillatory activities across a broad frequency [4-55 Hz] band revealed extensive impairments in CVI visual processing. CVI groups showed markedly reduced early-onset evoked theta [4-6 Hz] activity regardless of task complexity. Moreover, while induced alpha [8-14 Hz] increased with task complexity in controls, possibly reflecting distractor suppression, this modulation was absent in the CVI group. Finally, CVI participants also showed an overall delayed and sustained induced gamma response [30-45 Hz]. Results revealed that visuospatial processing in CVI is associated with substantial alterations in EEG activity across a broad range of oscillatory frequencies (theta, alpha, gamma rhythms) implicated in both local and distributed levels of neural processing. Moreover, both their evoked (time and phase-locked) and induced (non-time nor phase-locked) components are impaired, revealing widespread deficits in feedforward as well as feedback connectivity.

Finally, in the last chapter (Chapter 5), I highlighted the conclusions from these three studies.

Chapter 2

Short-term monocular deprivation boosts neural responsiveness to audio-visual events for the undeprived eye

2.1 Introduction

While neuroplasticity of the visual system is maximal during development (Hubel and Wiesel, 1970; Hensch, 2005; Espinosa and Stryker, 2012; Levelt and Ḧubener, 2012; Reh et al., 2020), evidence that a certain degree of plasticity is retained in the adult visual cortex has accumulated (Karmarkar and Dan, 2006; Spolidoro et al., 2009; Espinosa and Stryker, 2012; Hensch and Quinlan, 2018). Studies in adults employing psychophysics and neuroimaging methods showed that a brief period of MD, a pivotal model for testing the plasticity of the visual system, alters the ocular balance by strengthening visual processing of the deprived eye and weakening the undeprived eye (Castaldi et al., 2020). These functional changes reflect ocular dominance shifts in V1 in favor of the deprived eye (Lunghi et al., 2015a; Binda et al., 2018) and are supposedly driven by homeostatic plasticity (Lunghi et al., 2015b), the mechanism involved in preserving the cortical excitatory-inhibitory balance (Turrigiano, 2012). Besides this well-documented MD effect on visual processing, little is known about how MD affects multimodal processing.

Alterations induced by MD seem to impact beyond visual processing. At the behavioral level, short-term MD was found to affect the interplay between sensory modalities (Lo Verde et al., 2017; Opoku-Baah and Wallace, 2020). Overall, results were consistent with a decreased multisensory interplay for the deprived eye, in which the visual processing is generally strengthened following MD, and vice versa, an increased multisensory interplay for the undeprived eye, in which visual processing is typically weakened following MD. However, the neural correlates of MD effects on multisensory processes are still unknown. To fill this gap, we exploited the model of MD to elicit short-term plasticity

and investigated specific changes in visual and audio-visual processes for the deprived and undeprived eye. Overall, this study aimed to address whether a brief period of monocular visual experience in adulthood can affect the neural processing associated with multisensory audio-visual events and which are the underpinning neural mechanisms.

Here, we combined psychophysical and electrophysiological approaches. We employed the sound-induced flash illusion (Shams et al., 2000, Hirst et al., 2020), in which the number of perceived flashes can be biased by the number of concurring beeps. To investigate the impact of MD on visual processing, we measured neural oscillations in response to a single flash before and after a deprivation phase. To determine the existence of an audio-visual MD effect, the analysis focused on neural oscillations elicited by the fission illusion trials in which a single flash is coupled with two beeps, and two flashes can be perceived (Shams et al., 2000). This illusion reveals the impact of auditory input on visual processing in case of conflictual audio-visual information.

Neural correlates associated with visual and audio-visual processing are characterized by their spectral, temporal, and spatial properties. Reflecting high and low neuronal excitability cycles, neural oscillations reveal perceptual organization in both visual (Jensen et al., 2014; VanRullen, 2016) and multisensory analyses (Cooke et al., 2019; Lennert et al., 2021). We expected MD to induce changes in alpha activity, which is known to reflect levels of inhibition (Klimesch et al., 2007; Klimesch, 2012), and, thus, increase the visual system excitability for the deprived eye (Lunghi et al., 2015a). Moreover, we hypothesized MD to alter responses in the gamma range. Gamma activity has been as well associated with excitatory-inhibitory balance (Jensen et al., 2010; 2012), and its modulation was found to be involved in eliciting a perceptual fission illusion (Bhattacharya et al., 2002; Mishra et al., 2007; Lange et al., 2011, 2013; Balz et al., 2016).

Importantly, distinct components of neural oscillations characterize different types of processing according to the direction of information flow: while the evoked activity, which is phase-locked to the stimulation, has mainly been associated with feedforward processing (thalamo-cortical), the induced oscillatory activity, which is not phase-locked to the onset of the stimulus, has mainly been associated with feedback

processing (cortico-cortical connectivity, Klimesch et al., 1998; Tallon-Baudry and Bertrand, 1999; Chen et al., 2012). Studies in humans and non-human animal models demonstrated that permanent sensory deprivation primarily affects induced oscillatory activity (Bottari et al., 2016; Yusuf et al., 2017; Bednaya et al., 2021). As homeostatic plasticity is an intrinsic feedback mechanism (Turrigiano and Nelson, 2004), we predicted to primarily observe changes in induced oscillatory activity following temporary MD for both visual and audio-visual processing. Finally, source modeling was employed to investigate the neural sources of short-term plasticity effects.

2.2 Materials and Methods

2.2.1 Participants

Since the effect of MD on multisensory processing was unknown, we estimated the minimum sample size needed to reach the expected effect of MD on visual processing as previously reported in the literature. We expected the MD effect on visual processing to be at occipito-parietal electrodes, in the alpha range [8-14 Hz] (Lunghi et al., 2015a), and within the first stages of visual processing [0-120 ms] (comprising the earliest visual evoked potential, C1 wave, known to be modulated by MD; Lunghi et al., 2015a). The power analysis was performed by simulating our planned analysis (t1-t0 Deprived eye vs. t1-t0 Undeprived eye) on the alpha frequency power using a cluster-based permutation test (Wang and Zhang, 2021). The analysis revealed an estimated minimum sample size of 17 participants (for further details on sample size estimation, see Supplementary materials Chapter 2 Figure S2.1). Note that previous studies investigating the effect of MD using EEG analyzed up to 16 participants (Lunghi et al., 2015a; Zhou et al., 2015; Schwenk et al., 2020).

To determine individual suitability for the main experiment (EEG experiment), twenty-seven potential participants completed a preliminary behavioral assessment (see the section below) in order to assess whether they met the following inclusion criteria: (i) to perceive the fission illusion with the dominant eye (i.e., >20% illusory rate), and (ii) to not be completely biased by the sound in the illusory conditions (i.e., >95% illusory rate). Out of twenty-seven young adults tested (mean age 28.22 ± 2.41 SD, twelve males and fifteen females), six participants

were excluded as they did not meet these inclusion criteria or could not comply with the experimental instructions (see Supplementary materials Chapter 2). Out of the 21 participants who performed the main experiment, one further participant was excluded due to his poor behavioral performance (the number of errors was 3 SD above the group mean in the conditions in which only auditory stimuli were presented, i.e., the control conditions). The final sample included 20 young-adult participants (mean age 28.45 ± 2.67 SD, eight males and twelve females). They all had normal or corrected-to-normal vision (visual acuity ≥ 8/10) and did not report hearing deficits or a history of neurological conditions. Since one EEG and one behavioral dataset, from different participants, went lost due to technical issues during acquisitions, the analyzed data sample included 19 behavioral and 19 EEG datasets.

The study was approved by the local Ethical Committee (Comitato Etico di Area Vasta Nord Ovest Regione Toscana protocol n. 24579). Each participant signed a written informed consent before taking part in the experiment. The experimental protocol adhered to the principles of the Declaration of Helsinki (2013).

2.2.2 Stimuli and apparatus

The experiment was performed in a dimly lit and sound-attenuated chamber (BOXY, B-Beng s.r.l., Italy). Participants were comfortably sitting in front of the apparatus, with their eyes at a distance of 60 cm from the monitor. Visual stimuli were presented on an LCD monitor (60 Hz refresh rate; 24.5 inches; 1920 × 1080 screen resolution), and audio stimuli were delivered via a single speaker (Bose® Companion 2, series III multimedia) located below the screen and aligned with its center. Stimuli were flashes and beeps. Both visual and audio stimuli were created using Matlab (The Mathworks, Inc. - version 2017b). The audio stimulus was a 7 ms quadratic beep with a 3.5 kHz frequency and a sampling rate of 44.1 kHz, which was presented at about 75 dB. The visual stimulus was a 2° diameter grey dot displayed 5° below the center of the screen for 17 ms (corresponding to 1 frame) on a black background. The contrast level of the grey dot was selected individually via a staircase procedure to elicit the fission illusion in about 50% of trials (Pérez-Bellido et al., 2015, see below Preliminary behavioral assessment). Stimuli were delivered using E-Prime® software (version 2, Psychology

Software Tools, Inc. www.pstnet.com). The Audio/Visual (AV) Device (Electrical Geodesics, Inc.) was employed to ensure accurate optimal synchronization between the presented stimuli and the recorded EEG traces.

2.2.3 Experimental Design

The whole procedure consisted of two main parts performed on two separate days: a preliminary behavioral assessment and the main experiment, in which the dominant eye was deprived of patterned visual input using a translucent eye patch. In both the preliminary behavioral assessment and the main experiment, participants performed a monocular visual discrimination task.

2.2.3.1 Monocular visual discrimination task

Participants were asked to report the number of perceived flashes (0, 1, or 2) while task-irrelevant beeps (0, 1, or 2) were presented. Responses were given by pressing one of three keypad buttons using the right-hand fingers. In each trial, audio (A) and visual (V) stimuli could be presented coupled or isolated, constituting eight conditions: half the conditions were unisensory and comprised single or couples of visual or auditory events (visual: V and VV; auditory: A and AA) and the other half were multisensory (coherent audio-visual stimulation: AV and AVAV; illusory audio-visual stimulation: AVA and VAV, for a schematic summary of all conditions see the table reported in Figure 2.1a). Unisensory auditory trials (i.e., A and AA) represented control conditions. They were employed to ensure that participants correctly performed the task (participants with a number of errors 3 SD above the group mean were excluded from the analyses as described in the Participants section). The presentation order of the conditions was randomized.

Since our main aim was to explore changes in the neural response to audio-visual events caused by a short-term MD, the main analysis focused on the audio-visual condition inducing fission illusion (AVA). Generating an unstable percept, this illusion allows investigating of subtle changes in audio-visual processing. As a control, we investigated changes in the unisensory visual condition (V). Notably, the visual

stimulus was the same single flash in AVA and V conditions.

All trials started with a grey fixation cross presented at the center of the screen on a black background. After 717 ms, the stimulation was delivered. In the case of the fission illusion (i.e., AVA), each visual and auditory stimulus was separated by one frame (i.e., 17 ms; see an example for AVA condition in Figure 2.1a and Supplementary materials Chapter 2). Following the stimulation, a blank screen appeared for 500 ms (response-free time window), then the fixation cross became white, and participants were asked to respond within 1 second (except for the staircase procedure, in which participants had infinite time to respond; see Preliminary behavioral assessment). As soon as the response was given, a blank screen was presented for 300 ms before the beginning of the subsequent trial. Participants were asked to maintain their gaze at the fixation cross throughout the duration of the trial.

2.2.3.2 Preliminary behavioral assessment

The ocular dominance via the Porta Test (see Supplementary materials Chapter 2), the visual acuity via the eye chart, and the rate of the illusory percept during the monocular visual discrimination task were measured to verify if the participant could take part in the main experiment.

Once ocular dominance and visual acuity were tested, participants performed two short versions of the monocular visual discrimination task. The first short version comprised a staircase procedure (see Supplementary materials Chapter 2 for details) that was used to identify, at the individual level, the luminance contrast between the grey dot and the black background needed to elicit the fission illusion in about 50% of trials (Pérez-Bellido et al., 2015). Participants performed this test monocularly, with the dominant and non-dominant eye (the order was randomized). The contrast level for the dominant and non-dominant eye did not differ within-participant ($t(26)= -1.466$, $p=0.155$). The second short version of the monocular visual discrimination task (30 trials for each of the following conditions V, VV, AVA, VAV, A, and 6 for AA, AV, AVAV) was then performed with the dominant eye (with the contrast identified by the staircase procedure) to evaluate whether the participant was fulfilling the inclusion criteria to take part in the main experiment (see Participants section).

Previous evidence revealed that individual sensory preference (Audio or Visual) impacts multisensory processing (Giard and Perronet, 1999). To assess whether individual sensory predisposition might affect multisensory short-term plasticity, participants monocularly performed a speeded object recognition task based on auditory, visual, and audio-visual information (see Supplementary materials Chapter 2 for details). Each participant's Sensory-Preference (Audio or Visual) was classified for each eye, and no significant difference was found between them ($p>0.68$). Sensory-Preference was an additional measure that we took into consideration: for this reason, the N within the Audio and Visual groups were not balanced.

2.2.3.3 Main experiment

Participants recruited in the main experiment came to the laboratory a second time on a different day. Since the main experiment lasted about five hours, the data were always acquired in the morning (approximately between 9 am and 2 pm) to avoid possible confounds associated with the circadian cycle or related to (visual) activities performed before the experiment. Each participant repeated the short version of the monocular visual discrimination task with the dominant eye comprising the staircase procedure to ensure the test-retest reliability of the selected visual stimulus contrast (no significant difference was found between the contrast levels measured in the two assessments; $t(20)=0.637$, $p=0.532$).

A brief practice of 16 trials was run before the main experiment. Participants performed the monocular visual discrimination task, with each eye, before (t0) and after (t1) a period of monocular deprivation (MD) (see Figure 2.1b), while their EEG signal was recorded. Thus, each participant performed a total of four sessions of the monocular visual discrimination task (i.e., at t0 and t1, both with the dominant and the non-dominant eye). Note that whether they started with the dominant or the non-dominant eye was counterbalanced across participants. MD consisted of 150 minutes in which the dominant eye was occluded by a translucent eye patch, following a validated procedure (Lunghi et al., 2011). From now on, we will refer to the dominant eye as the 'Deprived eye' and to the non-dominant eye as the 'Undeprived eye'.

To prompt active and controlled multisensory interactions with the environment during the MD phase, participants were engaged in predefined activities. Since the physical activity was demonstrated to boost short-term homeostatic plasticity in the adult visual cortex (Lunghi and Sale, 2015), all participants were engaged in the following activities: table football, table hockey, ping pong, and billiards, each of them lasting 15 minutes. The EEG cap was always kept on the scalp for the entire experiment duration.

Each monocular session (i.e., t0 Deprived, t0 Undeprived, t1 Deprived, and t1 Undeprived) comprised 100 trials for the conditions V, VV, AVA, VAV, A, and only 30 trials for the conditions AA, AV, AVAV, and was divided into five blocks (118 trials each) lasting about 5 minutes each. The number of trials was chosen to keep the duration of the monocular session within the estimated length of the MD effect (which has been demonstrated to be present for up to 90 minutes but substantially decreases after 15 minutes; see Lunghi et al., 2011).

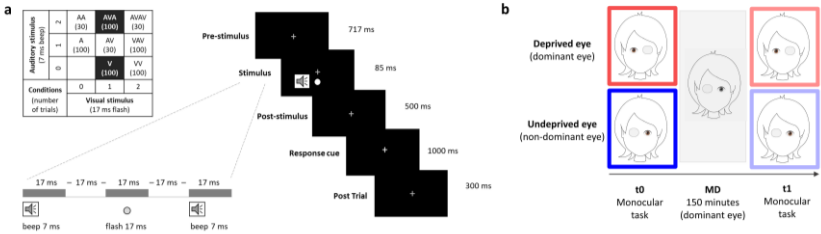

Figure 2.1. Schematic illustration of the experimental paradigm. (a) The top left table shows all the possible combinations of the stimuli (visual stimuli V and auditory stimuli A), representing all the eight possible conditions (conditions of interest are highlighted, and the number of trials in each condition is shown in brackets). On the right, an example of a single trial presentation in AVA condition is depicted. (b) Experimental procedure showing the four sessions performed with the Deprived eye (upper line, red contour) and the Undeprived eye (bottom line, blue contour). At t0 and t1, participants performed the visual monocular task with each eye (eye order was counterbalanced across participants). Between t0 and t1, participants wore a translucent eye

patch on the dominant eye (Deprived eye) for 150 minutes (MD phase).

2.2.4. EEG recording and preprocessing

EEG data were collected continuously during the four monocular task sessions (i.e., t0 Deprived, t0 Undeprived, t1 Deprived, and t1 Undeprived), using Electrical Geodesics EEG system with 64-channels (EGI; 500 Hz sampling rate). Offline, the data of the four sessions were concatenated at the individual level to detect common stereotypical artifacts. Data were preprocessed by implementing a validated approach (Stropahl et al., 2018; Bottari et al., 2020). The continuous recordings were filtered (low-pass cut-off at 40 Hz, Hanning filter, order 500; high-pass cut-off at 1 Hz, Hanning filter, order 100) and downsampled to 250 Hz to reduce the computational time. The filtered and downsampled data were segmented into consecutive 1-second epochs and cleaned using joint probability criterion: segments displaying an activity with a joint probability across all channels larger than 3 SD were removed (pop_jointprob function of EEGLAB; Delorme et al., 2007). Independent Component Analysis (ICA) based on the extended Infomax (Bell and Sejnowski, 1995; Jung et al., 2000a, 2000b) was then performed. The resulting ICA weights were saved and applied to the raw continuous unfiltered data (Stropahl et al., 2018; Bottari et al., 2020). Components associated with stereotypical artifacts, such as eye blinks and eye movements, were identified and removed using a semiautomatic procedure (CORRMAP, Viola et al., 2009). The data were then low-pass and high-pass filtered (100 Hz, filter order 100; 0.1 Hz, filter order 500) with a Hanning filter. Noisy channels were identified based on visual inspection and then interpolated using spherical spline interpolation (mean interpolated electrodes per subject 2.32 ± 2.26 SD) and re-referenced to the average. Finally, the residual power line fluctuations at 50 Hz were removed using the CleanLine EEGLAB plugin (https://github.com/sccn/cleanline). The EEG data were then split again into the original four sessions. Each session was then segmented into epochs of 2.2 seconds, from -1 to 1.2 seconds with respect to the onset of the stimulation. Noisy epochs were then rejected based on the joint probability across channels (Delorme et al., 2007) with a threshold of 3 SD (mean epochs rejected per subject in each session for V condition: t0 Deprived 12% ± 4 SD, t0 Undeprived 12% ± 6 SD, t1 Deprived 14% ±

5 SD, and t1 Undeprived 12% ± 5 SD, and for AVA condition: t0 Deprived 12% ± 6 SD, t0 Undeprived 12% ± 5 SD, t1 Deprived 12% ± 5 SD, and t1 Undeprived 14% ± 6 SD). All these steps were performed with EEGLAB software (Delorme and Makeig, 2004). Data were then imported into Fieldtrip (Oostenveld et al., 2011) to perform time-frequency decomposition and statistical analyses.

2.2.5 Time-frequency decomposition

Time-frequency decomposition of the EEG data was performed within each session and separately for the visual and audio-visual conditions. Within each condition and session, we first extracted the induced power at a single trial level after subtracting the evoked activity (that is, subtracting from each trial the ERP computed averaging across trials without low-pass filtering). Time-frequency decomposition of single-trials was computed at each channel, separately for low (2-30 Hz) and high (30-80 Hz) frequency ranges. The oscillations in low frequencies were estimated using a Hanning taper with a frequency-dependent window length (4 cycles per time window) in steps of 2 Hz. Oscillations with higher frequencies were estimated using a Multitapers method with Slepian sequence as tapers, in steps of 5 Hz with a fixed-length time window of 0.2 seconds and fixed spectral smoothing of ± 10 Hz. For both frequency ranges, the power was extracted over the entire epoch (from -1 to 1.2 seconds) in steps of 0.02 seconds. Then, the average across trials was computed at the individual level within each session (t0 Deprived, t0 Undeprived, t1 Deprived, t1 Undeprived), conditions (V and AVA), and frequency range (low and high). The resulting oscillatory activity was baseline-corrected to obtain the relative signal change with respect to the baseline interval. For the low-frequency range, the baseline was set between -0.7 and -0.3 seconds, while for the high-frequency range, it was between -0.2 and -0.1 seconds. The low-frequency range, having longer cycles, required a wide baseline for the appropriate estimation of slow oscillations and was kept temporally distant from the stimulus onset to avoid temporal leakage of post-stimulus activity into the baseline period. The same procedure, without ERP subtraction from single trials, was implemented to estimate the total power. The baseline-corrected evoked power was computed by subtracting the baseline-corrected induced power from the baseline-corrected total power.

2.2.6 Source reconstruction

To better characterize the neural alterations induced by MD, source estimation of the neural effects was performed using Brainstorm software (Tadel et al., 2011) on preprocessed EEG data. Sources were extracted by applying a dynamic statistical parametric mapping (dSPM; Dale et al., 2000), adopting minimum-norm inverse maps to estimate the locations of scalp electrical activities. For each dataset, we used single trials pre-stimulus baseline [− 0.1 to 0.002 s] to calculate single subject noise covariance matrices and to estimate individual noise standard deviations at each location (Hansen et al., 2010). The boundary element method (BEM) provided in OpenMEEG was adopted as a head model; the model was computed on the first dataset and then applied to all the others (default parameters in Brainstorm were selected). Source estimation was performed by selecting the option of constrained dipole orientations (Tadel et al., 2011). Time-frequency decomposition was computed for each participant on the estimated sources at the single-trial level using the same approach described for the time-frequency decomposition performed at the sensor level.

2.2.7 Statistical analysis

2.2.7.1 Behavioral data

For each participant, we computed the d-prime (d') as visual and audio-visual sensitivity indices: d' = z(p hits) - z(p false alarms), where z is the inverse cumulative normal function, and p is the proportion of hits and of false alarms out of signal and noise, respectively. Values equal to 0 or 1 were corrected as 1/n and (n-1)/n, respectively, with n being the number of signal or noise trials. To compute the visual d', we defined as hits, trials in which participants perceived one flash (V condition) and correctly responded 'one'. Consequently, false alarms were trials in which two flashes were presented (VV), and participants responded to having seen one flash. To compute the audio-visual d', we defined, coherently with the fission illusion literature, false alarms AVA trials in which participants reported two flashes (Watkins et al., 2006; Whittingham et al., 2014; Pérez-Bellido et al., 2015; Vanes et al., 2016; Keil, 2020). Thus, AVAV trials in which participants correctly responded 'two flashes' were considered hits. Note that the audio-visual sensitivity

(d') is inversely related to the amount of fission illusion: smaller d' indicated a greater amount of illusory percepts and vice-versa (note that Response means of each condition are reported in Supplementary materials Chapter 2 Figure S2.2).

Two mixed-design ANOVA, with Eye (Deprived and Undeprived) and Time (t1 and t0) as within-subjects factors, and Sensory-Preference (Audio and Visual) in the Deprived eye and Sensory-Preference (Audio and Visual) in the Undeprived eye as between-subjects factors, were performed separately on visual and audio-visual d' values. The Sensory-preference between-subjects factors were inserted in order to control their impact on the visual and audio-visual perception.

2.2.7.2 Neural oscillations

Oscillatory activity occurring after stimulus onset was analyzed separately for visual (V) and audio-visual (AVA) trials to assess MD impact on visual and audio-visual processing. Time-frequency analyses were separately performed for induced and evoked oscillatory activity for both low [4-30 Hz] and high [30-80 Hz] frequency ranges.

To assess the impact of MD, we subtracted the oscillatory activity recorded before MD from the oscillatory activity recorded after MD (i.e., t1 minus t0). This difference was computed separately for the Deprived and Undeprived eye. From now on, PowChangeDeprived represents relative changes in power due to MD for the Deprived eye, and PowChangeUndeprived the relative changes in power due to MD for the Undeprived eye.

To compare the impact of MD on Deprived and Undeprived eye, a series of non-parametric cluster-based permutation tests were performed via a paired-sample t-test without a priori assumptions (i.e., across all electrodes, time-points, and frequencies) between PowChangeDeprived and PowChangeUndeprived. We used the Monte Carlo method with 1000 random permutations; cluster-level statistics were calculated taking the sum of the t-values within every cluster, with an alpha level of 0.05 (two-tailed) and a minimum neighbor channel = 1. Identified clusters were considered significant at $p<0.025$ (corresponding to a critical alpha level of 0.05 in a two-tailed test). We focused on the post-stimulus

activity, and thus, statistical tests were performed for the entire response-free time window, that is, from 0 to 0.5 seconds. The time period after 0.5 seconds from the stimulation onset was discarded to prevent including motor artifacts. If a significant difference due to MD emerged in this test (PowChangeDeprived vs. PowChangeUndeprived), we assessed whether differences between the two eyes emerged at t0 or t1. To this end, two planned comparisons (i.e., t0 Deprived vs. t0 Undeprived and t1 Deprived vs. t1 Undeprived) were performed using the same cluster-based permutation analysis approach and the same parameters reported above. In case a significant difference between Deprived and Undeprived eye would emerge only at t1 and not at t0, it would be indicative of a specific effect of the MD manipulation and rule out possible differences between the two eyes at baseline.

2.2.7.3 Correlations between neural and behavioral changes

After assessing the normality of the data with Shapiro-Wilk tests, Pearson correlations were employed to assess whether the neural changes related to short-term MD were associated with behavioral changes. When multiple correlations were performed to the same dataset, their results were compared employing a bootstrap method adapted for independent samples (see https://github.com/GRousselet/blog/tree/master/comp2dcorr).

The datasets and code used in the present study are available from the corresponding author on reasonable request.

2.3 Results

2.3.1 Behavioral data

2.3.1.1 Unisensory visual

The mixed-design ANOVA on visual d' with Eye (Deprived and Undeprived) and Time (t1 and t0) as within-subjects factors and Sensory-preference in the Deprived or in the Undeprived eye as between-subjects factor revealed a significant main effect of Time ($F(1,15)=13.52$, $p=0.002$). No main effects of Eye, Sensory-Preference in the Deprived or in the Undeprived eye, nor other interaction effects were found (all $ps>0.1$). These findings suggest a general decrease of sensitivity at t1 (mean d' ±

SE for each session: t0 Deprived 1.44 ± 0.21; t1 Deprived 1.13 ± 0.22; t0 Undeprived 1.37 ± 0.26; t1 Undeprived 1.14 ± 0.23; see Figure 2.2a).

2.3.1.2 Audio-visual

The mixed-design ANOVA performed on audio-visual d' revealed a significant main effect of Eye ($F(1,15)=7.53$, $p=0.015$), showing that the Undeprived eye was less susceptible to the fission illusion (mean d' ± SE for each session: t0 Deprived 0.58 ± 0.16; t1 Deprived 0.53 ± 0.19; t0 Undeprived 0.84 ± 0.23; t1 Undeprived 0.66 ± 0.17). A tendency towards significance emerged for the interaction between Eye, Sensory-Preference in the Deprived eye, and Sensory-Preference in the Undeprived eye ($F(1,15)=4.01$; $p=0.064$). This tendency might suggest that the participant's Sensory-Preference had an eye-specific impact; being an Audio-subject or a Visual-subject might affect the level of the fission illusion perceived with that eye (in Deprived eye mean d' ± SE A-group: 0.52 ms ± 0.19; V-group: 0.69 ms ± 0.20; in the Undeprived eye A-group: 0.65 ms ± 0.20; V-group: 0.96 ms ± 0.36). No significant main effects of Time, Sensory-Preference in the Deprived or in the Undeprived eye, nor other interactions emerged (all ps>0.08). Notably, a strong fission illusion was elicited in both eyes as highlighted by the small d' measured in each of the four sessions (see Figure 2.2b).

Since no main effect of the Sensory-Preference emerged neither in visual nor in audio-visual ANOVAs, the analyses of EEG activity were performed on the whole group.

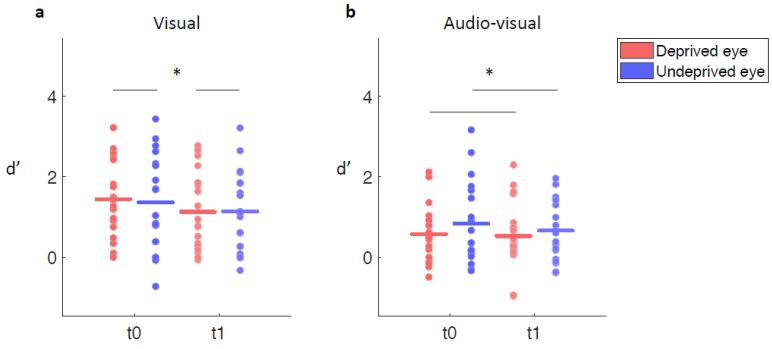

Figure 2.2. Behavioral performance computed as sensitivity (d'). (a) Both in visual and (b) audio-visual conditions, the group mean d' is reported for t0 and t1 within each eye (Deprived and Undeprived); superimposed dots represent single subjects' data; significant differences are highlighted with *. Sensitivity in the visual condition decreased after MD in both Deprived and Undeprived eye. Fission illusion in the audio-visual condition was greater for the Deprived than Undeprived eye.

2.3.2 Neural oscillations

To specifically investigate whether MD primarily affected feedback and/or feedforward connectivity, we assessed the impact of MD on induced and evoked neural oscillations associated with the processing of visual and audio-visual stimuli.

2.3.2.1 Unisensory Visual

Induced power. The cluster-based permutation test performed on induced oscillatory activity within the low-frequency range [4-30 Hz] revealed a significant difference for PowChangeDeprived vs. PowChangeUndeprived ($p<0.009$) spanning from occipital to frontal regions. MD elicited a marked decrease of induced activity in the alpha range [10-16 Hz] between 0 to 0.12 seconds selectively for the Deprived eye (see Figure 2.3a, b). While no significant effects were found when comparing the oscillatory activity between the two eyes at t0 (all $ps>0.51$), the comparison performed on induced oscillatory activity measured at t1 revealed a significant difference ($p<0.002$) between Deprived and Undeprived eye for the power in the alpha range [10-16 Hz]. These planned comparisons confirmed a direct effect of MD, and excluded possible confounds due to differences between the eyes at baseline. To further investigate the time-course of the MD effect in the alpha range, we tested the difference between t1 and t0 for each eye (i.e., Deprived, Undeprived). For each session and participant, we extracted the mean induced alpha power [10-16 Hz] measured across three occipital electrodes (E36, E38, E40, which corresponded to the peak of the statistical effect in the PowChangeDeprived vs. PowChangeUndeprived cluster-based permutation test). A series of paired t-tests were performed between t0 and t1 for each eye, at each time-point within the whole-time window of interest [0-0.5 s] (FDR

corrected, q=0.05). A significant difference was found only for the Deprived eye, showing a clear decrease in the alpha synchronization after MD (from 0 to 0.14 s; for Undeprived eye all ps>0.97; see Figure 2.3c).
No significant differences between PowChangeDeprived and PowChangeUndeprived were found in the high-frequency range [30-80 Hz] (all ps>0.67, see Figure S2.3 Supplementary materials Chapter 2).

Evoked power. Cluster-based permutation analyses on evoked oscillatory activity were performed contrasting PowChangeDeprived vs. PowChangeUndeprived to test whether MD alters feedforward visual processing. No significant differences emerged in either low or high frequencies (all ps>0.13, see Figure S2.4 Supplementary materials Chapter 2).

In sum, a visual MD effect emerged selectively for the Deprived eye and in the induced oscillatory activity within the alpha range.

Source analysis. We investigated the electrical sources of the visual MD effect. To this end, a permutation paired t-test (1000 randomizations) was performed at the source level, on the power in the alpha range [10-16 Hz] between t0 and t1 for the Deprived eye (time window [0-0.5 s]; FDR correction was applied on the time dimension). Results revealed that the visual MD effect was mainly located within the right hemisphere and comprised the superior parietal gyrus, the superior occipital gyrus, intraparietal and subparietal sulcus, and extended to calcarine sulcus (corrected p-threshold: 0.003; see Figure 2.3d).

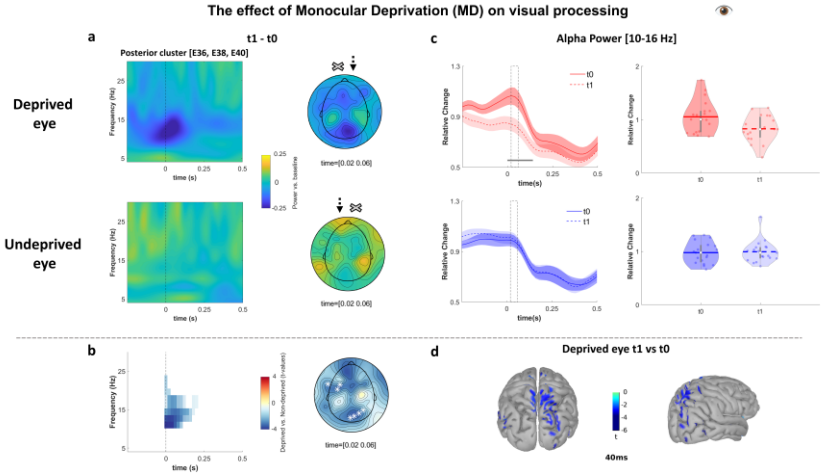

Figure 2.3. The effect of Monocular Deprivation (MD) on visual processing, visual MD effect. (a) Oscillatory activity calculated as the difference between t1 minus t0 at each eye: PowChangeDeprived (upper row) and PowChangeUndeprived (bottom row) are plotted as a function of time [-0.25 - 0.5 s] and frequency [4-30 Hz]. The plots show the average across occipital electrodes (E36, E38, E40); 0 s indicates stimulus onset. Topographies in the alpha range [10-16 Hz] at a representative time window [0.02 - 0.06 s]; arrows indicate which eye was stimulated (here depicted a participant with right-eye dominance); crosses represent the eye covered by a translucent patch. (b) Statistical results. Time-frequency plot highlighting significant differences between PowChangeDeprived and PowChangeUndeprived identified by the cluster-based permutation test ($p<0.025$, two-tailed) and the corresponding topography for the alpha range [10-16 Hz] at a representative time window [0.02 - 0.06 s]; electrodes belonging to the significant cluster are highlighted with white asterisks. (c) Time-course at the group level of the mean power in the alpha range [10-16 Hz] at t0 and t1 (data are averaged across electrodes E36, E38, E40) separately displayed for the Deprived and the Undeprived eye (upper and bottom rows); shaded areas represent the standard error of the mean; the continuous horizontal grey line indicates the significant difference between t0 and t1 in the Deprived eye (from 0 to 0.14 s; $p<0.05$, FDR corrected). The

dashed grey boxes represent the time window [0.02 - 0.06 s], comprising the alpha peak, in which the power in the alpha range [10-16 Hz] was extracted for each subject (across channels E36, E38, E40) and shown in the corresponding violin plots (right side; each dot represents individual data). (d) Source analysis performed to localize the visual MD effect; the image shows, at 40 ms after stimulus onset, the area in which the power in the alpha range [10 - 16 Hz] significantly decreased at t1 with respect to t0.

2.3.2.2 Audio-visual

After we assessed the impact of MD on unisensory visual processing (visual MD effect), we investigated whether MD can also affect audio-visual processing at the neural level. The induced and evoked oscillatory activities were tested separately within low and high-frequency ranges.

Induced power. The cluster-based permutation performed on induced oscillatory activity within the low-frequency range [4-30 Hz] between PowChangeDeprived and PowChangeUndeprived showed no significant effects (all ps>0.45, see Figure S2.5 Supplementary materials Chapter 2). In contrast, the same analysis performed within the high-frequency range [30-80 Hz] revealed a significant effect in gamma activity ($p<0.015$). An increase in gamma activity [65-75 Hz] was found in the Undeprived eye between 0.16 and 0.26 s, mainly in posterior electrodes (see Figure 2.4a, b). The planned comparison showed no significant effect at t0 (all ps>0.07), while a significant difference between the two eyes emerged only at t1 ($p<0.022$), confirming that MD specifically guided the effect. To further investigate the time-course of the induced gamma effect, we tested the difference between t0 and t1 within each eye. For each session and participant, we extracted the mean induced gamma power [65-75 Hz] measured across two parieto-occipital electrodes (E40 and E42, which corresponded to the peak of the statistical effect in the PowChangeDeprived vs. PowChangeUndeprived cluster-based permutation test). A series of paired t-tests were performed between t0 and t1 for each eye, at each time-point within the whole-time window of interest [0-0.5 s] (FDR corrected, q=0.05). Only for the Undeprived eye, a significant effect was found (from 0.12 to 0.2 s; for Deprived eye all ps>0.5; see Figure 2.4c).

The gamma band increase during audio-visual processing in the Undeprived eye following MD might suggest an upweighting of the auditory modality. If this would be the case, a greater neural response in the gamma range to unimodal acoustic stimulation (A and AA condition) should emerge selectively for the Undeprived eye after MD. To this end, a hypothesis-driven ($p<0.05$, one tail) cluster-based permutation test was performed on the induced oscillatory activity in response to auditory stimuli (average across A and AA trials) in the high-frequency range [30-80 Hz] across all electrodes, frequencies, and time-points [0-0.5 s], between t0 and t1, separately in each eye. The analysis revealed a significant increase in gamma activity between 100 and 300 ms in response to auditory stimulation after MD ($p<0.04$), selectively for the Undeprived eye (see Figure 2.5). Conversely, no significant difference emerged for the Deprived eye ($p>0.35$). This significant effect emerged in parietal electrodes as for the audio-visual MD effect. These findings support our hypothesis that the increased induced gamma activity during audio-visual processing is due to an upweighting of auditory input.

Evoked power. When the difference between PowChangeDeprived and PowChangeUndeprived was tested in the evoked power, no significant difference was found within the low-frequency range (all $ps>0.09$), nor within the high-frequency range ($p>0.05$, see Figure S2.6 Supplementary materials Chapter 2).

To sum up, the audio-visual MD effect selectively emerged for the Undeprived eye in the induced gamma power. This neurophysiological change seems to be driven by increased responsiveness to auditory inputs.

Source analysis. We investigated the sources of the audio-visual MD effect. To this end, a permutation paired t-test (1000 randomizations) was performed at the source level, on the power in the gamma range [65-75 Hz] between t0 and t1 for the Undeprived eye (time window [0-0.5 s]; FDR correction was applied on the time dimension). Results revealed that audio-visual MD effect was mainly located at the cortical level around the right intraparietal sulcus (corrected p-threshold: 0.002; see Figure 2.4d).

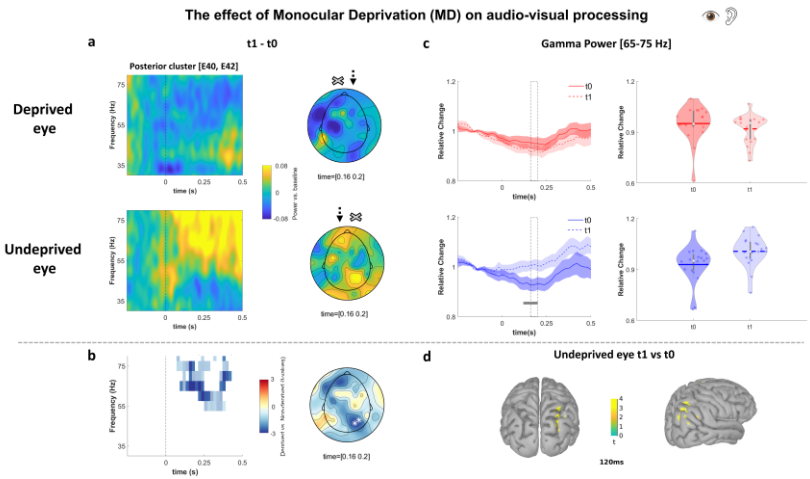

Figure 2.4. The effect of Monocular Deprivation (MD) on audio-visual processing, audio-visual MD effect. (a) Oscillatory activity calculated as the difference between t1 minus t0 at each eye: PowChangeDeprived (upper row) and PowChangeUndeprived (middle row) are plotted as a function of time [-0.25 - 0.5 s] and frequency [30-80 Hz]. The plots show the average across posterior electrodes (E40, E42); 0 s indicates the stimulus onset. Topographies in the gamma range [65-75 Hz] at representative time window [0.16 - 0.2 s]; arrows indicate which eye was stimulated (represented in a participant with a right-eye dominance), and crosses represent the eye covered by a translucent patch. (b) Statistical results. Time-frequency plot highlighting significant differences between PowChangeDeprived and PowChangeUndeprived identified by the cluster-based permutation test ($p<0.025$, two-tailed) and corresponding topography for the gamma range [65-75 Hz] at a representative time window [0.16 - 0.2 s]; electrodes belonging to the significant cluster are highlighted with white asterisks. (c) Time-course at the group level of the mean power in gamma range [65-75 Hz] at t0 and t1 (data are averaged across electrodes E40, E42) separately displayed for the Deprived and the Undeprived eye (upper and bottom rows); shaded areas represent the standard error of the mean; the continuous horizontal grey line indicates a significant difference between t0 and t1 for the Undeprived eye (from 0.12 to 0.2 s after

stimulus onset; p<0.05, FDR corrected). The dashed grey boxes represent the time window [0.16 - 0.2 s] in which the power in the gamma range [65-75 Hz] was extracted for each subject (across channels E40 and E42) and shown in the corresponding violin plots (right side). (d) Source analysis performed to localize the audio-visual MD effect; the image shows at 120 ms after stimulus onset the area in which the power in the gamma range [65-75 Hz] significantly increases at t1 with respect to t0.

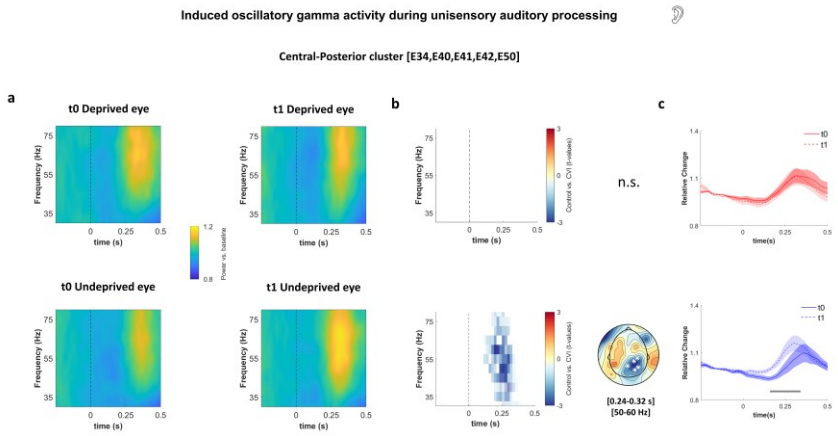

Figure 2.5. Increased induced gamma activity for the Undeprived eye after MD during auditory processing. (a) Oscillatory activity at t0 and t1 are plotted as a function of time [-0.25 - 0.5 s] and frequency [30-80 Hz] for the Deprived (upper row) and Underprived eye (bottom row). The plots show the average across central-posterior electrodes (E34, E40, E41, E42, E50); 0 s indicates the stimulus onset. (b) Results of the cluster-based permutation test are shown in the time-frequency plots and highlight significant differences between t0 and t1, which emerged only for the Undeprived eye. Topography shows the results of the cluster-based permutation test for the Undeprived eye in the gamma range [50-60 Hz] over a representative time window [0.24 - 0.32 s]; white asterisks highlight significant electrodes (E34, E40, E41, E42, E50). (c) Time-course at the group level of the mean power in gamma range [50-60 Hz] at t0 and t1 (data are averaged across electrodes E34, E40, E41, E42, E50),

separately displayed for the Deprived and the Undeprived eye (upper and bottom rows); shaded areas represent the standard error of the mean; the continuous horizontal grey line indicates a significant difference between t0 and t1 for the Undeprived eye (from 0.16 to 0.34 s after stimulus onset; $p<0.05$, FDR corrected).

2.3.3 Association between neural and behavioral changes due to MD

For visual and audio-visual conditions, we investigated the degree of association between brain activity alterations and changes in behavioral performance. The average power at the frequencies of interest was extracted within a time window and across channels that resulted significant in the cluster-based permutation tests (visual and audio-visual MD effects). At the individual level, we computed the normalized difference between t1 and t0 within each eye ([PowChangeDeprived/t0 Deprived] * 100; [PowChangeUndeprived/t0 Undeprived] * 100). Shapiro-Wilk tests confirmed that data in each condition were normally distributed (all ps >0.05). Thus, within each condition (i.e., visual and audio-visual) and for each eye (i.e., Deprived and Undeprived), the power change was correlated with the corresponding change in sensitivity between t0 and t1 using Pearson's correlation coefficient.

2.3.3.1 Unisensory Visual

We first tested whether observed changes of oscillatory activity in induced alpha power following MD (visual MD effect) were associated with changes in behavioral performance. To this aim, we extracted the average power in the 10-16 Hz range between 0.02 and 0.06 s from the three significant electrodes (E36, E38, and E40) for each session. Then, the normalized t1-t0 difference of PowChangeDeprived and PowChangeUndeprived was computed.

A significant positive correlation between normalized PowChangeDeprived and visual sensitivity change in the Deprived eye (d' change) was found ($r(16) = 0.492$, $p=0.038$). Following MD, the visual sensitivity in the Deprived eye decreased in parallel with a reduction in induced alpha power in the same eye. When the correlation between induced alpha change and visual sensitivity change was tested for the Undeprived eye, no significant effect was found ($p>0.99$).

2.3.3.2 Audio-visual

Next, we tested whether the increase in induced gamma after MD period (audio-visual MD effect) was associated with illusory fission percept. Thus, within each session, the induced power between 65 and 75 Hz was extracted within the 0.16-0.2 s time window and across the two significant posterior channels (E40 and E42). Then, the normalized t1-t0 difference of PowChangeDeprived and of PowChangeUndeprived was computed. No significant correlation was found neither for the Deprived eye nor for the Undeprived eye (all ps>0.43). However, at the behavioral level, a tendency for an interaction between illusion perception and sensory preferences was found ($F(1,15)=4.01$, $p=0.06$), indicating that Visual subjects tended to experience less illusion than Audio subjects, especially in the Undeprived eye (see section Audio-visual in the Behavioral Results). Interestingly, the perception of the multisensory input is known to partially depend on individual sensory predisposition (e.g., Giard and Perronet, 1999; Hong et al., 2021). Therefore, despite this was not the focus of the paper, we additionally explored whether the association between neural and behavioral changes might be affected by individual sensory preference. Specifically, we calculated the correlation between PowChangeUndeprived and audio-visual d' change in the Undeprived eye within Audio and Visual groups, classified according to participants' Sensory-Preference (estimated for the same eye). Pearson correlation revealed a significant negative correlation in the V-group ($r(3) = -0.937$; $p=0.019$), while a tendency toward a significant positive correlation was found in the A-group ($r(11) = 0.513$; $p=0.073$). The two correlations significantly differed (difference=1.45 CI [0.17 1.80]. Since Pearson correlations were performed, the confidence interval was adjusted as described in Wilcox (2009); see Supplementary materials Chapter 2 Figure S2.7). While these results are based on an explorative analysis and small sub-samples, they seem to suggest that the audio-visual MD effect might have a different impact on the illusory percept according to the participants' Sensory-Preference: in V-group, the increase of induced gamma activity in the Undeprived eye was positively associated with a fission illusion increase (smaller d' after MD), while in A-group the increase of induced gamma activity seemed to be associated with a fission illusion decrease (larger d' after MD).

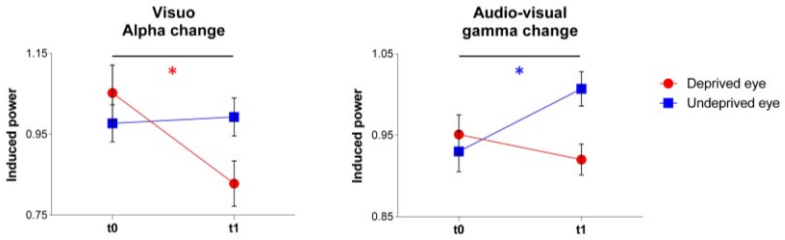

Figure 2.6. Visual and audio-visual MD effects on induced oscillatory activity. The plots show the % normalized power change due to MD in unisensory visual and multisensory audio-visual processing. On the left, the visual MD effect: decreased induced alpha power selectively for the Deprived eye (red) during unisensory visual processing. On the right, the audio-visual MD effect: enhanced induced gamma power selectively for the Undeprived eye (blu) during audio-visual processing. Each dot represents the group mean and bars the SE. Significant differences are highlighted with * (red indicates effect for the Deprived eye and blu for the Undeprived eye).

2.4 Discussion

In this study, adult neural plasticity of both unisensory visual and multisensory audio-visual processes was investigated to assess whether the impact of MD extends beyond visual processing. Induced and evoked oscillatory activity changes both in visual and audio-visual processing were measured after 150 minutes of altered visual experience (brief MD). Induced alpha associated with the early phase of visual processing (<150ms) decreased after MD selectively for the Deprived eye. Conversely, induced gamma associated with audio-visual processing increased after MD only in the Undeprived eye, within a later temporal window (~100-300ms). Notably, both visual and audio-visual processing alterations were found selectively for the induced component of neural oscillations (see Figure 2.6). Source modeling linked both the visual and audio-visual MD effects to the right parieto-occipital cortex. Our data reveal the specific neural signatures of temporary MD effects on visual and audio-visual processes and shed light on their shared

feedback nature. We demonstrated that a brief period of monocular visual experience in adulthood specifically changes the neural response to multisensory audio-visual events because of plasticity in feedback connectivity.

2.4.1 Spectro-temporal properties of the visual MD effect

The observed visual MD effect is in line with previous studies (Lunghi et al., 2015a, 2015b; Zhou et al., 2015; Binda et al., 2018; Schwenk et al., 2020). The reduced alpha synchronization observed when the task was performed with the Deprived eye after MD is consistent with increased excitability to compensate for the absence of stimulation during the deprivation phase. Source modeling suggested that the alpha reduction was mainly localized in the right hemisphere in superior parieto-occipital areas, with some activities extending to primary visual areas (calcarine sulcus). These results confirm the modulation of alpha rhythm induced by short-term plasticity, previously shown in the frequency domain as a change in alpha peak amplitude (Lunghi et al., 2015a), and characterize the spectro-temporal properties of this neural effect. Namely, a selective decrease of alpha synchronization [10-16 Hz] occurs in the early stages of visual processing (<150ms). Notably, only induced activity (i.e., not phase-locked to stimulus onset) was altered by MD, revealing the feedback nature of visual short-term plasticity. Overall, these results are coherent with spectroscopy data showing an increase of excitability in the early visual cortex as indicated by reductions of inhibitory gamma-aminobutyric acid (GABA) concentration after short-term MD (Lunghi et al., 2015b). Moreover, selectively for the Deprived eye, a significant correlation was found between the decrease in induced alpha activity and the decrease in visual sensitivity after MD, suggesting a potential link between this neural change and the ability to discriminate temporal aspects of visual processing.

2.4.2 The impact of MD on audio-visual processing

Previous behavioral studies have shown that multisensory perception can be altered by MD (Lo Verde et al., 2017; Opoku-Baah and Wallace, 2020). By measuring changes in neural oscillations, we assessed neural mechanisms underpinning multisensory short-term plasticity and revealed the specific enhancement of induced gamma activity [65-75 Hz]

selectively for the Undeprived eye when processing audio-visual input. The audio-visual MD effect involved the right intraparietal sulcus, suggesting its central role in short-term plasticity induced by MD.

We hypothesized that the audio-visual MD effect could be due to a crossmodal upweighting of the other modality (i.e., audition). To this end, we tested whether the neural response to unimodal auditory stimuli was increased following MD in each eye. The observation that gamma response to auditory input increased following MD selectively for the Underprived eye confirmed our hypothesis. This result revealed that short-term plasticity following MD alters both visual and auditory neural representations. Interestingly, alterations of neural excitability due to temporary binocular deprivation were previously shown to increase heteromodal responses in the visual cortex (Merabet et al., 2008).

From a neurophysiological perspective, it is important to remark that neural profiles of short-term plasticity following MD seem to depend on the type of input at hand. While the visual stimulus was the same in visual and audio-visual conditions, short-term plasticity was characterized by specific oscillatory fingerprints (Siegel et al., 2012): alpha decreased during visual processing while gamma increased during audio-visual and auditory processing.

To what extent does this neural alteration interact with individuals' sensory predisposition? In the Undeprived eye, the correlation between enhanced gamma activity in audio-visual processing and behavioral performance seems to indicate opposite MD impacts on illusory perception with respect to participants' Sensory-Preference. Although preliminary, this result opens the possibility that the upweighting of auditory information during audio-visual processing after MD affects visual perception according to individual sensory preference. Coherently with the extreme flexibility and adaptability of multisensory functions (Giard and Perronet, 1999; Fujisaki et al., 2004; Van Atteveldt et al., 2014), the perception of the multisensory input after MD might change as a function of individual sensory predisposition. This inference should be further verified with psychophysics experiments (see Rohe et al., 2019), designed to directly estimate auditory modality's weight changes during audio-visual processing after MD. Interestingly, a recent study investigating cross-modal recalibration highlighted how

individual variability in one sensory modality (visual reliability) differently affects recalibration of the other modality (audition) (Hong et al., 2021).

Binocular input was shown to be critical for developing audio-visual perception: anomalies in different audio-visual perceptual tasks were reported in cases of monocular enucleation (Moro and Steeves, 2018a, 2018b), individuals affected by early monocular cataracts (Chen et al., 2017), and people suffering from amblyopia (Narinesingh et al., 2015, 2017; Richards et al., 2017). The present results, revealing that MD induces short-term plasticity of audio-visual processing, encourage possible treatments of audio-visual anomalies associated with MD. Increasing evidence in animal studies supports clinical treatment of adult amblyopia (Hensch and Quinlan, 2018), and crucially a recent study conducted with adult people affected by amblyopia has shown that MD combined with physical exercise could be a promising clinical intervention to promote visual recovery (Lunghi et al., 2019). Future studies might help in understanding whether multisensory audio-visual processing could also benefit from this novel clinical treatment.

2.4.3 The pivotal role of induced cortical response in experience-dependent plasticity

Both visual and audio-visual MD effects were selectively found in induced neural oscillations, likely reflecting main alterations in feedback processing integrating sensory input and ongoing cortical activity (Galambos 1992; Klimesch et al., 1998; Tallon-Baudry and Bertrand, 1999; Chen et al., 2012; Keil et al., 2022). Instead, the evoked phase-locked activity (feedforward), related to the processing within the thalamo-cortical pathway (Galambos 1992; Keil et al., 2022), was not affected.

Visual MD effect was found in the induced alpha band, which was previously demonstrated to be drastically impaired by the transient absence of visual experience during development (Bottari et al., 2016). Animal studies involving congenital deaf cats demonstrated that induced and not evoked oscillatory activity in the auditory cortex is extremely reduced across a wide range of frequency bands (e.g., Yusuf et al., 2017). The authors hypothesized that the absence of sensory stimulation prevents the development of neural mechanisms allowing

the integration of sensory signals and internal representations. Evidence of alterations of induced oscillatory activity following sensory deprivation was reported not only within modality, for visual (Bottari et al., 2016) and auditory systems (Yusuf et al., 2017), but also cross-modally. In humans, early-onset deafness selectively affects induced oscillatory activity associated with visual processing (Bednaya et al., 2021). The present audio-visual MD effect (increased induced gamma activity) provides evidence in the same direction also for multisensory processing. Taken together, this evidence suggests a substantial alteration of cortico-cortical feedback activities, in case of sensory input absence in both developmental and adult brain, for unisensory and multisensory functions. This is in line with previous evidence suggesting that the plasticity of feedback connectivity represents an extremely flexible mechanism to process sensory information according to changing demands (Polley et al., 2006).

2.4.4 Limitations of the study

Here, we focused on neural oscillations changes and given the time constraints intrinsic in the MD effect (which is maximum within the first 15 minutes following the deprivation, Lunghi et al., 2011), we could not insert a direct measure of ocular dominance, which is usually assessed with binocular rivalry (e.g., Lunghi et al., 2011). Thus, we relied on eye-specific oscillatory activity alterations selectively at t1 (and their lack at t0) as indications of the change in interocular excitability balance: the decreased alpha during visual processing is compatible with the strengthening of the Deprived eye after MD. While a clear reduction of strength for the Undeprived eye (i.e., increased alpha activity) did not emerge, this is in line with the literature: the strongest impact of MD is known to be on the Deprived eye, while the opposite effect on the Undeprived eye was found to be much smaller (Lunghi et al., 2015a; Binda et al., 2018) or even absent (Zhou et al., 2015). Thus, it is possible that larger sample sizes are required to measure neural effects on the Undeprived eye during visual processing. Further studies might help to assess whether depriving the non-dominant eye will lead to the same MD effects. However, given the absence of difference at t0, we can rule out the possibility that our effects are due to baseline differences between the dominant and the non-dominant eye.

Noticeably, the visual MD effect emerged here for the Deprived eye, while the audio-visual MD effect emerged only for the Undeprived eye. While these effects are in line with previous behavioral studies (Lo Verde et al., 2017; Opoku-Baah and Wallace, 2020), they also support a crucial role of MD in inducing flexible alterations of interocular excitability balance and, in turn, in audio-visual processes. Moreover, although an interaction between MD and eye dominance cannot be excluded, a recent study reported that the MD effect was the same regardless of whether the dominant or the non-dominant eye was deprived (Schwenk et al., 2020).

Finally, while the interaction between sensory preference and gamma change in audio-visual processing seems of interest, a larger sample with a balanced number of subjects with visual and auditory sensory preferences is needed to confirm our intriguing preliminary result on how multisensory plasticity can be affected by individual sensory predisposition.

2.5 Conclusions

These results demonstrated that a brief period of monocular visual experience in adulthood is able to change the neural response not only to visual stimuli but also to multisensory events. The data unveiled the spectral fingerprints of adult short-term plasticity induced by a brief period of MD for visual and audio-visual processing. We found enhanced excitability (i.e., decreased induced alpha activity) for the Deprived eye during an early phase of visual processing, and we demonstrated the presence of neural alterations beyond the visual processing. Gamma activity associated with audio-visual processing was increased by MD at a later latency and only when the task was performed with the Undeprived eye. The analyses of responses to unimodal auditory input indicate an upweighting of sound input following MD, selectively for the Undeprived eye. Importantly, these distinct neural effects were selectively found in the induced neural oscillations, revealing that experience-dependent plasticity mainly involves alterations in feedback processing not only during development but also in adulthood. This observation is consistent with the existence of a general mechanism shared across sensory modalities and across the life cycle.

Chapter 3

Neural tracking of speech envelope is delayed in cochlear implanted children

3.1 Introduction

Since a seminal publication in 2007 (Luo and Poeppel 2007) paved the road, a multitude of studies revealed that brain activity at a slow timescale (around theta range 4–8 Hz) temporally aligns with the dynamic regularities occurring in speech. The possibility to objectively measure this neural tracking represents today a validated tool to understand the neural representation of speech. In particular, consistent evidence exists that speech envelope, the signal-amplitude modulation over time, is tracked by the auditory cortex oscillatory activity. Such matching is thought to align the auditory-cortex neural activity to the stimulus time-course (phase alignment). Current models suggest that intrinsic oscillating neural signals matching input frequencies provide a mechanism for encoding speech, parsing the signal into temporal windows leading to subsequent analysis and then comprehension (Giraud and Poeppel, 2021; Obleser and Kayser, 2019). Neural tracking of speech envelope is not an epiphenomenon; if neural entrainment to speech-signal is poor, intelligibility is also impaired (Vanthrnhout et al., 2018). While the vast majority of studies investigated neural tracking of speech in adults, recent evidence has revealed that it occurs already in 4 (Attaheri, et al., 2022) and 7 months (Kalashnikova et al., 2018; Jessen et al., 2019; Attaheri, et al., 2022) infants, suggesting a role of this mechanism already in early development. However, to what extent the development of this specific form of neural entrainment requires early exposure to sound and, thus, to speech is unknown.

Typical brain development requires temporal overlapping between the intrinsic maturation of neural systems and environmental input.

Conditions of sensory deprivation represent crucial natural models for the study of such brain-environment interdependences (Amedi et al., 2017; Ricciardi et al., 2020; Bottari and Berto, 2021; Röder et al., 2021). Furthermore, rare contexts in which a deprived sense can be restored provide unprecedented opportunities for assessing whether a specific sensory input is required, within specific periods of life, for the emergence of sensory and cognitive functions (Kral et al., 2019; Röder and Kekunnaya, 2021). In deaf children, auditory deprivation can impact well beyond sensory processing and become language deprivation (Kral and O'Donoghue, 2010). Thanks to cochlear implants (CI), partial but successful auditory restoration is available (Winn and Nelson, 2022). However, even if implantation is performed early in life (i.e., at about one year of age), in the case of congenital profound bilateral deafness, CI cannot prevent delayed sound and speech exposure. Sensitive periods for the discrimination of certain speech features can close within the first year of life (Ruben, 1997; Werker and Hensch, 2015). Thus, both the age at the onset of hearing loss and the age at which auditory experience is restored are fundamental for language development in CI individuals. Indeed, these two factors heavily contribute to the implant outcome (for review, see Kral et al., 2019). However, while the date of cochlear implantation is always known, the definition of deafness onset in humans is more elusive.

The great importance of early implantation (i.e., early auditory restoration) is supported by studies assessing language acquisition. No deficits in learning new words were reported in two-three years old prelingually deaf children who received cochlear implants before 14 months of age, whereas infants implanted later had worse abilities compared to hearing controls (Houston et al., 2012). Congenitally deaf children implanted before 4 years of age showed progressively better trajectories of language development when implanted before 2 years of age or even better before 1 year (Holt and Svirsky, 2008). Congenitally and early deaf children who underwent implantation younger than 18 months had higher comprehension and expression scores and a steeper improvement rate than those implanted later, even if after 3 years of implant experience, CI children did not match hearing children performance (Niparko et al., 2010). However, it is important to highlight that language development extends until the teenage years (Ruben,

1997), and indeed, significant improvements were reported even 10 years after children's implantation (Beadle et al., 2005; Uziel et al., 2007; Geers et al., 2008).

The impact of delayed access to sounds and speech has also been assessed in neurophysiological studies. In CI individuals, optimal responsiveness of auditory cortices to simple linguistic sounds depends on the onset of auditory input. A series of seminal studies uncovered a sensitive period of the central auditory system within 3.5 years of age (Sharma et al., 2002a, 2005). The latency of early auditory responses, occurring about 50 ms after stimulus onset (P1 wave), was comparable between congenitally deaf children (or with severe to profound hearing loss by 1 year of age) implanted within 3.5 years of age and typical developing hearing children. Conversely, children implanted later tended not to reach age-appropriate neural response latency. Similar findings emerged investigating higher-order auditory processing occurring at about 100ms after stimulus onset (N1 wave; Eggermont and Ponton, 2003; Sharma et al., 2015). Due to technical limitations, the activity of the temporal cortex in CIs has been measured so far in reaction to simple and often short-lived sounds, such as syllables. Thus, an unsolved key question is to what extent the CI provides the possibility to develop hearing-like responses to naturalistic speech in the auditory cortices. Yet it is unknown whether and how the auditory cortex receiving sounds via CI is capable of operating at multiple levels of analysis required to understand speech.

In this study, we aimed to answer this question and assess whether the ability of the auditory cortex to efficiently track speech envelope depends on the availability of auditory input in the first months of life or not. That is, we investigated the presence of a perinatal sensitive period in which auditory input must be present for the development of the auditory neural tracking of speech envelope.
To these aims, we used electrophysiology to measure the degree of synchronization between brain activity and continuous speech in hearing children and children with different onsets of bilateral profound deafness (congenital or not) who received cochlear implants. Differences in auditory response functions between the congenital deaf (CD) group and the group of children who develop deafness (DD) would indicate a crucial role of auditory experience in the first months of life for the

development of neural tracking of speech envelope. The onset of deafness, whether children were congenitally deaf, was characterized using objective measures: otoacoustic emission, evaluation of auditory brain-stem responses (ABR), and, when possible, confirmed with genetic tests. To investigate neural tracking of speech, we employed a forward encoding model to predict EEG responses from selected stimulus features. In particular, we used a temporal response function (TRF) to linearly map the envelope speech feature and the neurophysiological responses (Crosse et al., 2016; 2021). As in previous studies from infants to adults (Mirkovic et al., 2015; J. A. O'Sullivan et al., 2015; Kalashnikova et al., 2019; Nogueira et al., 2020; Attaheri, et al., 2022; Keshavarzi et al., 2022;), we estimated the neural tracking of broad band speech envelope 2-8 Hz frequency range because low-frequencies oscillations are crucial for speech comprehension (Peelle and Davis, 2012).

3.2 Materials and Methods

3.2.1 Participants

A total of 47 children participated in the study. They belong to three groups according to their access to auditory input: a group of profound congenital bilateral deaf children (congenital deaf, CD), a group of children who become profound bilateral deaf during development (delayed deaf, DD), and a group of hearing controls children (HC) who never experienced auditory deprivation. Tirthy cochlear implanted children (mean age: 8.8 ± 3.5 fifteen females and fifteen males) were recruited at the Meyer Hospital of Florence (Italy) and the IRCCS Materno Infantile Burlo Garofolo of Trieste (Italy).

All CD children received a diagnosis of congenital profound bilateral deafness. First, they did not pass the neonatal screening for otoacoustic emissions which is performed before the hospital discharge (typically < 1 week). Second, they received a diagnosis of profound bilateral deafness (hearing thresholds ≥ 90 dB in both ears) following the evaluation of auditory brain-stem responses (ABR) within two months of age (range 21-60 days). In contrast, DD children had at least some auditory experiences after birth (minimum 15 months). To ensure the presence of such auditory experience, we combined the following clinical

information: 1) whether they passed otoacoustic emissions neonatal screening at least with one ear; 2) an ABR indicating normal hearing before the diagnosis of deafness or a diagnosis of deafness that was not profound made by ABR or behavioral test (hearing thresholds < 90 dB in at least one ear); 3) family report indicating residual hearing for the first months of life. All DD patients received a diagnosis of profound bilateral deafness through behavioral hearing thresholds (age range 15-65 months) before cochlear implantation (in case the exact date of this test was not available, we estimated the onset of profound bilateral deafness two months before the date of the first cochlear implantation; N=9).

All cochlear-implanted children included in the final sample were diagnosed with profound bilateral deafness and received cochlear implantation at least six months before the present study (Sharma et al., 2002) to ensure a stable implant functioning and that some auditory experience had been accumulated by the auditory system (see Table 1 for more detailed CI participants' information). One child was excluded because they took part in the experiment only one month after the activation of cochlear implants. Another two-year-old child was discarded because they could not comply with the experiment.

The final sample of cochlear implanted participants comprised fifteen CD children (mean age: 8.70 years; SD: 3.61, seven females and eight males) and thirteen DD children (mean age: 9.58 years; SD: 3.35, eight females and five males). A group of hearing controls (HC) age- and gender-matched were recruited as a control group (N=17; mean age: 8.89 years; SD: 2.84, six females and eleven males). No significant difference emerged between the three groups neither for age ($F(2)=0.28$; $p=0.76$) nor for gender ($\chi2(2)=2.04$; $p=0.36$). HC children were recruited among public schools in Lucca (Italy) and at the MultiLab of Milano-Bicocca University (Italy). None of the children who participated in the study had any additional sensory deficits or neurological disorders (medical records and/or family reports). All participants were oralists, and their first language (L1) was Italian (two CD, one DD, and one HC participants were bilingual). The mean age at cochlear implantation was 28.67 months (range: 11-132) for the CD group and 58.46 months (range: 17-120) for the DD group. The mean duration of auditory experience

with cochlear implants was 74.73 months (range: 23-151) for the CD group and 55.46 months (range: 11-178) for the DD group.

The study was approved by the local Ethical Committee (Comitato etico Regionale per la sperimentazione clinica della Regione Toscana: Numero registro 34/2020, and Comitato etico congiunto per la ricerca espressione di parere delibera n. 17/2020). Before participating in the experiment, written informed consent was signed by the participants' parents and by the children themself if older than seven years old. The experimental protocol adhered to the principles of the Declaration of Helsinki (2013).

Table 3.1 CI Participant's clinical characteristics

Participant	Group	Gender	Age (years)	Screening Otoacoustic Emissions	Test indicating some hearing experience before implantation (threshold < 90 dB)			Test indicating profound bilateral deafness diagnosis (threshold ≥ 90 dB)			Cause of deafness	Familiarity	Implant information				Age first hearing aids before IC (months)	Bilinguism	Gestation, type of birth
					Age	Value ABR / autometry left ear	Value ABR / autometry right ear	Age	Value ABR / autometry left ear	Value ABR / autometry right ear			Side	Age first implant (months)	Age second implant (months)	Experience with CI (months)			
CI 1	CD	famele	6	not pass bilateral	n.a.	n.a.	n.a.	38 days	95	100	Connexina 26	yes	Bilateral	11	36	61	6	no	
CI 2	CD	famele	14	not pass bilateral	n.a.	n.a.	n.a.	25 days	100	90	Connexina 26	no	Bilateral	132	160	39	1	no	
CI 3	CD	male	13	not pass bilateral	n.a.	n.a.	n.a.	49 days	90	90	Connexina 26 heterozygosis	no	Right	84		69	6	no	
CI 4	CD	famele	10	not pass bilateral	n.a.	n.a.	n.a.	25 days	90	90	Connexina 26	no	Left	16		106	6	no	NICU
CI 5	CD	male	7	not pass bilateral	n.a.	n.a.	n.a.	21 days	100	100	Connexina 26 CMV infection	yes	Left	28		50	5,5	no	twin pregnancy without complications
CI 6	CD	male	7	not pass bilateral	n.a.	n.a.	n.a.	21 days	100	100	Connexina 26 CMV infection	yes	Left	25		53	5,5	no	twin pregnancy without complications
CI 7	CD	male	15	not pass bilateral	n.a.	n.a.	n.a.	31 days	100	100	CMV during pregnancy	no	Right	23		151	never used	no	
CI 8	CD	famele	3	not pass bilateral	n.a.	n.a.	n.a.	57 days	100	100	Connexina 26	yes	Bilateral	11	11	23	6	no	
CI 9	CD	male	6	not pass bilateral	n.a.	n.a.	n.a.	60 days	>100	>100	Connexina 26	yes	Bilateral	11	12	54	2,5	no	
CI 10	CD	famele	9	not pass bilateral	n.a.	n.a.	n.a.	30 days	>90	>90	Prematurity and perinatal complications	no	Bilateral	16	31	92	5	no	premature birth (25 weeks) ceasarean delivary. NICU
CI 11	CD	famele	6	not pass bilateral	n.a.	n.a.	n.a.	33 days	> 90	> 90	Connexina 26	no	Bilateral	11	12	54	3	yes	
CI 12	CD	famele	5	not pass bilateral	n.a.	n.a.	n.a.	34 days	100	100	CMV infection	yes	Bilateral	13	13	45	7	no	
CI 13	CD	male	12	not pass bilateral	n.a.	n.a.	n.a.	49 days	> 90	> 90	Unknown (not syndromic, not genetic)	no	Bilateral	22	72	116	4	no	
CI 14	CD	male	11	not pass bilateral	n.a.	n.a.	n.a.	40 days	> 90	> 90	Unknown (not syndromic, not genetic)	no	Bilateral	13	27	115	5	no	
CI 15	CD	male	9	not pass bilateral	n.a.	n.a.	n.a.	40 days	>100	>100	Waanderburg sindrome	yes	Bilateral	14	35	93	1	no	

Participant	Group	Gender	Age (years)	Screening Otoacoustic Emissions	Test indicating some hearing experience before implantation (threshold < 90 dB)			Test indicating profound bilateral deafness diagnosis (threshold ≥ 90 dB)			Cause of deafness	Familiarity	Implant information				Age first hearing aids before IC (months)	Bilinguism	Gestation, type of birth
					Age	Value ABR / autometry left ear	Value ABR / autometry right ear	Age	Value ABR / autometry left ear	Value ABR / autometry right ear			Side	Age first implant (months)	Age second implant (months)	Experience with CI (months)			
CI 16	DD	famele	9	not pass bilateral	24 months	85	90	64 months	Before implantation tested for profound bialteral deafness		Unknown (not syndromic, not genetic)	yes	Bilateral	66	66	45	24	no	birth at 31 weeks; ceasarean delivary. TIN
CI 17	DD	famele	12	not done	5 months	60	60	118 months	Before implantation tested for profound bialteral deafness		Renal tubular acidosis and EVA	yes	Right	120		21	6	no	
CI 18	DD	male	10	pass bilateral	17 months	80	90	106 months	Before implantation tested for profound bialteral deafness		Connexina 26 CMV infection	no	Left	108		16	18	yes	
CI 19	DD	male	12	pass bilateral	65 months	decrease hearing loss 45-100	decrease hearing loss 45-100	120 months	Before implantation tested for profound bialteral deafness		Connexina 26 CMV infection	no	Bilateral	73	122	68	72	no	
CI 20	DD	famele	6	not pass bilateral	screening ABR pass			29 months	>100	>100	2 genetic variants of TBCID24 in compound heterozygosity	yes	Right	35		37	30	no	birth at 41 weeks; vaginal delivary
CI 21	DD	famele	7	left pass	3 years	60	65	52 months	Before implantation tested for profound bialteral deafness		CMV 7 months of pregnancy	no	Left	54		24	38	no	premature birth at 8 months
CI 22	DD	male	6	pass bilateral	n.a.	n.a.	n.a.	28 months	>100	>100	genetic causes: variations in WFS1 ed USH 2A in heterozygosis	no	Bilateral	32	50	39	30	no	
CI 23	DD	male	8	not pass bilateral	3 months	80	80	82 months	Before implantation tested for profound bialteral deafness		perinatal suffering, NICU, diabetes	no	Right	84		12	6	no	perinatal suffering, NICU, diabetes
CI 24	DD	famele	9	not pass bilateral	1°ABR normal, 2° ABR at 29 months pathological			34 months	Before implantation tested for profound bialteral deafness		Unknown	yes	Bilateral	36	36	70	30	no	
CI 25	DD	male	12	not pass bilateral	2 months	75	55	55 months	Before implantation tested for profound bialteral deafness		enlarged vestibular aqueduct	no	Bilateral	57	99	80	6	no	
CI 26	DD	famele	16	pass bilateral	1 years	diagnosis with ABR		15 months	Before implantation tested for profound bialteral deafness		CMV infection	no	Right	17		178	6	no	
CI 27	DD	famele	5	pass bilateral	n.a.	n.a.	n.a.	30 months	>100	90	Connexina 26	yes	Left	42		11	32	no	
CI 28	DD	famele	13	not pass bialteral	Familiy reported some hearing and language development and then deterioration			35 months	>100	>100	Connessina 26	no	Bilateral	36	36	120	34	no	

3.2.2 Stimuli and Experimental procedure

3.2.2.1 Speech Stimuli

The speech stimuli were ~ 3 minutes length stories read by an Italian speaker. We chose different stories according to the children's age in order to provide each participant with speech materials suitable for their age. Three different age ranges - from 3 to 6, from 7 to 10, and from 11 to 15 years old – were defined according to Italian school cycles. For each age group, we selected ten stories from popular Italian books suitable for that age range. Stories were read by a person whose diction has been formally trained and were recorded in a sound attenuated chamber (BOXY, B-Beng s.r.l., Italy) with an iPhone 7 (camera with 12MP, video resolution in HD, 720p with 30fps, at a sampling frequency of 48000 kHz) and an external condenser microphone (YC-LM10 II, Yichuang). All audio recordings were imported in iMovie (version 10.3.1), the noise reduction at 100% was applied, and each file was cut to have 2 seconds of silence before the title of the story and a few seconds of silence at the end of the story. Then, the audio was imported in Audacity® (version 2.4.2, https://www.audacityteam.org/ using ffmpeg and lame functions to isolate the audio from the video). The audio files imported in Audacity were preprocessed with the following steps: they were converted from stereo to mono, amplified (default value in Audacity and avoid clipping were selected), down-sampled to 44100 Hz, and set to a 32-bit sample. Finally, we imported all audio files in Matlab to perform RMS equalization to achieve an equal loudness for all the stimuli (RMS value = 0.0337).

Speech stimuli were presented to participants using Psychopy® software (PsychoPy3, v2020.1.3), and the sound was delivered by a single front-facing loudspeaker (Bose Companion® Series III multimedia speaker system, country, USA) placed in front of the participants behind the computer screen, approximately 70 cm distance from their heads. Stimuli were delivered at ~80 dB, measured at the place of the loudspeaker (Meterk MK09 Sound Level Meter).

3.2.2.2 Task and Experimental Procedure

Participants were asked to listen to the stories carefully while looking at a cross displayed at the center of the screen. At the beginning of each story, a white cross was displayed, and after two seconds of silence, participants listened to the title of the story, and then the story began. A colored cross was presented in the middle of the screen (the color was randomly generated and changed every 1 to 20 sec to maintain children's gaze) throughout the duration of the story. At the end of each story, children were asked to answer two comprehension yes/no questions. For younger children (age range between 3-6 years), questions were performed verbally by the narrator's voice, and the yes/no answers were supported by drawings representing the contents. Comprehension questions mainly aimed to encourage children to pay attention to the story. For older children (>7 years old), questions were presented via text on the screen and were also read by the experimenter. Each participant was presented with four stories, randomly drawn among the ten selected for their age range to obtain more generalizable results (six participants listened to only three stories due to time constraints of the experimental session). Narrated stories were unknown to most of the participants (two children had previously heard one story each).

3.2.2.3 Extraction of Acoustic Envelope

For each subject, the audio file of each listened story was loaded, and the first 6 seconds were discarded, as for the EEG signal. All stories were concatenated in the same order they were presented and segmented into corresponding 1-minute-long trials, resulting in 10 trials of speech envelope per subject (or seven trials for subjects who have listened to only three stories). Then for each trial, we extracted the acoustic envelope taking the absolute value of the Hilbert transform of the original piece of the story and applying a low-pass filter with 8 Hz cut-off (3rd-order Butterworth filter, filtfilt MATLAB function). Then the resulting signal was downsampled to 64 Hz to be matched with the EEG data (e.g., Mirkovic et al., 2015; J. A. O'Sullivan et al., 2015). Finally, envelopes were normalized by dividing by the maximum value to optimize cross-validation for the estimation of the regularization parameter (Crosse et al., 2016; Bednaya et al., 2022).

3.2.2.4 EEG recording and preprocessing

EEG data were collected continuously during the entire experimental session, using a Brain Products system (ActiCHampPlus) with elastic caps (Easy cap Standard 32Ch actiCAP snap) suited for children and having 32 active channels (500 Hz sampling rate). Note that for CI participants, electrodes placed very close to the magneto of the cochlear implants were disconnected (mean: 3.39 ± 1.50; range 1-7). Continuous EEG data acquired during each story presentation were concatenated and offline preprocessed using EEGLAB toolbox (Delorme and Makeig, 2004), implementing a validated preprocessing pipeline (Stropahl et al., 2018; Bottari et al., 2020). Continuous EEG recordings were low-pass filtered (cut-off at 40 Hz, Hanning, order filter 50), downsampled to 250 Hz to reduce the computational time, and high-pass filtered (cut-off at 1 Hz, Hanning filter order 500). The filtered downsampled data were segmented into consecutive 1-second epochs. Noisy segments were removed using joint probability (pop_jointprob function of EEGLAB, threshold across all channels = 3 SD; Delorme et al., 2007). These data were submitted to Independent Component Analysis (ICA, based on the extended Infomax, Bell and Sejnowski, 1995; Jung et al., 2000a, 2000b). The computed ICA weights were applied to the continuous raw data (Stropahl et al., 2018; Bottari et al., 2020). Components associated with stereotypical blinks and eye movements artifacts were identified and removed using CORRMAP, a semiautomatic procedure (Viola et al., 2009). For CI participants, the mean number of removed components was 2.07 ± 0.38, and for HC 2.00 ± 0.00. The cleaned data were low-pass filtered (40 Hz filter order 50), downsampled to 250 Hz, and high-pass filtered (0.1 Hz, with a Hanning filter order 5000). Noisy channels were identified based on the automatic bad channel detection algorithm (clean_channels function of clean_data plugin of EEGLAB; correlation threshold = 0.8 and sample size =1; all the other parameters were kept as default). Noisy channels were then interpolated using spherical spline interpolation (mean interpolated electrodes per subject ± SD, in CI participants: 1.8 ± 1.5, in HC: 2.29 ± 1.45). Disconnected channels nearby the magneto of the cochlear implant were also interpolated. Following

interpolation, data were re-referenced to the average reference. EEG data were then band-pass filtered according to the envelope frequency of interest: between 2 and 8 Hz (Hanning, for 2 Hz cut-off order filter 250, for 8 Hz cut-off order filter 126) as previously performed (Bednaya et al., 2022; Mirkovic et al., 2015; J. A. O'Sullivan et al., 2015). The timing of each epoch was adjusted to +99 ms onset delay measured by the AV device (EGI). Then preprocessed EEG data of each listened story were epoched starting from 6 seconds and keeping 2.5 minutes. The first 6 seconds of each story included 2 s of silence, the reading of the story title, and the very beginning of the story, which was removed to avoid as much as possible the stimulus onset response (Crosse et al., 2021). Finally, epochs were downsampled to 64 Hz, concatenated, and segmented into 1-minute-long trials, resulting in 10 trials per subject (or seven for the children in which we collected only three stories). Trials were created in order to perform a cross-validation procedure in the analysis. To optimize the cross-validation procedure during the estimation of the regularization parameter, data were z-scored (Crosse et al., 2016).

3.2.3 Estimation of TRF

The Forward Model. To investigate how speech envelope is encoded in the brain of CI children, we use a linear forward model known as temporal response function (TRF, incorporated in mTRF toolbox, Crosse et al., 2016). TRF can be seen as a filter that describes the mapping between ongoing stimulus features (here envelope) and the ongoing neural response. This approach allows to predict previously unseen EEG responses from the stimulus feature (i.e., envelope) and has been extensively used to model the neural tracking of continuous speech envelope (Obleser and Kayser, 2019). Mathematically, TRF is described by the following function:

$$r(t,n) = \sum_{\tau} w(\tau,n)s\,(t-\tau) + \varepsilon(t,n),$$

Where t = 0, 1, … T is time, r(t,n) is the neural EEG response from an individual channel n at time t, s is the stimulus feature(s) at each moment (t – τ), τ is the range of time-lags between s and r, w(τ,n) are the calculated regression weights over time-lags, and ε(t,n) is a residual response at each channel n at time t not explained by the TRF model (Crosse et al., 2016). Specifically, TRF at each time-lags (τ) represents how the unit change in the amplitude of the speech envelope would affect the EEG response τ ms later (Lalor et al.,2009).

We fitted separate TRF models at the single subject level to predict response in each of the 32 EEG channels from the speech envelope [2-8 Hz], using time-lags from -100 to 600 ms indicating the relationship between the stimulus and the neural response from 100 ms before to 600 ms later. For example, the TRF at -100 ms time-lag represents how amplitude change of the speech envelope would affect the EEG response at 100 ms earlier, while TRF at 600 ms time-lag represents how amplitude change of the speech envelope would affect the EEG response at 600 ms later (the same is for all the time-lags comprised in the time-lag window). Provided that the TRF model is conducted separately for each channel, their interpolation during preprocessing (in case of bad channels or in case of the vicinity with the cochlear implant) had no effect on the model results. To train the model, a leave-one-out cross-validation procedure was used. All 1-minute trials except one were used to train the model to predict the neural response from the speech envelope, and the left-out trial was used to test the model. This procedure was performed for each trial; the prediction model for every trial was computed and then averaged together to obtain the TRF model for each channel.

Regularization Parameter Estimation. Importantly, the regularization parameter was estimated to avoid overfitting in the regression model obtained by the training data. Overfitting consists of fitting the noise in the data unrelated to the stimulus, thus preventing generalization to different datasets. Regularization is achieved by selecting TRF models' optimal regularization parameter (λ). A set of ridge values (λ = 10^−6, 10^−5,…, 1, 10, …, 10^11, 10^12) is used to compute the model for time-lags from -100 to 600 ms through leave-one-out cross-validation procedure. To determine the optimal regularisation parameter (λ) for each participant, we used the mean squared error (MSE) value – averaged across trials and electrodes – between the actual and the

predicted EEG responses; the λ value reaching the lowest MSE value was selected. The identified λ value was 10^3 for most participants, and in order to generalize results, we decided to keep λ constant across all channels and participants.

Chance-level Estimation. To assess the ability of TRF models to predict neural responses and verify that neural tracking was above chance in all groups, we computed a null TRF model for each participant (Combrisson & Jerbi, 2015). We permuted the 1-minute pairs of trials to obtain mismatched envelope and EEG response pairs, and then, TRF models were fitted on these randomly mismatched trials of speech envelopes-EEG responses (mTRFpermute function with 1000 iterations; Crosse et al., 2016, 2021). Then, all these null TRF models computed across the iterations were averaged to obtain a null TRF model used as a control. This procedure was done separately for each participant.

3.2.4 Statistical Analysis

We computed the accuracy percentage for each participant at the behavioral level (on the number of correct yes/no answers) to assess whether there was a difference across the three groups (HC, CD, DD) through univariate ANOVA with *group* as a between-subject factor.

To test whether we could extract an auditory temporal response function (TRF model) within each group, we first selected a cluster of four central channels (Cz, Fz, FC1, FC2; note that none of these channels were disconnected in CI children) typically capturing at the scalp level auditory responses with evoked potentials (for review see Steinschneider et al., 2001) and auditory response functions (e.g., Jessen et al., 2019; Paul et al., 2020). Then, we performed comparisons between the TRF model and the null TRF by running paired t-tests within time-lags [0 - 600 ms] (i.e., every 15 ms) separately for HC, CD, and DD (two-tailed, q=0.05, FRD correction, Benjamini and Yekutieli, 2001).

To test differences in the spatiotemporal profile of averaged TRFs between groups, we performed cluster-based permutation tests (Maris and Oostenveld, 2007) in FieldTrip toolbox (Oostenveld et al., 2011). A cluster was defined along electrodes x time-lags dimensions, the minimum number of neighboring electrodes was set at 2, and cluster-level statistic was the sum of the t-values within each cluster, with an

alpha level of 0.025 (two-tailed test). Cluster-based permutation tests were performed at the whole brain level (across all electrodes) and time-lags from 0 to 600 ms, using the Monte-Carlo method with 1000 permutations. Identified clusters were considered significant with p-value lower than 0.025 (accounting for both positive and negative clusters). First, we performed a cluster-based permutation test with F-statistics including all three groups. In case of a significant effect, we performed the same cluster-based permutation test using independent-samples t-statistics between pairs of groups (HC vs. CD, HC vs. DD, and CD vs. DD) to highlight the group differences ($p < (0.025/3)$, Bonferroni correction).

In order to test whether CI children's TRF profile is affected by earlier implantation (here after, *age first implant*), we performed a linear regression model with age at first implant as independent variable to characterize individual TRFs. In addition to *age first implant*, we added *age*, and *age hearing aids* as independent variables. Chronological age (*age*) was inserted in the model, given the broad age range of our sample. The age at which hearing aids were provided to the children (*age hearing aids*) was inserted to test whether precocious hearing aids use affects the brain response (TRF).

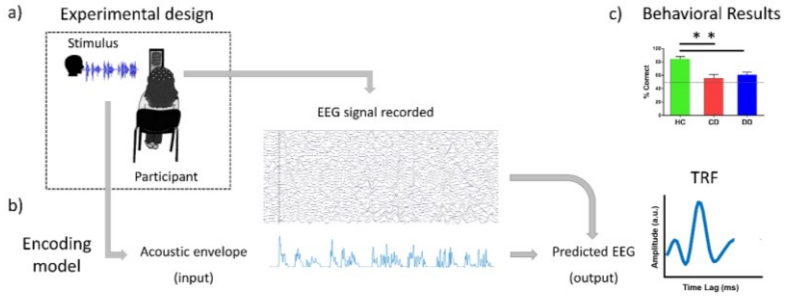

Figure 3.1. Schematic illustration of the experimental design and analysis method. a) Experimental design shows the participant listening the story (speech stimulus). b) The schema shows the performed encoding model. The speech envelope of the stimulus is extracted and with the corresponding EEG signal is used to compute the model to predict the EEG, TRF is the estimated model. c) The bar plot shows % of correct

response to the comprehension question in each group (HC, CD, DD), mean ± SE are plotted, the dashed line represents chance level.

3.3 Results

3.3.1 Behavioral data

The ANOVA performed on the mean behavioral accuracy with *group* (HC, CD, DD) as a between-subject factor revealed a significant group effect ($F(2,42)=12.08$, $p<0.001$). Post-hoc tests (Bonferroni correction) revealed a significant difference between HC and both CI groups (HC vs. CD $p<0.001$; HC vs. DD $p=0.002$); no significant difference emerged between the two CI groups. Even if our behavioral measure was simple due to the investigated population of children, results suggest that the comprehension of the content story is significantly more complex for CI children (both CD and DD) than for HC children. However, if tested against 50% (chance level), the DD group, as well as the HC group, showed a performance significantly higher than the change level, while CD did not (HC: $p<0.001$; DD: $p=0.018$; CD: $p=0.37$).

3.3.2 Neural tracking

First, within each group, we contrasted the TRF with null TRF at a central cluster of electrodes which typically capture auditory response functions (Cz, Fz, FC1, FC2). We observed clearly defined auditory response functions in all groups of children using the envelope regressor. Significant differences between the TRF and the null TRF emerged in each group. In HC children, the auditory response function was characterized by a prominent frontocentral positivity (0–125ms) peaking at ~60ms and a second central negativity (200-300ms) peaking at ~250ms (see Figure 3.2a). In contrast, in both CD and DD groups, the auditory response function comprised only the first frontocentral positivity (30-200ms) peaking at ~120ms (see Figure 3.2b,c).

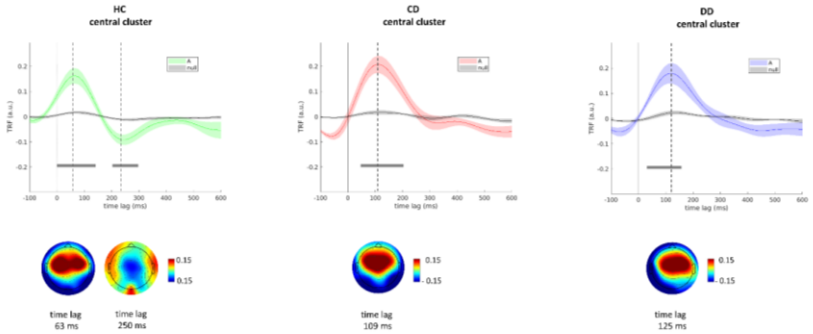

Figure 3.2. Central cluster TRF within each group of children. Grand average TRFs (green HC, red CD, and blue DD) and grand average null TRFs (black). Here plotted averaged TRFs in a central cluster of electrodes (Cz, Fz, FC1, FC2) at -100 and 600 time-lags. Shaded areas represent SE across participants for both TRFs and null TRFs. Grey horizontal bars indicate time-lags (between 0 and 600 ms) at which TRFs differed significantly from the null TRF ($p < 0.05$, FDR-corrected). Grey dashed vertical lines indicate the peaks of significant positive and negative deflection of auditory response functions, and the corresponding topography is displayed below.

Having assessed the existence of an auditory response function in each group, we investigated whether the neural tracking of the speech envelope differed as a function of the onset of hearing input, thus across the three groups. To this end, we compared the auditory response functions performing a cluster-based permutation test via F-statistics without any a priori assumption (across all channels and all time-lags between 0-600 ms) across the three groups. This test revealed a significant effect ($p<0.001$). To understand which group differences guided the effect, we performed three cluster-based permutation tests via independent samples t-statistics between group pairs. A significant difference emerged between HC and CD groups; a positive cluster emerged between 125 and 265 ms ($p<0.001$). Similarly, the comparison between HC and DD groups revealed a significant positive cluster ($p<0.001$) at the same time-lags window [125 - 265 ms]. In contrast, the

cluster-based permutation test between the two CI groups (CD vs. DD) did not reveal any significant difference (0 positive and 0 negative clusters were found). These results revealed that neural tracking of speech envelope is delayed in both CI groups (i.e., CD and DD) compared to HC children. Strikingly, the absence of a difference between CD and DD indicates that neural tracking is not affected by the lack of hearing input in the first months of life.

3.3.3 Clinical characteristics and neural tracking in CI participants

Previous studies revealed that implantation age affects the development of the auditory evoked potentials and, in particular, the P1 wave latency (Sharma et al., 2002a). Thus, we assessed whether the age at implantation could explain the delay of the auditory response function in CI participants. To have a more stable estimation of the latency of the peak of the first positive auditory response, we computed the global field power (GFP; Lehmann and Skrandies, 1980), and we extracted for each participant the peak latency of the frontocentral positivity. We performed a linear regression model with *age first implant*, *age*, and *age hearing aids* as independent variables and the latency of the first peak of the auditory response function (*P1 TRF latency*) as the dependent variable. Results showed a significant effect of *age first implant* (β=0.688, SE=0.228, p=0.006), and a significant effect of *age* (β= -0.491, SE=0.120, p=0.021). No significant effect of the *age hearing aids* was found (p=0.912). These data highlighted that the earlier children were implanted, the less delayed the first peak of the auditory response function. The effect of age suggested that the latency of the auditory response decreased with the development. In CI children, we were particularly interested in testing whether there was an impact of the use of the implant. Thus, we computed the variable experience with implant = age – (age first implant + 1 month, to account for implant activation time). Then we performed a second linear regression with *experience with implant* as the independent variable and *P1 TRF latency* as the dependent variable. The model showed that *experience with implant* significantly explained the delayed latency of the first positive peak of the auditory response function (β= -0.529, SE=0.159, p=0.003). Note that in a linear regression model with *age* as a unique independent variable, the effect of age was nonsignificant (p=0.24), suggesting that the impact of age emerged in the first model

was not representing the chronological age, but mainly the increased experience with the implant during the development.

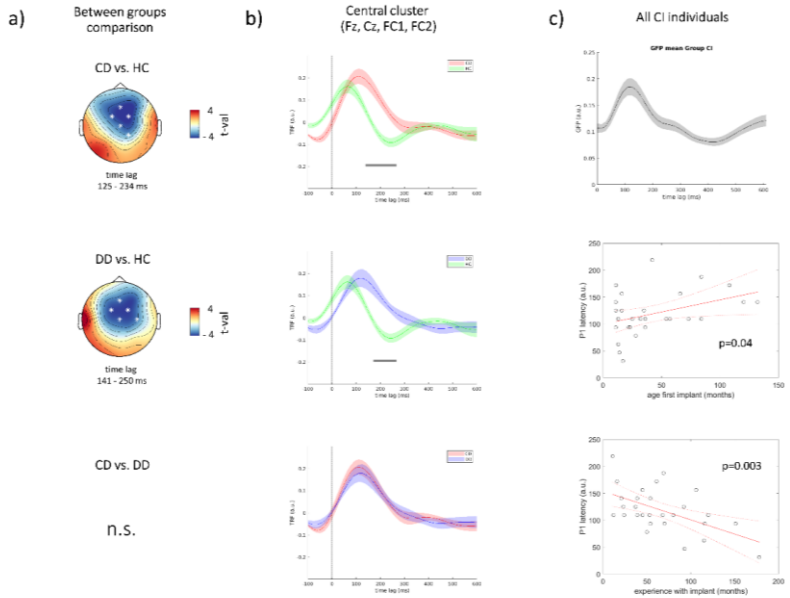

Figure 3.3. Delayed auditory response function in CI children. a) Topographies depict statistical differences emerged in each cluster-based permutation test performed between group pairs. Significant electrodes are highlighted with asterisks. b) Auditory response function (TRF) at the central electrodes in each group across -100 600 time-lags; in each TRF continuous line represents the group mean, the shaded area the SE across participants. Grey horizontal bars highlight significant differences between groups. c) Top. Global field power (GFP) of the auditory response function across all CI children (both CD and DD) over time-lags [0-600 ms]. Regression models testing the impact of early implantation on P1 TRF latency (middle) and the impact of implant experience on P1 TRF latency (bottom) for all CI children.

3.4 Discussion

In this study, we aimed to investigate (1) whether CI allows the developing of hearing-like neural response to speech envelope and (2) to assess whether the first months after birth comprise a sensitive period for the development of the speech envelope neural tracking. To these aims, we assessed how speech envelope is encoded in the brain using a linear forward model (TRF) in two groups of CI children, congenital (CD) and delayed deaf (DD), and in a control group of hearing children (HC). In all groups of children (i.e., HC, CD, and DD), we found a clearly defined auditory response function. The between groups comparison revealed significantly delayed auditory response function in both CD and DD groups compared to HC. No significant difference emerged in the auditory response function of the two groups of CI children (CD vs. DD). However, linear regressions performed over all CI children (both CD and DD) revealed that the latency of the auditory response function was affected by the age at which partial hearing was restored with cochlear implants and by the time of children's experience with cochlear implants. The earlier the child received the cochlear implant and the longer their experience with the implant, the less delayed the neural tracking.

3.4.1 Neural tracking of speech envelope in CI children

In both congenital deaf (CD) and delayed deaf (DD) children, we measured a clear auditory response function, indicating that neural tracking to speech envelope develops in CI children. This is coherent with evidence showing that early cochlear-implanted children perceive and understand speech (Osberger et al., 2002; Kral and O'Donoghue, 2010). However, two main differences with hearing children emerged: for both CD and DD children, the auditory response function was characterized by a delayed first response (frontocentral positivity peaking at ~120 ms, while in HC at ~60 ms) and the absence of the subsequent phase (central negativity peaking in HC at ~250 ms).

Delayed neural tracking in CI children is coherent with traditional auditory evoked potential data, showing delayed P1 wave in CI children as a measure of immature acoustic neural response (Eggermont and Ponton, 2003; Sharma et al., 2005). A recent study assessing neural

tracking to continuous speech in individuals with hearing deficits showed that the severity of hearing impairment is positively associated with neural tracking delay (Gills et al., 2021). Moreover, hearing control showed delayed neural tracking when presented with a speech stimulus in a noisier background. Coherently, difficult acoustic listening conditions, such as when speech was presented in noise, induced delayed auditory evoked response to simple speech stimuli, measured with traditional ERPs, in hearing listeners, both in adults and children (Billings et al., 2011; Gustafson et al., 2019). Delayed entrainment to speech envelope was also reported for compressed speech in poor readers (Abrams et al., 2009). These findings suggest that delayed neural tracking in CI could be indicative of poor acoustic system efficiency. Both a deficit of functional development caused by auditory deprivation and impaired processing due to the degraded input could explain current results. Of note, using backward modeling, it was shown that while speech envelope reconstruction is possible in CI but is less accurate than in hearing individuals, decoding accuracy also decreases for hearing participants when speech is presented using a vocoder to simulate speech perception in CI participants (Nogueira et al., 2020).

The central negativity, which did not emerge in CD and DD groups, in HC emerged at about 200 ms and, thus, is linked to higher stages of speech processing. Interestingly, a central negativity at ~ 250ms was demonstrated to be modulated by attentional processing in CI late deaf adults during dichotic listening (Paul et al., 2020). Smaller N1 was found for the attended stream than for the unattended one. In CD and DD children, the absence of the central negativity could represent attentional deficits to the auditory stimulus. One possibility is that a degraded acoustic signal is more complicated to process. In support of this hypothesis, a recent paper using noise-vocoder speech demonstrated that the second response peaking at about 200 ms was strongly reduced when the speech was degraded (Chen et al., 2022). Alternatively, the ability to categorize speech information in meaningful units could be impaired due to anomalous auditory experience throughout the language development period. This would prevent the possibility of relying on high-level representations that help predict and interpret sensory input. Studies on animal models with congenital deafness have revealed that the absence of acoustic stimulation during development

would induce a disconnection between low and high auditory areas (Kral et al., 2017).

3.4.2 Is there a sensitive period for the neural tracking of the speech envelope?

No difference emerged between neural tracking in CD and DD groups. These two groups of CI children are very homogenous, except for their deafness onset. CD children were born deaf and received the first acoustic information only after cochlear implantation, while DD children have at least some auditory experiences since birth. Contrasting these two groups of children provided the rare opportunity to test whether acoustic stimulation at a very early stage of development is necessary to develop neural tracking of speech envelope in CI children. The substantial overlapping between the auditory response functions in CD and DD groups (see Figure 3.3b) convincingly revealed that this is not the case. Interestingly, a recent fNIRS study (Mushtaq et al., 2020) showed that 8 years old congenitally or early-onset deaf CI children who were implanted on average at two years of age did not differ from hearing control children in the neural response to speech, neither to amplitude modulation (i.e., envelope), suggesting that early acoustic stimulation might not be needed for neural response to speech envelope.

The first period after birth is known to be crucial for the development of basic acoustic functions (see Sanes and Wolley, 2011). However, speech processing requires multiple complex functions, and a series of sequential sensitive periods extend along the development (Ruben, 1997; Werker and Hensch 2015). Thus, it is possible that if a sensitive period for envelope speech tracking exists, it could be more protracted than the first months of life. On the one hand, behavioral data showed that individuals who were born deaf and received cochlear implants before six years of age understand speech, highlighting the high plasticity of the auditory system within six years of life (Manrique et al., 1999). On the other hand, the fact that in our data, a different neural tracking emerged between CI and HC could endorse the existence of a protracted sensitive period. Only testing an additional group of CI children with late deafness onset (e.g., > 6 years of age) would answer this question.

Finally, it is interesting to note that DD children performed better than the chance level in the comprehension questions, while CD children's performance did not differ from chance. Even if, due to the age of children, we could not estimate precise behavioral measures of speech content understanding, from our simple comprehension measure, we can hypothesize that difference between congenital and delayed deafness would emerge by assessing neural tracking to other linguistic features (e.g., Di Liberto et al., 2015). For instance, the ability to discriminate phonetic features represents a fundamental milestone in language development that, in typical development, occurs within the first 12 months (Kuhl, 2004). Thus, we can hypothesize that neural tracking of phonetic features would be differently affected in CD and DD children. A result in this direction would be indicative that the first months are critical for the development of the neural tracking of phonetic features. Further investigation using an extensive number of different predictors would help to clarify whether the first months after birth comprised a sensitive period for the neural tracking of any speech features or not.

3.4.3 Early implantation and experience with implant enhance neural tracking efficiency

Since no difference emerged between the two groups of CI children (i.e., CD and DD) we assessed whether relevant clinical characteristics could explain the delayed auditory response function. This is particularly important to rule out the possibility that delayed brain response is only due to CI transmission. First of all, we expected that the latency of the frontocentral positivity could be modulated by the age at which the auditory input is restored. Linear regression showed that children who received earlier cochlear implants had less delayed auditory response functions. Coherently with traditional data collected with short-lived speech sounds (e.g., "ba"; Sharma et al., 2002a; 2002b; 2005; 2015), our results highlight the benefit of early implantation and extend it to the development of neural tracking of continuous speech. Conversely, we did not find evidence that the age of hearing aids use improved the neural tracking latency. Similarly, Niparko and colleagues (2010) found evidence of the importance of the earliest implantation, instead of

prolonged hearing aids use, on behavioral measures of speech comprehension.

To understand neural tracking to speech envelope in children with CI, a crucial aspect, despite the effective chronological age, is how long children have had experience processing acoustic information after implantation. Our data show that experience with implants had a significant impact on the latency and, thus, on the development of neural tracking efficiency. The more experience the child has with the implant, the less delayed their brain response to speech envelope. This result is coherent with data showing significant improvement with long-term cochlear implant use (Beadle et al., 2005; Uziel et al., 2007; Geers et al., 2008). More experience with implants allows children to tune the development of auditory functions needed to process speech material and to deal with degraded acoustic information provided by the implant.

Taken together, these results support the hypothesis that the delayed neural tracking observed in CI is mainly due to less efficient speech processing associated with a developmental issue of the auditory system and highlight the pivotal role of auditory experience for typical neural tracking development.

3.4.4 Limitations and future directions

EEG data of CI children are not free from CI artifacts. We are aware that Somers and colleagues developed a method (2019) allowing analysis on EEG free-artifact time windows. To this aim, temporal gaps, short enough (4 ms) to not affect the speech understanding, are periodically inserted (every 25 ms) in the stimulation to avoid the electrical activities of the implant. However, this method consists of providing participants with degraded speech information and requires the extension of the experimental session since the collected data are decimated in the analysis to keep only the free-artifact EEG traces. Our task required consecutive minutes of attention to speech and was already demanding for children, especially younger ones. Thus, we reasoned that providing them with a degraded speech signal would represent an additional effort to accomplish the task. Importantly, the artifact decay within 2 ms after the stimulus (Deprez et al. 2017); therefore, we would expect contamination artifact only in the time-lags around zero. Moreover, the

fact that our main result, delayed TRF in CI, was found to be modulated by clinical CI children's characteristics (early implantation and experience with implant) rules out the possibility that delayed neural tracking is simply caused by CI artifact.

A final limitation of this study is that we tested only speech stimuli, and thus, we cannot disentangle whether our results are specific to the speech envelope or would characterize neural tracking of any continuous envelope. Speech represents a special stimulus for its extreme relevance in human development and is crucial from a clinical perspective. Further studies are needed to clarify whether the delayed neural tracking is specific to speech or is due to a general impairment of auditory processing in CI children.

3.5 Conclusion

We showed that neural tracking of speech envelope is clearly measurable in CI children. Compared with hearing control children, auditory response function in CI children, both CD and DD, is delayed. The absence of difference between CD and DD indicates that neural tracking of speech envelope is possible even in the absence of auditory input in the first months of auditory system development after birth. Importantly, the latency of the auditory response is affected by the age at which partial hearing was restored with cochlear implants and by the experience children had with implants. The earlier children have been exposed to acoustic experience thanks to the implant, and the longer their experience with processing auditory stimuli with the CI, the more efficient (less delayed) their speech envelope neural tracking.
In conclusion, our data indicate that if congenital deafness is treated early, a period of absence of acoustic experience after birth does not prevent the development of speech envelope neural tracking as in their delayed deaf pairs. Moreover, and extremely promising from a clinical point of view, these findings show that early implantation and long-term use of the implant are beneficial for speech processing in ecological situations.

Chapter 4

Altered Neural Oscillations Underlying Visuospatial Processing in Cerebral Visual Impairment (CVI)

4.1 Introduction

The childhood condition characterized by visual impairment due to damage or maldevelopment of retrochiasmatic visual processing pathways represents a brain-based visual disorder known as Cerebral Visual Impairment (CVI; Sakki, et al., 2018, Dutton and Lueck 2015). Due to improved neonatal care and overall awareness, CVI prevalence has steadily risen, and nowadays, it is the leading cause of pediatric visual impairment in developed countries (Good et al., 2001; Philip and Dutton, 2014). Despite presenting as a significant public health concern, the neurophysiological basis of CVI remains poorly understood. Early neurological damage to visual pathways and higher-order processing areas of the brain can be very heterogeneous and, thus, leads to heterogeneous clinical presentations of visual dysfunctions in CVI (Boot, et al., 2010; Fazzi et al., 2007; Lam, et al., 2010; McKillop and Dutton, 2008). Visual acuity, visual field function, contrast sensitivity, and oculomotor function can all be impaired to varying degrees. Noteworthy, deficits associated with higher-order visuospatial and attentional processes have been identified, even in cases where visual acuity and visual field functions are at normal or near-normal levels (Boot et al., 2010; Dutton, 2013; Philip and Dutton, 2014; Weinstein et al., 2012). Individuals with CVI often report difficulties interacting with complex and cluttered visual scenes (Dutton, et al., 2004; Jacobson et al., 1996; Lam, et al., 2010; McDowell and Dutton, 2019). For example, an individual with CVI may have difficulties finding a favorite toy placed in a toybox or recognizing a familiar person in a crowd, despite being able to identify them easily when presented in isolation (Jacobson et al., 1996; Lam et al., 2010; McKillop and Dutton, 2008). A deeper understanding of these high-order visual processing impairments in CVI individuals remains crucial to better understand the neurophysiological basis of the condition, avoid the risk of misdiagnosis (particularly in the

setting of normal visual acuity and visual field function), and fine-tune potential adaptive strategies to improve individual's autonomy and well-being.

In clinical practice, visual-evoked potentials (VEPs), typically measured by averaging neural activity in response to the passive viewing of simple visual stimuli, have been used to assess the integrity of afferent visual pathways and functions (such as visual acuity) in CVI, particularly in the case of infants and/or nonverbal patients who may not be able to undergo formal ophthalmic testing (Good, et al., 2001; Skoczenski and Norcia, 1999; Watson et al., 2010; see Chang and Borchert, 2020 for review). However, clinical VEPs remain limited with respect to characterizing processing within visual areas beyond primary visual cortex (V1) and the underlying neurophysiological basis of higher-order visual processing deficits in CVI. That is, in the presence of typical VEP responses, it is not possible to rule out the presence of higher-order processing deficits. In this regard, the analysis of neural oscillatory activity may be more informative as to how information is encoded, transferred, and integrated within the brain (Buzsaki and Draguhn, 2004; Siegel et al., 2012). Specifically, analyzing neural oscillations allow investigation of both sensory-driven (i.e., evoked) neural activity as well as the process of integration of sensory inputs with ongoing neural activity. The latter is the induced component of neural oscillations, which is not time- or phase-locked to stimulus onset (Galambos, 1992; Keil et al., 2022; Klimesch et al., 1998). Distinct components of neural oscillations were associated with different types of processing according to the direction of information flow, that is, feedforward and feedback (Chen et al., 2012; Tallon-Baudry and Bertrand, 1999). Anomalies in evoked activity are more likely to reveal impairments of feedforward information flow of the thalamocortical pathway, while abnormal induced activity tends to be indicative of deficits in feedback cortico-cortical connectivity. Several neurodevelopmental conditions have been consistently associated with abnormal oscillatory activity (Edgar et al., 2015; Gandal et al., 2010; Goswami, 2011, 2014; Heim et al., 2011; Murphy and Benítez-Burraco, 2017). Therefore, neural oscillations have the potential to represent a valid tool to characterize neural profiles also in CVI. In particular, to assess whether visuospatial deficits in this population are mainly driven by aberrant early stage (i.e., feedforward)

sensory input or are the result of impaired higher-order (i.e., feedback) visual processing mechanisms. In turn, this could be useful for identifying potential biomarkers of CVI and designing specific visuospatial training strategies.

In a preliminary study, we found that in CVI, the analysis of EEG activity during visual search was associated with a dramatic reduction in alpha desynchronization following the onset of a visual scene (Bennett et al., 2021). Given that alpha desynchronization is an important neural signal associated with visuospatial attention and distractor suppression (Peylo, et al., 2021), these findings provided early evidence of altered neural processing in relation to higher-order visual perceptual deficits observed in this population. In this study, we aimed to extend this finding by further investigating the neurophysiological basis of higher-level visual alterations occurring in CVI. We combined eye-tracking and EEG to measure behavioral performance and neural oscillations during a virtual-reality-based visual search task in which we manipulated the levels of task difficulty related to visual complexity. By investigating a broad frequency range [4-55 Hz] of neural oscillations, as well as their evoked and induced related activity associated with overt visual search performance, we are in the position to better characterize which aspects of high-level visuospatial computations are affected in CVI participants compared to age-matched controls with neurotypical development.

4.2 Methods

4.2.1 Participants

A total of 26 individuals were recruited in this study. Ten participants were previously diagnosed with CVI (3 females, mean age: 17.5 years old ± 2.59 SD) by experienced clinicians specializing in neuro-ophthalmic pediatric care. Diagnosis was based on a directed and objective assessment of visual functions, including visual acuity, contrast, visual field perimetry, color, and ocular motor functions. A thorough refractive and ocular examinations were carried out, as well as an extensive and integrated review of medical history (including developmental, birth, and gestational), neuroimaging, and electrophysiology records (Chandna et al., 2021; Fazzi et al., 2007; Jacobson et al., 2004). Input regarding visual behaviors was collected

using standardized questionnaires and inventories (McCulloch et al., 2007; Ortibus et al., 2011). All participants with CVI had visual impairments related to pre- or perinatal neurological injury and/or neurodevelopmental disorders. Causes of CVI included hypoxic-ischemic injury related to prematurity (including periventricular leukomalacia; PVL), hypoxic/ischemic encephalopathy (HIE), seizure disorder, as well as genetic and metabolic disorders. Four out of the 10 CVI participants were born preterm (i.e., prior to 37 weeks gestation). Associated neurodevelopmental comorbidities included spastic and dystonic cerebral palsy. Best corrected visual acuities in the better seeing eye ranged from 20/20 to 20/60 Snellen (0.0 to 0.5 logMAR equivalent). CVI participants were also categorized according to previous functional criteria (Dutton, 2015). The distribution of our study population was limited to categories 2 and 3 (definition of category 2: 40% defined as "have functionally useful vision and cognitive challenges" and category 3: 60% defined as "functionally useful vision and who can work at or near expected academic level for their age group"). For a full list of CVI participant details, see Table 1. All CVI participants had a level of visual acuity, intact visual field function within the area corresponding to the visual stimulus presentation, as well as fixation and binocular ocular motor function sufficient for the purposes of completing the behavioral task requirements (including eye tracking calibration; see Supplementary materials Chapter 4 for further details). Exclusion criteria included any evidence of oculomotor apraxia, intraocular pathology (other than mild optic atrophy), uncorrected strabismus, visual field deficit corresponding to the area of testing, uncontrolled seizure activity, as well as cognitive deficits precluding the participant from understanding the requirements of the study.

Structural MRIs from CVI participants were assessed for brain lesion severity according to a reliable and validated semi-quantitative scale. The scoring procedure has been described in detail elsewhere (Fiori, 2014). Briefly, raw scores for each brain structure (e.g., lobe, subcortical structures, corpus callosum, and cerebellum) were calculated and summed to provide a global (total of cortical and subcortical) lesion score, whereby a higher score is indicative of a greater degree of brain injury (see Figure S4.1 Supplementary materials Chapter 4).

Sixteen individuals with neurotypical development (5 female, mean age: 19.2 years old ± 2.14 SD) were recruited as comparative controls. Control participants had normal or corrected to normal visual acuity and no previous history of any ophthalmic (e.g., strabismus, amblyopia) or neurodevelopmental (e.g., epilepsy, attention deficit disorder) conditions. The control and CVI groups were not statistically different with respect to mean age [$t(24) = 1.806$, $p = 0.084$].

Formal written consent was obtained from all the participants and a parent/legal guardian (in the case of a minor). The study was approved by the investigative review board of the Massachusetts Eye and Ear, Boston MA, USA, and carried out in accordance with the Code of Ethics of the World Medical Association (Declaration of Helsinki) for experiments involving humans.

Table 4.1 - CVI Participant Demographics

Subject ID	Sex	Age	Associated Cause of CVI	Preterm/Term Birth	CVI Classification	Distance Visual Acuity OD - OS (Snellen)	Distance Visual Acuity OD - OS (LogMAR equivalent)	Global (Total) Lesion Score (n/48)
1	female	15	birth complication, global developmental delay	term	2	20/30 - 20/30	0.2 - 0.2	
2	female	17	meningitis, infarct	term	3	20/50 - 20/60	0.4 - 0.5	8,5
3	male	19	decreased placental perfusion	preterm	2	20/25 - 20/25	0.1 - 0.1	2,5
4	female	21	periventricular leukomalacia	preterm	2	20/50 - 20/40	0.4 - 0.3	21
5	male	19	focal cortical atrophy, seizure disorder	term	3	20/60 - 20/60	0.5 - 0.5	16
6	male	15	genetic	term	3	20/20 - 20/20	0.0 - 0.0	4
7	male	16	infection	term	2	20/25 - 20/25	0.1 - 0.1	11,5
8	male	22	periventricular leukomalacia	preterm	3	20/40 - 20/25	0.3 - 0.1	26
9	male	16	unspecified, developmental delay	term	3	20/20 – 20-20	0.0 - 0.0	2
10	male	14	periventricular leukomalacia	preterm	3	20/25 – 20/25	0.1 - 0.1	16,5

4.2.2 Visual search task

The behavioral task was a static object visual search based on a previously designed desktop VR-based naturalistic environment called the "virtual toybox" (complete details regarding the design of the task can be found in (Bennett et al., 2018). Briefly, the task represents a simulated rendering of a toy box viewed from overhead, first-person perspective (Figure 4.1 Participants were instructed to search, locate, and fixate a specific target toy (a blue truck) placed randomly among surrounding toys (and without overlap) serving as distractors in a 5 x 5 array. The target toy remained constant and was unique with respect to shape and color in order to create a “pop out” effect when presented with the other distractor toys (akin to feature search). The arrays of toys were presented in a trial-by-trial fashion and in pseudorandom order.

Two levels of task complexity ("Low" and "High") were used. In the Low task condition, the target toy was surrounded by one unique distractor toy presented on a uniform background. In the High task condition, the target was placed alongside 9 unique distractor toys and superimposed upon a cluttered background scene designed to make target recognition more difficult (see Figure 4.1). At a viewing distance of 60 cm, the virtual toybox subtended approximately 38 x 38 deg of visual. An equal number of Low and High task conditions were presented. A trial consisted of viewing the toybox scene for 2 sec followed by 1 sec of a blank gray screen with a central fixation target. This was repeated 50 times per run, and 4 runs were collected (a total of 200 trials). Each run lasted less than 2.5 min, with a brief rest period between each run.

The visual environment was developed using the Unity 3D game engine version 5.6 (Unity Technologies) and on an Alienware Aurora R6 desktop computer (Intel i5 processor, NVidia GTX 1060 graphics card, and 32 GB of RAM; Alienware Corporation). In house 3D object models were created in house using Blender modeling software (Blender Foundation). The visual search task was run using Presentation software (https://www.neurobs.com) to control simultaneous EEG event markers and signal recording (see below).

Participants were seated comfortably in a quiet room and 60 cm in front of a 27" LED monitor (ViewSonic 27" Widescreen 1080p; 1920 x 1080 resolution). Visual search patterns (X,Y coordinate positions of gaze on the screen) were captured under binocular viewing conditions using a Tobii 4C Eye Tracker system (Tobii Technology AB, Stockholm, Sweden; see Supplementary materials Chapter 4). While participant performed the task EEG activity was recorded via a wireless 20-channel Enobio system (Neuroelectrics, Barcelona, Spain).

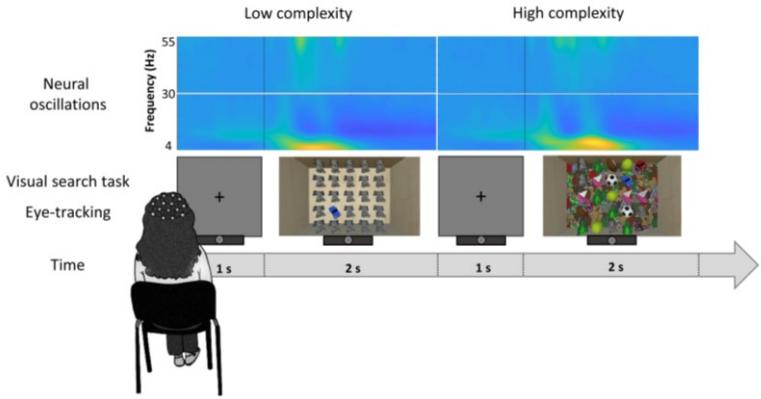

Figure 4.1. Experimental design. The figure shows an example of a participant that is performing the task. Two trials are shown, one for each condition (Low complexity on the left and High complexity on the right). While participant is performing the visual search task, their eye-gaze pattern and neural activity are recorded (putative neural oscillations are shown in the top row).

4.2.3 Eye-gaze pattern in a visual search task

To successfully search for a target in a complex visual scene, people look for it by moving their eye across the visual stimuli, and when they find it, the target is fixated (see figure S4.2 Supplementary materials Chapter 4 for an example of the heatmaps of the eye-gaze pattern). Thus, visual search performance was quantified using three objective outcomes based on eye-tracking data captured while participants initially viewed, searched, located, and then fixated the target. We computed the success rate, the reaction time, and the gaze error. (1) Success rate (expressed as a percentage) is a measure of accuracy indicating whether a participant could find and fixate the target on a given trial. Successful fixation was defined as a sustained gaze that remained within the outer contour of the target for a minimum time of 0.4 sec. (2) Reaction time indicates how much time participants need to find the target on the screen. It was defined as the first moment the participant's gaze arrived within the outer contour of the target and remained fixated for at least 0.4 sec. (3)

Gaze error was a continuous measure of participants' precision in locating and accurately fixating the target (Bennett et al., 2018, 2021). This precision measure is defined as the distance between the center of the target and the participant's gaze position, and it was computed based on the sampling rate of the eye-tracker (90 Hz). As a supplemental outcome, we also determined how often/long participants were looking at and away from the screen on a given trial based on the continuous recording of the position of the gaze. For this purpose, the off-screen metric represents the number of gaze points per trial that fell outside the screen bounds and thus serves as an index measure of test compliance and reliability (Bennett et al., 2021; see Supplementary materials Chapter 4).

Statistical analyses were carried out using a mixed-model repeated measure ANOVA (group as a between factor and condition as a within factor) conducted separately for each of the behavioral measures. Statistical analyses were performed using IBM SPSS, Statistics Software Package v26, SAS Studio, and MATLAB Statistics Toolbox.

4.2.4 Neurophysiological data acquisition, Signal Processing, and Analysis

Electrophysiological data were collected in a clinical setting. Therefore, to facilitate the data acquisition in a clinical population, a simple and practical EEG was used: a wireless 20-channel Enobio system (Neuroelectrics, Barcelona, Spain). This system with only 20 electrodes allows a very fast montage and minimizes patients' discomfort. Note that the electrodes were arranged according to the standard 10-20 international system and, thus, covered the entire cap. An additional reference channel was connected using an ear clip and placed on the participant's right ear lobe. EEG was acquired online while participants performed the task, with a sampling rate of 500 Hz.

EEG signal preprocessing was performed by implementing a validated pipeline to clean the data, promoting reproducibility (Bottari et al., 2020; Stropahl et al., 2018). Offline, each participant's continuous dataset was low-pass filtered (cut-off at 40 Hz, Hanning filter, order 50) and high-pass filtered (cut-off at 1 Hz, Hanning filter, order 500; see (Winkler et al., 2015), downsampled to 250 Hz, segmented into consecutive 1-second

epochs, and cleaned by using joint probability algorithm (epochs displaying an activity with a joint probability across all channels exceeding the 3 SD threshold were removed; (Delorme et al., 2007). Then, Independent Component Analysis (ICA) based on the extended Infomax (Bell and Sejnowski, 1995; Jung et al., 2000a; Jung et al., 2000b) was then performed, and the resulting weights were applied to the raw continuous unfiltered data (Bottari et al., 2020; Stropahl et al., 2018). Components associated with stereotypical blinks were identified and removed using a semiautomatic procedure (CORRMAP (Viola et al., 2009). The template for the blink components was chosen within the control group to ensure the selection of a typical artifact, and the template was used to find blink components across all participants, both in control and CVI individuals (mean of components removed for each individual in the CVI group=0.9 ± 0.0.32 SD, and in the control group=0.94 ± 0.25 SD; see in Supplementary materials Chapter 4 Figure S4.3 the topography of each component which was removed in each participant). All EEG activities associated with eye movements was retained because of the overt task. Indeed, eye movements, being required by our ecological approach, are intrinsically related to meaningful visual activities that represent what we want to investigate in this study. Thus, we retained all eye movements components to avoid the risk of removing associated brain activity. Datasets were then low-pass and high-pass filtered (60 Hz, filter order 26; 0.1 Hz, filter order 1000) with a Hanning filter. Each continuous EEG was then segmented into epochs of 3 seconds, from -1 to 2 seconds with respect to the onset of the stimulation, and split between Low and High level of complexity trials. Noisy channels were identified based on visual inspection and then interpolated using spherical spline interpolation (mean interpolated electrodes per subject in the CVI group: 1.7 ± 1.06 SD; in the Control group: 1.1 ± 0.84 SD). Following visual inspection, we rejected epochs exceeding a threshold of 150 uV within the [-0.5 - 1 s] time window representing contaminated portions of the EEG signal. Remaining epochs were further cleaned, using as rejection method joint probability across channels (Delorme et al., 2007) with a threshold of 3 SD. In total the mean epochs rejected per subject in the CVI group were 12.7% ± 6.6 SD for Low complexity trials and, 11.2% ± 5.6 SD High complexity trials; in the Control group: 8.4% ± 2.9 SD Low complexity trials, and 8.6% ± 2.4 SD High complexity trials, no significant difference

between groups emerged, all ps>0.07. Finally, we re-referenced data to the average, and a 40 Hz low-pass filter (order 50) was applied only before the computation of event-related potential (ERP). All these steps were performed with EEGLAB software (Delorme and Makeig, 2004). Data were then imported in Fieldtrip (Oostenveld et al., 2011) to perform time-frequency decomposition, event-related potential (ERP) and statistical analyses.

Since the literature on CVI is mainly based on event-related potentials, we extracted ERPs separately for Low and High level of complexity within each group (CVI and Control). The data were baseline corrected, using as baseline the time window between -0.1 to 0 seconds before the stimulus presentation.

Primary analysis of acquired EEG activity was focused on oscillatory activity associated with visual search behavior. To this end, time-frequency decomposition of the EEG data was performed separately for Low and High level of complexity within each group (CVI and Control). At the single participant level, we first extracted the induced power at each single trial after subtracting from each epoch the not filtered ERP (i.e., event-related potentials computed for each participant without 40 Hz low-pass filter) to get rid of the evoked activity from each trial. Single-trial's time-frequency decomposition was computed at each electrode, separately for low- [2-30 Hz] and high- [30-55 Hz] frequency ranges. The higher-frequency range was investigated up to 55 Hz to avoid line noise contamination (i.e., 60 Hz). Within the low-frequency range [2-30 Hz], oscillatory power was estimated using a Hanning taper with a frequency-dependent window length (4 cycles per time window) in steps of 2 Hz. Within the higher-frequency range [30-55 Hz], oscillatory power was estimated using a Multitapers method with Slepian sequence as tapers, in steps of 5 Hz with a fixed-length time window of 0.2 seconds and fixed spectral smoothing of ± 10 Hz. For both low- and high-frequency ranges, the power was extracted over the entire epoch (from -1 to 2 seconds) in steps of 0.02 seconds. Then, the average across trials was computed at the single-subject level within condition (i.e., Low and High level of complexity) and for low- and high-frequency ranges. The resulting oscillatory activity was baseline-corrected to obtain the relative change with respect to the baseline period. For the low-frequency range, the baseline was set between -0.7 and -0.3 seconds,

while for the higher-frequency range, between -0.2 and -0.1 seconds. Low frequencies, having a longer cycle, required a baseline window wider for appropriate estimation of slow oscillations and farther away from zero to avoid temporal leakage of post-stimulus activity into pre-stimulus baseline. The same procedure was implemented without ERP subtraction from single trials to estimate the total power from which the baseline-corrected evoked power was computed by subtracting the baseline-corrected induced power.

The same statistical approach was applied to all extracted electrophysiological measures. To investigate whether there was an interaction effect between group and task complexity on ERPs and oscillatory activities (i.e., evoked and induced components; low and high-frequency ranges), we estimated the neural response change between conditions (differential activity computed High minus Low level of task complexity) within each group. Non-parametric cluster-based permutation, without a priori assumptions, was performed between Control and CVI groups on the difference between conditions (High-Low). The Monte Carlo method with 1000 random permutations was applied, and cluster-level statistics were calculated by taking the sum of the t-values within every cluster (minimum neighbor channel = 1; alpha level of 0.05, two-tailed). Identified clusters were considered significant at $p<0.025$ (alpha=0.05, two-tailed). For ERPs, the cluster-based permutation analyses were performed across all electrodes and time points within the time window [0 - 0.5 s]. For time-frequency, statistical analyses were performed across all electrodes, time points within the time window [0 – 1] s, and across all frequencies within low [4-30 Hz] and high [30-55 Hz] frequency ranges, and separately performed for induced and evoked oscillatory activities.

If a significant effect of interaction emerged, we assessed the difference between conditions within each group (i.e., Low vs. High complexity within control group and Low vs. High complexity within CVI group), and the difference between the two groups within each condition (i.e., controls vs. CVI in the High complexity and control vs. CVI in the Low complexity). These effects were all investigated with the same cluster-based permutation analysis approach and the same parameters reported above ($p<0.025$, alpha=0.05, two-tailed). In contrast, in the case of absence of interaction, we collapsed the two conditions, performing the

average between High and Low levels of task complexity. The same cluster-based permutation analysis approach was performed between neural activity in control and CVI groups ($p<0.025$, alpha=0.05, two-tailed).

4.3 Results

4.3.1 Visual Search Task Performance

We examined visual search performance on the effect of task complexity level with respect to all outcomes of interest. We conducted a series of two-way repeated measure ANOVAs with group (CVI and control) as between-subject factor and task complexity (High and Low) as within-subject factor. In general, for all outcomes of interest (including success rate, reaction time, and gaze error), we found a significant group difference between the control and CVI groups, with the CVI group being associated with an overall impairment in visual search performance. A task complexity difference between Low and High conditions was found in reaction time and gaze error. No interaction effect between task complexity and group emerged.

With respect to success rate, CVI participants showed a lower mean success rate compared to controls. A repeated measure ANOVA showed that the CVI group had a significantly lower success rate (Low: 84.06 % ± 21.18 SD, High: 81.30 % ± 22.24 SD) than the control group (Low: 99.22 % ± 2.15, High: 98.28 % ± 3.84) [$F(1,24) = 9.141$ $p = 0.006$, $\eta p2 = 0.276$]. There was no effect of complexity level [$F(1,24) = 2.36$, $p = 0.137$, $\eta p2 = 0.090$] and no interaction effect between group and level of complexity on success rate [$F(1,24) = 0.57$, $p = 0.458$, $\eta p2 = 0.023$].

Mean reaction times were also higher in the CVI group than in controls, and this difference was also statistically significant. A repeated measure ANOVA showed that the CVI group had a significantly higher reaction time (Low: 1447.39 ± 297.85 ms, High: 1519.07 ± 259.22 ms) than the control group (Low: 1035.38 ± 109.54 ms, High: 1122.30 ± 151.59 ms) [$F(1,24) = 29.27$, $p < 0.001$, $\eta p2 = 0.55$]. There was a significant effect of complexity level [$F(1,24) = 6.69$, $p = 0.016$, $\eta p2 = 0.218$], but no interaction effect [$F(1,24) = 0.062$, $p = 0.806$, $\eta p2 = 0.003$] on reaction time. This suggests that the effect of task complexity on reaction time was consistent across groups.

Finally, mean gaze error (an index for visual search accuracy) was significantly higher in the CVI group compared to controls. A two-way repeated measure ANOVA showed that the CVI group had a significantly higher gaze error (Low: 6.61 ± 2.62 arc degrees, High: 7.37 ± 2.76 arc degrees) than the control group (Low: 3.14 ± 0.84 arc degrees, High: 3.39 ± 1.02 arc degrees) [$F(1,24) = 27.275$, $p < 0.001$, $\eta p2 = 0.532$]. There was a significant effect of complexity level [$F(1,24) = 11.985$, $p = 0.002$, $\eta p2 = 0.333$], but no interaction effect [$F(1,24) = 2.931$ $p = 0.100$, $\eta p2 = 0.109$] on gaze error. This indicates that the effect of task complexity on gaze error was consistent across groups.

Examining putative associations between visual acuity in CVI participants (based on the LogMAR value of the better-seeing eye) and each of the behavioral visual search outcomes did not reveal any significant statistical correlations (all ps>0.24). Moreover, age did not emerge to be correlated with any behavioral measures of interest (all ps>0.53).

Taking together, these behavioral results indicate that, as expected, CVI participants have worse performance than control participants, highlighting the challenge that a similar everyday visual exploration would be for them. However, absolute values of success rate (average 82%, see Figure 4.2) reveal that CVI individuals were able to perform the task successfully. Given these results, we assumed that the task was particularly suitable for investigating the neurophysiology associated with overt behavior visual search.

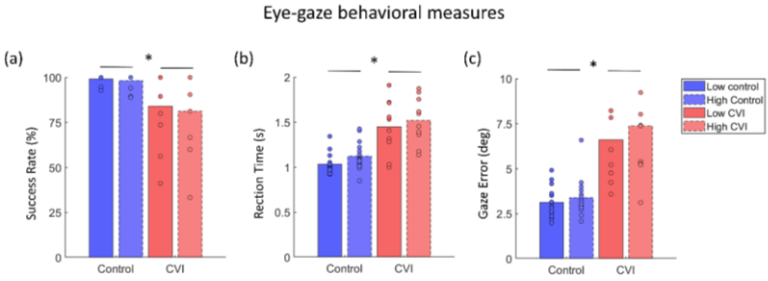

Figure 4.2. Behavioral measures. Three bar plots, one for each behavioral measure, show means and individual data (superimposed dots) for each level of complexity (Low and High) in the control and CVI groups. (a) Success Rate are reported, (b) Reaction Time, and (c) Gaze error.

4.3.2 Event Related Potentials (ERPs)

No significant differences emerged in the ERPs (all ps>0.034). However, visual inspection revealed a smaller P300 amplitude in the CVI compared to the control group (see Supplementary materials Chapter 4 Figure S4.4).

4.3.3 Neural oscillations

Evoked power. Within the low-frequency range [4-30 Hz], a cluster-based permutation test performed on the neural response change between the two levels of complexity contrasting the control and CVI groups revealed the absence of a significant interaction (all ps>0.03). Thus, we collapsed the levels of task complexity, and a cluster-based permutation revealed a significant difference between the two groups ($p<0.004$). In the control group, the presentation of the visual stimulus elicited a marked theta activity [4-6 Hz] between 150 and 500 ms, starting at occipital regions and extending to central areas. This pattern was nearly absent in CVI participants (see Figure 4.3a,b).

No significant differences emerged at high-frequency range [30-55 Hz] (all ps> 0.1; see Supplementary materials Chapter 4 Figure S4.5).

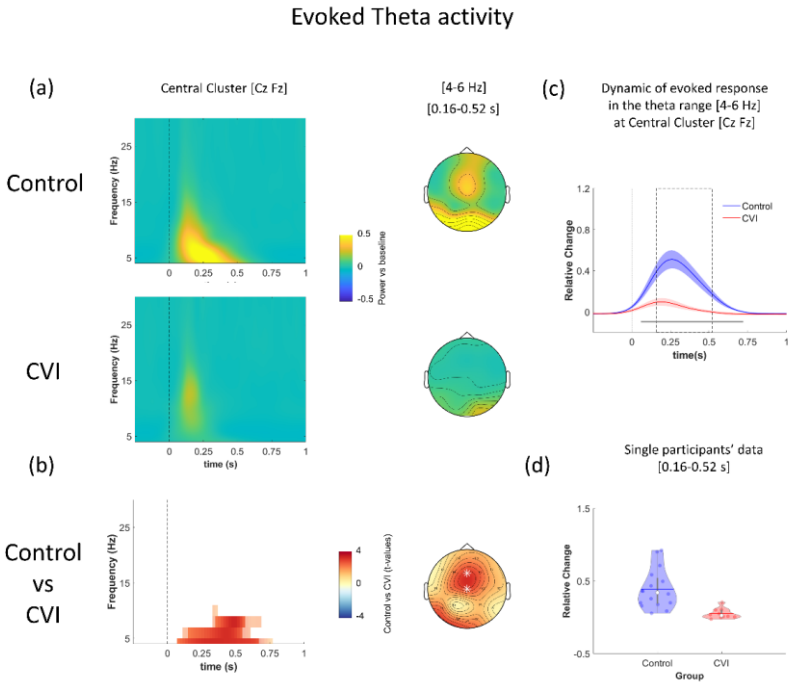

Figure 4.3. Evoked theta activity. (a) Oscillatory activities calculated as the average across Low and High level of complexity within each group (control upper row and CVI bottom row) are plotted as a function of time [-0.25 - 1 s] and frequency [4-30 Hz]. The plots show the average between two representative central electrodes (Cz, Fz); 0 s indicates stimulus onset. On the right side, topographies in the theta range [4-6 Hz] at a representative time window [0.16 - 0.52 s]. (b) Statistical results. Time-frequency plot highlighting significant differences between Control and CVI groups identified by the cluster-based permutation test ($p<0.025$) and the corresponding topography for theta range [4-6 Hz] at a representative time window [0.16 - 0.52 s]; electrodes belonging to the significant cluster are highlighted with white asterisks. (c) Time-course at the group level of the mean power in the theta range [4-6 Hz] for control and CVI individuals (data are averaged across two representative central electrodes Cz, Fz); shaded areas represent the standard error of the mean; the continuous horizontal grey line indicates

the significant difference between CVI participants and the control group (from 0.08 to 0.72 s; FDR corrected). The dashed grey boxes represent the time window [0.16 - 0.52 s], comprising the theta peak, in which the theta power [4-6 Hz] was extracted for each subject (across channels Cz, Fz) and shown in the corresponding violin plots (d), each dot represents individual data.

Induced power. Within the low-frequency range [4-30 Hz], a cluster-based permutation test performed on the neural response change between task complexity conditions and contrasting the control and CVI groups revealed a significant interaction between condition and group ($p<0.005$). This interaction effect emerged in the alpha frequency band [8-14 Hz] at the occipital level between 250 and 500 ms (see Figure 4.4a,b). We explore this further by performing a cluster-based permutation analysis between High and Low complexity within each group. In the control group, we found a significant alpha modulation, extending into the beta band, associated with task complexity ($p<0.001$). In contrast, no difference emerged in CVI participants (all $ps>0.04$). Moreover, when we investigated the difference between groups within each level of task complexity, a cluster-based permutation analysis revealed a significant difference between the two groups for both Low and High levels of complexity (Low, $p<0.001$; High, $p<0.005$). In particular, the CVI group showed a reduction in the alpha [10-16 Hz] desynchronization (>500 ms) within occipital channels in the Low condition, and this difference also extended to beta activity [12-22 Hz] at the High level of task complexity (see Supplementary materials Chapter 4 Figure S4.6).

Within the high-frequency range [30-55 Hz], a cluster-based permutation test performed on the neural response change between the two levels of task complexity and contrasting the control and CVI groups revealed the absence of a significant interaction (all $ps>0.04$). Thus, we averaged at the individual level the oscillatory responses across Low and High levels of complexity, and a cluster-based permutation analysis revealed a significant difference between the two groups ($p<0.01$). The effect emerged between 300 and 700 ms in the occipital-parietal area. In the CVI groups, delayed induced gamma [30-45 Hz] activity appeared to emerge compared to controls (see Figure 4.5a,b).

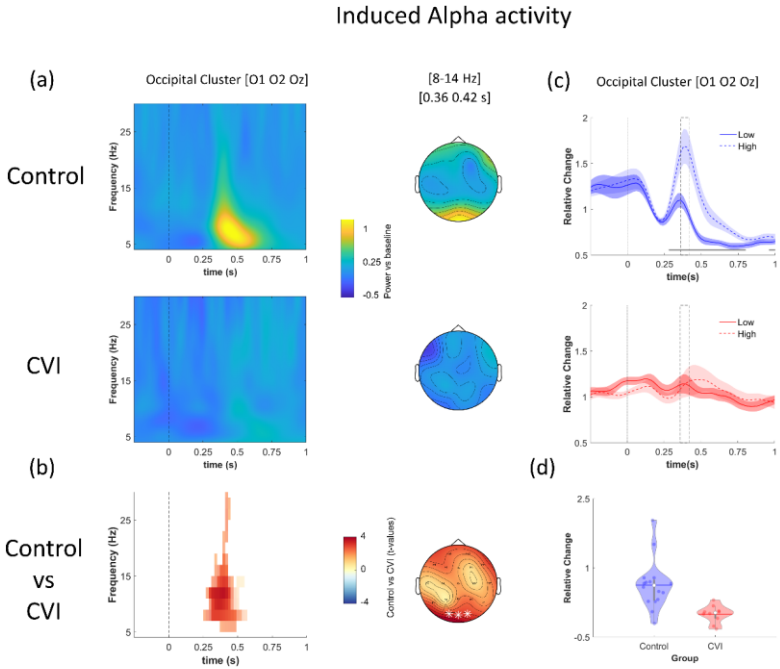

Figure 4.4. Induced alpha activity. (a) Oscillatory activity calculated as the difference between High minus Low levels of complexity is plotted within each group (Control, upper row, and CVI, bottom row) as function of time [-0.25 - 1 s] and frequency [4-30 Hz]. The plots show the average across three representative occipital electrodes (O1, O2, Oz); 0 s indicates stimulus onset. On the right, topographies in the alpha range [8-14 Hz] at a representative time window [0.36 - 0.42 s]. (b) Statistical results. Time-frequency plot highlighting significant differences between Control and CVI groups identified by the cluster-based permutation test ($p<0.025$) and the corresponding topography for the alpha range [8-14 Hz] at a representative time window [0.36 - 0.42 s]; electrodes belonging to the significant cluster are highlighted with white asterisks. (c) Time-course of the mean power in the alpha range [8-14 Hz] separately for Low and High level of complexity are shown for control and CVI groups (upper and bottom row respectively, data are averaged

across three representative central electrodes O1, O2, Oz); shaded areas represent the standard error of the mean; the continuous horizontal grey line indicates the significant difference between Low and High level of complexity in the control group (from 0.28 to 0.8 s; $p<0.05$, FDR corrected). The dashed grey boxes represent the time window [0.36 - 0.44 s], comprising the alpha peak, in which the power in the alpha range [8-14 Hz] was extracted for each subject (across channels O1, O2, Oz) and shown in the corresponding violin plots (d), each dot represents individual data.

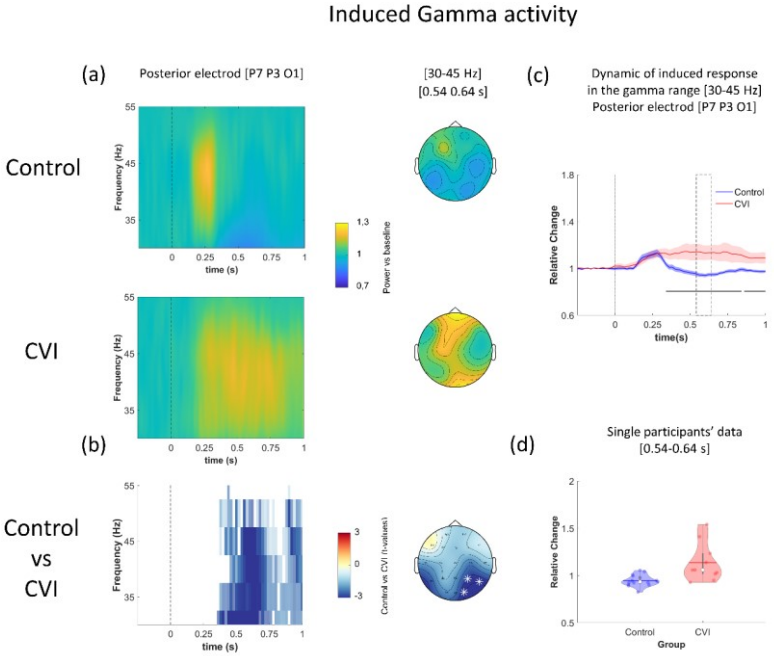

Figure 4.5. Induced gamma activity. (a) Oscillatory activity calculated as the average across Low and High level of complexity within each group (Control, upper row, and CVI, bottom row) is plotted as a function of time [-0.25 - 1 s] and frequency [30-55 Hz]. The plots show the activity at the representative posterior electrode (P7; P3; O1); 0 s indicates stimulus onset. On the right, topographies in the gamma range [30-45 Hz] at a

representative time window [0.54 - 0.64 s]. (b) Statistical results. Time-frequency plot highlighting significant differences between Control and CVI groups identified by the cluster-based permutation test ($p<0.025$) and the corresponding topography for the gamma range [30-45 Hz] at a representative time window [0.54 - 0.64 s]; significant electrodes belonging to the significant cluster is highlighted with white asterisks. (c) Time-course at the group level of the mean power in the gamma range [30-45 Hz] for control and CVI groups (data averaged across representative posterior electrodes P7, P3, O1); shaded areas represent the standard error of the mean; continuous horizontal grey lines indicate significant differences between CVI participants and the control group (from 0.34 to 0.82 s and from 0.86 to 1 s; $p<0.05$, FDR corrected). The dashed grey boxes represent the time window [0.54 - 0.64 s], in which the power in the gamma range [30-45 Hz] was extracted for each subject (in the electrodes P7, P3, O1) and shown in the corresponding violin plots (d), each dot represents individual data.

4.4 Discussion

In this study, we assessed the neurophysiological basis underpinning high-level visuospatial dysfunction that characterizes CVI in a virtual-reality-based visual search task. Behavioral data confirmed that CVI participants showed impaired visual search performance compared to controls as indexed by decreased success rate as well as increased reaction time and gaze error. The analysis of both evoked and induced oscillatory activity within a broad frequency range [4-55 Hz] revealed widespread neurophysiological alterations associated with impaired visual search in CVI participants compared to controls. Specifically, we found markedly reduced evoked theta [4-6 Hz] activity in the CVI group regardless of the level of task complexity. Analysis of the induced oscillatory activity revealed that, overall, alpha response was markedly reduced in CVI compared to control participants. Furthermore, while induced alpha activity in controls was enhanced at higher complexity of the visual scene, this modulation was completely absent in CVI individuals. Moreover, the CVI group showed a delayed yet greater sustained induced gamma response compared to controls. These alterations in both evoked and induced components of neural

oscillations suggest that CVI are characterized by anomalies in both feedforward and feedback connectivity.

4.4.1 Impaired ocular pattern in CVI during ecological visual search

Notwithstanding the above chance level performance, behavioral data consistently revealed an overall impairment in visual search performance in CVI individuals compared to controls. Results showed that CVI participants were less likely, and took longer to find the target and that their search patterns were less accurate in finding the target compared to controls. Importantly, behavioral performance in CVI did not correlate with visual acuity, suggesting that impaired visual search could not simply be explained by reduced stimulus visibility and highlighting the brain-based nature of higher-order visual perceptual deficits associated with this condition. Overall, these effects indicate a dysfunctional ocular pattern in CVI during visual search, regardless of the level of complexity of the visual scene, ultimately revealing how challenging everyday visual exploration can be for CVI individuals. In general, these observations appear in line with the clinical profile of CVI with respect to visuospatial and visual attention processing deficits in this population (Fazzi et al., 2007; Philip and Dutton, 2014). The use of VR-based, behaviorally relevant tasks embedded within naturalistic visual scenes can help capture and characterize higher-order processing dysfunctions and functional visual abilities that are not assessed as part of a typical ophthalmological examination. Noteworthy, by asking for an overt ocular visual search, the task represented an ecological exploration of a naturalistic scene, a crucial aspect of assessing neural mechanisms underpinning behavioral impairments occurring in the real-world (Matusz et al., 2019).

4.4.2 Altered neural mechanisms involved in visual search in CVI

No significant differences emerged between CVI and control groups on the ERPs. Note that in the present study, we employed a conservative statistical approach without a priori assumptions (i.e., a cluster-based permutation across all electrodes and all time points). It is important to remark, especially for clinicians, that by observing the VEPs at posterior electrodes, CVI individuals seem to display a reduced P300 wave. A

more VEPs-oriented statistical analysis, across posterior electrodes only, showed a reduction of the P300 amplitude in the CVI group compared to controls (see Supplementary materials Chapter 4 Figure S4.4). Of note, any difference emerged at early ERP response.

Notwithstanding the conservative statistical approach, the analyses of neural oscillations clearly revealed significant differences between typical development and CVI individuals.

4.4.2.1 Time and phase-locked neural oscillations, feedforward processing

The analysis of the evoked oscillatory activity revealed a significant difference between CVI and control participants with respect to theta activity independently from the level of complexity. While a robust post-stimulus response in the evoked theta [4-6 Hz] was found within the first 500 ms in the control group, in CVI, theta activity was extremely dampened. Theta activity has been linked with the active sampling of input from the environment, with information processed at any given moment packed in each theta cycle (Colgin, 2013). Relevant to the present context, a successful visual search was found to be positively associated with post-stimulus theta amplitude in sighted individuals (Dugué et al., 2015). Moreover, a recent magnetoencephalography (MEG) study showed that children with CVI associated with cerebral palsy exhibited weaker theta oscillations during visuospatial processing (verMass et al., 2021). Interestingly, a subset of our study participants with CVI had visual acuities within normal/near normal levels, yet, impaired theta activity was still evident. This might suggest that the observed evoked theta impairment could be linked to a specific deficit in the organization of the neural response time and phase-locked to visual events. In other words, despite a proper visual input, feed-forward visual processing seems to be hampered as a result of CVI. Which structures could be responsible for this alteration of the neural response remains to be ascertained. Given CVI's subcortical lesions, it is possible that thalamo-cortical processing might be altered at the earliest steps, providing poorly organized input for cortical analyses.

4.4.2.2. Non-time and non-phase-locked neural oscillations, feedback processing

Analyzing induced oscillatory activity, we found evidence of two alterations in the CVI group associated with alpha [8-14 Hz] and gamma [30-45 Hz] ranges. While in the control group, occipital induced alpha synchronization increases as visual scenes become more complex, in CVI individuals, this modulation was absent. Given the well-established link between alpha and visual attention (Bagherzadeh et al., 2020; Clayton et al., 2018; Peylo et al., 2021; Romei et al., 2010), this finding would be consistent with the view that neural mechanisms implicated with selecting visually attended targets and suppressing task-irrelevant stimuli are impaired in CVI (Jensen et al., 2012; Klimesch, 2012). A recent study by Gutteling and colleagues (Gutteling et al., 2022) reported that alpha-oscillations might be especially involved in distractor suppression and play a key role in closing the perceptual gate to interferent input. The data presented here suggest that CVI participants, even with "functionally useful vision", may have specific deficits with the inhibition of distracting information. This neurophysiological data could well fit with clinical reports indicating that many individuals with CVI often appear overwhelmed in complex, cluttered, and busy visual environments.

In addition, CVI participants showed a delayed yet, sustained induced gamma activity within posterior regions of the scalp, independent of the level of complexity. It has to be noted that gamma activity was consistently associated with ocular movements such as micro-saccades (Yuval-Greenberg et al., 2008). Thus, it is possible that this aberrant pattern in gamma oscillatory activity in CVI could be related to their abnormal ocular pattern. Consistent with this view, our behavioral data suggest that gaze error (an index of gaze precision in locating and accurately fixating the target) was significantly higher in CVI compared to control participants. The continuous need to recalibrate gaze while searching, locating, and fixating the target might explain the pattern of sustained gamma band activity observed in CVI.

4.4.3 Neural markers of CVI and their use for clinical purposes

Results revealed strong impairment in CVI feedforward activity, as suggested by the almost absent evoked response in the theta range. This impairment in thalamo-cortical processing might represent a distinctive aspect of cerebral visual impairment. The fact that evoked activity was marked altered represents a difference compared with results stemming from investigations in visually deprived individuals due to peripheral damages. Peripheral damages, such as early-onset sensory deprivation in both visual (Bottari et al., 2016) and auditory modalities (Bednaya et al., 2021; Yusuf et al., 2017), strongly affected induced oscillatory activities.

Moreover, in the CVI group, widespread alterations also emerged for induced neural oscillations. That is, our findings indicate early onset neurological damage impacts the correct development of induced oscillatory activity as well. Along the development, the normal elaboration of feedforward connectivity, crucial for stimulus driven sensory processing, seems to precede the elaboration of feedback connectivity, which in turn is important for top-down control of sensory processing and learning (Dehaene-Lambertz and Spelke, 2015; Kral et al., 2017). It has been suggested that early stimulus-driven learning plays a crucial role in elaborating feedback connectivity (Batardière et al., 2002; Magrou et al., 2018). The present results suggest that feedback cortico-cortical connectivity not only needs external sensory input, as available in our CVI group, but requires intact central processing to fully develop and operate.

Vision plays a crucial role in different high-level functions, and thus, deficient visual processing can lead to widespread cognitive and social impairment (Chokron and Dutton, 2016; Chokron et al., 2021; Dutton, 2003; Dutton and Jacobson, 2001; Lueck et al., 2019; Pavlova, 2003). Visual deficits can be highly invasive in neurodevelopment and can cause deficits resembling autistic-like traits leading to confusion in diagnosis (Chokron et al., 2020). Notably, atypical visual processing was highly documented in autism (Robertson and Baron-Cohen, 2017), and sensory anomalies recently became a core feature of the disorder (American Psychiatric Association, 2013). Therefore, uncovering the neural mechanisms behind similar behavioral manifestations, like being overwhelmed in complex, cluttered environments, is crucial in the

differential diagnosis. Due to its brain-based origin and the associated higher-order visual deficits, CVI is distinct from ocular visual impairment and can lead to phenotypes close to neurodevelopment disorders. For this reason, diagnosis of CVI requires combined professional expertise such as ophthalmologists, neurologists, psychologists, and neuroscientists (McConnell et al., 2021).

Improving the neurophysiological characterization of high-level visual processing deficits can also guide the tuning of individualized treatments in this population. Even if little is known about neuroplasticity in CVI, the majority of children with CVI showed improvement in visual acuity when tested in a follow-up (Matsuba and Jan, 2006), and the prognosis for recovery was reported to be better in children who were early diagnosed (Huo et al., 1999). These data are consistent with the high plasticity of the visual system after early brain damage (Guzzetta et al., 2010). Fazzi and colleagues (Fazzi et al., 2021) showed important preliminary results with 6-months early intensive individualized visual training in infants with visual impairment. This training improves visual functions and developmental outcomes, with CVI showing a greater improvement than children with peripheral visual impairment. While these results suggest the importance of the availability of sensory input (Ricciardi et al., 2020), it allows hypothesizing that children with CVI would also benefit from early treatments focusing on high-level visual dysfunctions. The identification of effective treatments for these individuals falls beyond the scope of the present study; however, these results might indicate that treatments boosting distractor suppression and using alpha oscillations as a biomarker might represent a plausible approach.

4.4.4 Limitations and future studies

Electrophysiological data in this study were recorded using a 20-channel EEG system to facilitate acquisition in the clinical setting and minimize participant discomfort. Given the reduced number of electrodes employed, we could not perform source modeling to localize neural sources of the electrophysiological activity. Future studies using our visual search paradigm combined with high-density EEG are therefore needed to further characterize the nature of the associated electrophysiological activity.

The sample size of our CVI group is small and represents an important limitation of the study. The small number depends on the choice of recruiting CVI participants with homogenous visual abilities. Given the broad and complex clinical profile of CVI, we tested participants with narrower inclusion/exclusion criteria to focus on recruiting CVI individuals with "functionally useful vision" to minimize potential confounding factors. Nonetheless, future studies with a larger sample size could help to better characterize associations between impaired EEG activities and behavioral performances, which could not be assessed here.

4.5 Conclusion

Results from this study corroborate that participants with CVI are affected by pervasive deficits of visual search, even in visual scenes with low complexity. Their dysfunctional visual search was first observed in their ocular pattern and, most importantly, in neural oscillations. Marked alterations were observed in neural oscillations over a broad frequency range, suggesting widespread deficits within the visual system and implicating both local and distributed levels of neural processing. Finally, alterations of both evoked and induced components of oscillations suggest that both feedforward and feedback processing may be compromised in CVI.

Chapter 5

Conclusion

The studies collected in this dissertation revealed neural plasticity induced by different degrees of sensory perturbation, which we defined according to the three dimensions characterizing a deprivation model (i.e., *when*, *duration*, and *where*). The present findings expand our knowledge of experience-dependent plasticity in visual and auditory systems, showing distinct forms of alterations that depend on the degree of perturbation and sensory processing involved.

The first study (Chapter 2) showed that basic visual, audio-visual, and auditory processing could be altered in the adult brain following a low degree of perturbation, such as a short-lasting deprivation. On the one hand, we observed distinct signatures of plasticity depending on the sensory processing involved, revealing high specificity of the neural activity changes. On the other hand, the underpinning neurophysiological mechanism was shared across sensory systems: neural changes in this context emerged in feedback connectivity.
The second study (Chapter 3) showed that some basic functions (e.g., the neural tracking of speech envelope) develop despite a medium degree of sensory perturbation, even if deprivation starts at birth. However, some functional changes clearly emerged, indicating an altered developmental pathway of the sensory system. Importantly, the longer the experience provided to the restored sense, the more the neural system recovered, and neural response became similar to typical development.
The third study (Chapter 4) revealed that the neural oscillations during complex visual processing are massively impacted in case of a high degree of sensory perturbation. In this case, both feedback and feedforward connections, as well as a broad range of frequency bands, were affected, highlighting wide alterations in neural processing.

These results are now presented according to the three dimensions of the degree of perturbation space (when, duration, and where).

When dimension. Whether the deprivation occurs in adulthood or during development critically impacts the type of neural plasticity taking place.
When the adult brain receives a proper developmental experience, neural plasticity can still emerge in basic sensory processing and mainly involves feedback connectivity (study one). In contrast, when sensory information is anomalous during development, neural circuits follow an atypical trajectory (study two and study three). Study three showed that atypical sensory experience from birth widely impaired sensory processing. However, study two revealed that some functions, even if altered, can develop in the absence of correct sensory experience during development.

Duration dimension. How long the sensory perturbation lasts, short-term deprivation (study one), temporary deprivation (study two), or permanent deprivation (study three), differently affects neural plasticity. After short-term deprivation, the neural changes are subtle, specific for different sensory processes, and could represent an adaptive response to environmental changes. Conversely, the study of more protracted temporary deprivation (medium degree) indicated that a longer perturbation affects the efficiency of sensory processing, while persistent perturbation leads to a detrimental impact on functional processing.

Where dimension. Changes in neural response can be differently affected by where is the barrier that induces the sensory perturbation: peripheral occlusion of the sensory system (study one), peripheral lesion (study two), or central lesion (study three).
Peripheral occlusion, without lesioning the sensory system, induced alteration of feedback connectivity with distinct neural signatures for different sensory modalities. When the deprivation was caused by a lesion in the periphery of the sensory system, we observed an altered development of rather simple sensory processing functions. Instead, when the lesion was central, we found widespread processing alterations resulting in severe processing deficits at higher-level processing stages.

From this picture arises that different degrees of deprivation could differently impact multifaced aspects of neural processing: the type of processing (low vs. high-level functions), the extension of the neural

alterations (focus vs. spread), and the flexibility of the neural response. A low degree of perturbation (study one) affected basic functions; a medium degree of perturbation (study two) induced alteration but not disruption of a low-level function; while a high degree of perturbation (study three) revealed alterations during high-level processing. Extension of the neural changes seems to increase with a higher degree of perturbation, and the flexibility of the neural response seems to be higher with a low degree of perturbation.

However, since the studies in this dissertation are prototypical of a low, medium, and high degree of perturbation across all dimensions, we cannot disentangle the role of each dimension on the neural changes. Further studies could help to understand how manipulating the degree of perturbation in a single dimension (when, duration, or where) affects different aspects of neural plasticity and development. From a theoretical point of view, focusing on the degree of perturbation in the three-dimensional space could be insightful for understanding neural changes characteristics of different deprivation models. Moreover, this framework can help to reconcile different results in the literature. Finally, understanding the specific effect of different degrees of perturbation and characterizing their distinctive biomarkers could be extremely useful for clinical implications. This knowledge could help develop and assess the efficiency of specific sensory-experience-based training that could produce enriched environments to counteract deviant trajectories and repair detrimental neural plasticity.

Appendix

Supplementary materials Chapter 2

Simple size estimation for the main EEG experiment

We estimated the minimum sample size needed to replicate previous evidence of neural MD effect on visual processing. Starting from the previous electrophysiological (EEG) studies (Lunghi et al., 2015a), we expected the effect to be in the alpha range [8-14 Hz] in the first stages of the visual processing [0-120 ms] and in occipito-parietal electrodes (E33, E34, E36, E38). As planned for our main analyses, we contrasted the difference between t1 and t0 in the Deprived and Underpived eye. Using the data of four pilot subjects, through simulations suited for cluster-based permutation tests (500 randomizations; Wang and Zhang, 2021), we estimated a minimum sample size of 17 subjects to reach a power of 0.8 (lower threshold). Here, the final sample comprised 19 behavioral and 19 EEG datasets.

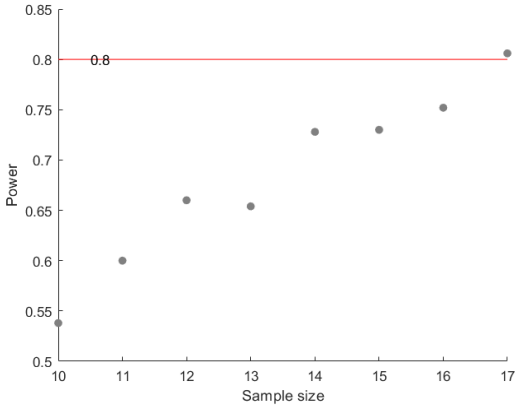

Figure S2.1. Sample Size Estimation. Expected statistical power at each sample size, starting from N=10, computed through simulations of time-frequency data on the total power (alpha = 0.05). Results showed that to achieve a power of 0.8 (red line), a minimum sample size of N=17 was

required.

Participants excluded after the preliminary behavioral assessment
Five participants were excluded as they did not meet the inclusion criteria of the study: one perceived the fission illusion only in a few trials (20% illusory rate), and the others were entirely biased by the sound on their visual perception (>95% illusory rate). Moreover, one participant was excluded because they could not comply with instructions (difficulties in responding within the response time window).

Conditions trials
In fission illusion (AVA condition), the visual stimulus was presented between the two auditory stimuli, with the inter-stimulus-interval (ISI) between each stimulus being a single frame (i.e., 17 ms). The same was done for fusion illusion (VAV condition): the audio stimulus was presented within the two visual stimuli (ISIs between the stimuli: 17 ms). Instead, in coherent multisensory conditions (i.e., AV and AVAV), each audio-visual couple was presented simultaneously. In the AVAV condition, the two couples of stimuli were presented with an ISI of 51 ms (that corresponds to three frames, 17 ms × 3), as in the conditions with two unisensory stimuli (i.e., VV, AA).

Porta Test
To assess participants' eye dominance, we used the Porta test. With both eyes open, the participant extends one arm and aligns the thumb finger with a distant object. Then participant alternates closing the eyes; when the thumb appears to "move," it means that the closed eye is the dominant one (https://web.archive.org/web/20080215220943/http://www.sportvue.com/support/dominance.php).

Staircase procedure on the AVA condition
The contrast level of the grey dot presented on the screen was selected for each individual via a one-up one-down staircase procedure. In the staircase procedure, 133 contrasts for the grey dots were implemented

(linearly spaced). When the subject's response corresponded to the perception of the fission illusion (i.e., response "two flashes"), the contrast decreased, while it increased after a non-illusion perception (i.e., response "one fash"). Wrong answers (i.e., response zero flashes) were not taken into account by the staircase procedure, and the same contrast was displayed again in the subsequent AVA trial. AVA condition trials were presented randomly with all the other conditions (i.e., A, AA, V, VV, VAV, AV, AVAV; maximum 15 trials for each condition). No more than three consecutive AVA trials could be displayed for a maximum of 99 trials. Flash contrast was randomly selected between 10 pre-selected contrasts in all the other conditions. The staircase procedure was considered completed when 16 reverses, changes of direction in the staircase, were reached. The threshold contrast value was computed as the mean of the last three levels of contrast that caused a reverse.

Speeded object recognition task

The speeded object recognition task was performed monocularly with the dominant (Deprived) eye and the non-dominant (Undeprived) eye in a randomized order.

We created two different objects: one was characterized by a small circle (1.7° diameter grey dot) and a high-pitch sound (quadratic beep with a 3.8 kHz frequency and a sampling rate of 44.1 kHz). While the other by a bigger circle (2° diameter grey dot) and a lower pitch sound (quadratic beep with a 3.5 kHz frequency and a sampling rate of 44.1 kHz). The visual and auditory features were coupled in accordance with previously reported crossmodal correspondences between auditory pitch and size of visual objects (see review Spence, 2011). In each trial, participants were presented with one of the two objects defined either by visual feature alone (unisensory visual condition), auditory feature alone (unisensory auditory condition), or by the combination of auditory and visual features, and they were asked to recognize as soon as possible which of the two objects was presented. Twenty trials for each condition (only audio, only video, audio-visuo × 2 objects) were randomly presented. Computing the median reaction times (RTs) at the single-subject level, only on correct trials and excluding the outliers above or

below 3 SD from the median of each condition, we compared RTs in unisensory visual and unisensory auditory trials to define the Sensory-Preference of each participant. Subjects with shorter RTs in unisensory visual trials were considered Visual, while those who were faster in unisensory auditory trials were considered Audio.

Behavioral results in all conditions

We reported here the mean of responses in each condition for each session. In all four sessions, we found an expected performance: when zero stimuli were presented, the means were close to zero, and the mean response increased when the number of visual stimuli increased (maximal when 2 Visual and 2 Auditory stimuli were presented); participants are clearly able to perform the task in all sessions. Notably, the fission illusion was elicited in all sessions; indeed, AVA cell (1 Visual and 2 Auditory stimuli) is always whiter than AV cell (1 Visual and 1 Auditory stimulus).

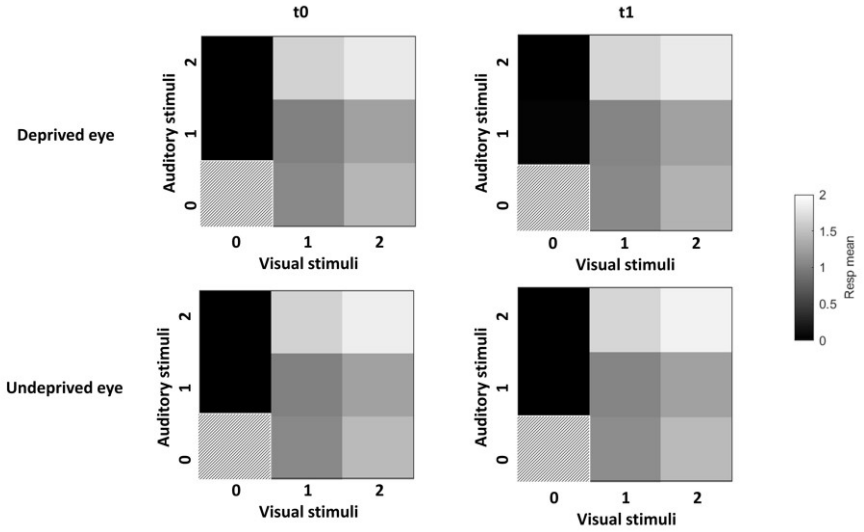

Figure S2.2. Mean of response for each condition in each session. The

heatmaps of the four sessions (t0 Deprived, t0 Undeprived, t1 Deprived, t1 Undeprived) are shown at the group level. Each square represents one of the eight possible conditions, according to the stimulations delivered (the condition zero-zero is absent in our experiment, for this reason, we fill this square up with dashed lines). The color code represents the mean responses: black = zero is the minimum, and white = two is the maximum.

Unisensory visual

Induced power. No significant differences between PowChangeDeprived and PowChangeUndeprived were found in the high-frequency range (all ps>0.6).

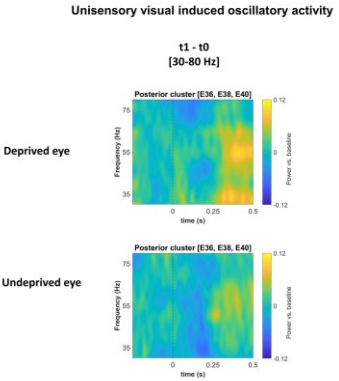

Figure S2.3. Time-frequency plots showing high-frequency induced oscillatory activity during visual processing. Oscillatory activity, calculated as the difference between t1 and t0 at each eye (upper row, PowChangeDeprived, t1 minus t0 at the Deprived eye, and bottom row, PowChangeUndeprived, t1 minus t0 at the Undeprived eye), are plotted as a function of time [-0.25 - 0.5 s] and frequency [30-80 Hz]. The data represent the average across occipital electrodes (E36, E38, E40); the

dashed line at 0 s indicates the stimulus onset.

Evoked power. No significant differences emerged in either low or high frequencies (all ps>0.13).

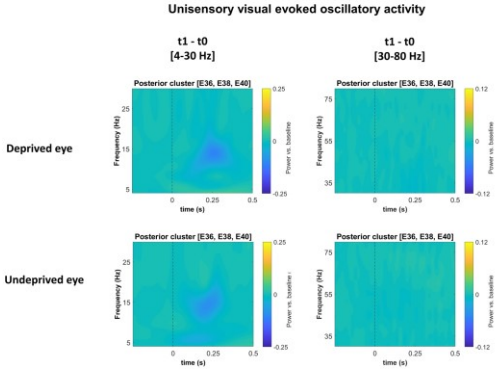

Figure S2.4. Time-frequency plots showing evoked oscillatory activity during visual processing. Oscillatory activity, calculated as the difference between t1 and t0 at each eye (upper row, PowChangeDeprived, t1 minus t0 at the Deprived eye and bottom row, PowChangeUndeprived, t1 minus t0 at the Undeprived eye), are plotted as a function of time [-0.25 - 0.5 s] and frequency [4-30 Hz] and [30-80 Hz] (left and right column, respectively). The data represent the average across occipital electrodes (E36, E38, E40); the dashed line at 0 s indicates the stimulus onset.

Audio-visual

Induced power. The cluster-based permutation performed between PowChangeDeprived and PowChangeUndeprived within the low-frequency range showed no significant effects (all ps>0.45).

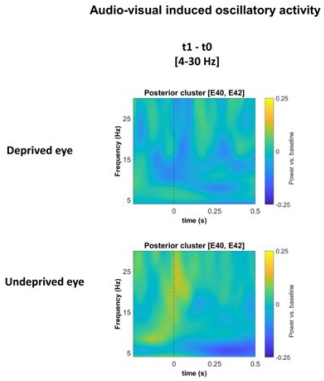

Figure S2.5. Time-frequency plots showing low-frequency induced oscillatory activity during audio-visual processing. Oscillatory activity, calculated as the difference between t1 and t0 at each eye (upper row, PowChangeDeprived, t1 minus t0 at the Deprived eye and bottom row, PowChangeUndeprived, t1 minus t0 at the Undeprived eye), are plotted as a function of time [-0.25 - 0.5 s] and frequency [4-30 Hz]. The data represent the average across two posterior electrodes (E40, E42); the dashed line at 0 s indicates the stimulus onset.

Evoked power. When we tested the difference between PowChangeDeprived and PowChangeUndeprived in the evoked power, no significant difference was found within the low-frequency range (all ps>0.09) nor within the high-frequency range (p>0.05).

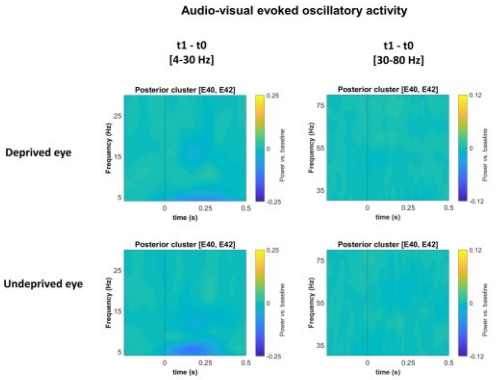

Figure S2.6. Time-frequency plots showing evoked oscillatory activity during audio-visual processing. Oscillatory activity, calculated as the difference between t1 and t0 at each eye (upper row, PowChangeDeprived, t1 minus t0 at the Deprived eye and bottom row, PowChangeUndeprived, t1 minus t0 at the Undeprived eye), are plotted as a function of time [-0.25 - 0.5 s] and frequency [4-30 Hz] and [30-80 Hz] (left and right column, respectively). The data represent the average across two posterior electrodes (E40, E42); the dashed line at 0 s indicates the stimulus onset.

Comparison between correlations in the audio-visual condition

After computing for A- and V- groups the correlations between normalized PowChangeUndeprived and d' change for the audio-visual condition in the Undeprived eye, we tested by means of the bootstrap method (Pernet, Wilcox & Rousselet, 2012) whether the difference between the two correlations was significantly different from zero. Since Pearson correlations were performed, the confidence interval was adjusted as described in Wilcox (2009).

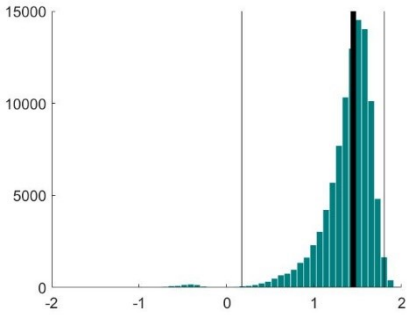

Figure S2.7. Difference between correlations in the Audio and Visual groups. The graph shows the distribution of the differences between correlations in the A- and V-groups (i.e., rA minus rV), computed by the bootstrap methods with 100000 repetitions. The thick black line is the difference between our correlations (rA-rV=1.45), and the thin lines indicate the CI [0.17 1.87].

Supplementary materials Chapter 4

Structural morphometry

Structural morphometry data were available from a subset of participants with CVI (n=9). Of these, 6 were scanned using a T1-weighted anatomical scan (TE 2.9 ms, TR 6.5 ms, flip angle 8°, isotropic 1 mm voxel size) which was acquired with a 32-channel phased array head coil (Philips 3T Elition X scanner). An additional 3 participants with CVI were scanned as part of a previous protocol (TE 3.1 ms, TR 6.8 ms, flip angle 9°, isotropic 1 mm voxel size) using an 8 channel phased array head coil (Philips 3T Intera Achieva). The volumes of predetermined thalamic nuclei (i.e., the lateral geniculate nucleus (LGN) and pulvinar) and the pericalcarine cortex were quantified for each subject in anatomical space using the FreeSurfer 7.2.0 (https://surfer.nmr.mgh.harvard.edu) (Dale, 1999; Fischl, 2002; Fischl, 1999; Fischl, 2004). Segmentations for subcortical and cortical ROIs were derived from a probabilistic thalamic atlas (Iglesias, 2018) and the Desikan-Killiany atlas (Desikan, 2006), respectively.

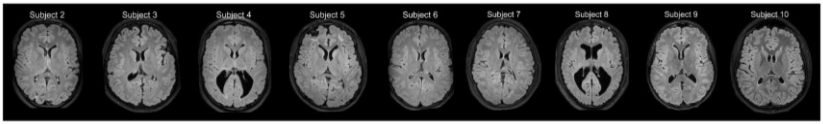

Figure S4.1. Structural morphometry CVI participants. Representative axial fluid-attenuated inversion recovery (FLAIR) images from CVI participants in the study (scanning could not be performed on participant 1 due to contraindications to MRI). Images illustrate examples of the underlying brain changes observed in CVI participants, such as ventriculomegaly (periventricular leukomalacia; PVL), white matter injury, and cortical atrophy.

Eye-tracking characteristics and information on the calibration

The system samples gaze data at a 90 Hz frequency using near infrared

illumination based on pupil-center corneal reflections. Prior to the first experimental run, eye tracking calibration was performed for each participant (Tobii Eye Tracking Software, v 2.9 calibration protocol) which took less than one minute to complete. The process included a 7-points calibration task (screen positions: top-left, top-center, top-right, bottom-left, bottom-center, bottom-right, and center-center) followed by a 9-points post calibration verification (the same 7 calibration points plus a center-left and center-right position). The accuracy criterion was determined by gaze fixation falling within a 2.25° (arc degree) radius around each of the 9 points and further confirmed by visual inspection prior to commencing data collection.

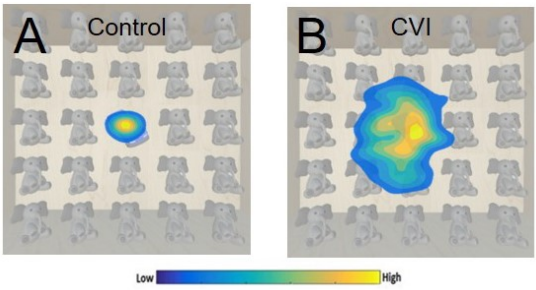

Figure S4.2. Eye-tracking data. Example of the heatmaps of the eye-gaze pattern, respectively for controls individuals with neurotypical development and CVI participants.

Test compliance

As an index of task compliance, we calculated off-screen percent values and found a statistically significant difference between the two groups (compare CVI low: 2.18 % ± 2.92 SD, CVI high: 3.30 % ± 4.81 SD and controls low: 0.11 % ± 0.15 SD, controls high: 0.33 % ± 0.52 SD) [$F(1,24) = 6.967$, $p < 0.014$, $\eta p2 = 0.225$]. The comparatively low off-screen percent values suggests that both groups maintained a high level of task compliance and engagement. However, the significantly higher mean

off-screen percent value in CVI suggests that, as a group, CVI participants were less able to maintain their gaze on the screen compared to controls. There was a significant effect of task difficulty [F(1,24) = 6.586, p = 0.017, ηp2 = 0.215], but no interaction effect between condition and group [F(1,24) = 2.976, p = 0.097, ηp2 = 0.110] with respect to off-screen percent values.

Removed blink components

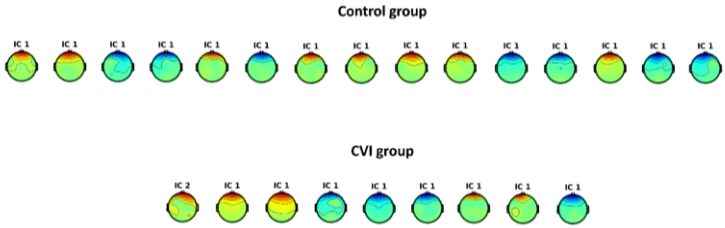

Figure S4.3. Removed blink components. Topography of each blink component which was removed in each participant. In each participant the first (IC 1) or the second (IC 2) component was removed. Only two participants, one control and one CVI, did not have the typical blink artifacts.

Visual Evoked Potential (VEP)

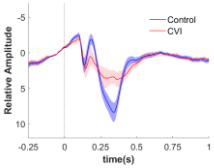

Figure S4.4. VEP. One-tailed positive cluster-based permutation performed on posterior electrodes ('P8' 'P4' 'Pz' 'P3' 'P7' 'O1' 'Oz' 'O2') within [0-0.5 s] revealed a significant difference between 300-400 ms ($p<0.045$), highlighting a decreased P300 in CVI participants.

Evoked activity high-frequency range

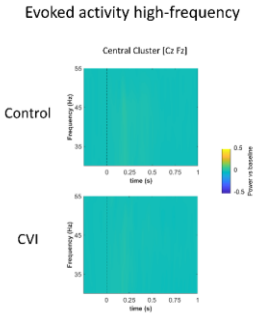

Figure S4.5. Evoked activity in high-frequency range. Oscillatory activities calculated as the average across Low and High level of complexity within each group (Control, upper row, and CVI, bottom row) as function of time [-0.25 - 1 s] and frequency [30-55 Hz]. The plots show the average between two central electrodes (Cz, Fz); 0 s indicates stimulus onset.

Difference between groups within each condition

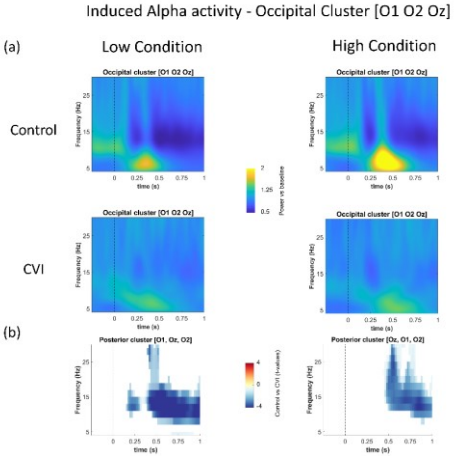

Figure S4.6. Induced alpha activity in Low and High conditions. (a)

activity is plotted within each group (Control, upper row, and CVI, bottom row) and within each condition (Low complexity, left column and High complexity, right column) as function of time [-0.25 - 1 s] and frequency [4-30 Hz]. The plots show the average across three occipital electrodes (O1, O2, Oz); 0 s indicates stimulus onset. (b) Statistical results in Low condition (left column) and High condition (right column). Time-frequency plot highlighting significant differences between Control and CVI groups identified by the cluster-based permutation test ($p<0.05$, two-tailed).

Possible correlations between anomalous neural responses, behavioral outcomes, and clinical profile of CVI individuals

We investigated putative associations between EEG activity, visual search performance, and the clinical profile: visual acuity, age, as well as available structural morphometry data (MRI) of our CVI participants using Spearman rank correlations followed by correction for multiple comparisons using False Discovery Rate (FDR) (Benjamini, 1995). Specifically, the relationship between EEG activity and the volumes of the LGN, pulvinar, and primary visual cortex were evaluated following adjustment for estimated total intracranial volume using residuals.

We observed a significant negative correlation between gaze error and the volume of the pulvinar nucleus ($r = -0.72$, $p = 0.03$). However, this did not survive FDR correction for multiple comparisons ($p = 0.63$). There were no significant correlations between any others behavioral outcomes and volume of the pulvinar, LGN, and pericalcarine cortex, respectively (all p values > 0.4). No statistically significant correlations between the volumes of the LGN, pulvinar, pericalcarine cortex and average theta, alpha, or gamma activity nor P300 amplitude, respectively (all ps > 0.4). We did not observe any significant correlations between EEG activity (average theta, alpha, or gamma activity nor P300 amplitude) and age (all ps > 0.1), LogMAR visual acuity (better seeing eye) (all ps > 0.1), and extent of neurological damage (as defined by global lesion scores; all ps > 0.1).

Bibliography

Abrams DA, Nicol T, Zecker S, Kraus N (2009) Abnormal cortical processing of the syllable rate of speech in poor readers. J Neurosci 29:7686–7693.

Amedi A, Hofstetter S, Maidenbaum S, Heimler B (2017) Task Selectivity as a Comprehensive Principle for Brain Organization. Trends Cogn Sci 21:307–310.

American Psychiatric Association (2013) American Psychiatric Association, 2013. Diagnostic and statistical manual of mental disorders (5th ed.).

Attaheri A, Choisdealbha ÁN, Di Liberto GM, Rocha S, Brusini P, Mead N, Olawole-Scott H, Boutris P, Gibbon S, Williams I, Grey C, Flanagan S, Goswami U (2022) Delta- and theta-band cortical tracking and phase-amplitude coupling to sung speech by infants. Neuroimage 247:118698

Beadle EAR, McKinley DJ, Nikolopoulos TP, Brough J, O'Donoghue GM, Archbold SM (2005) Long-term functional outcomes and academic-occupational status in implanted children after 10 to 14 years of cochlear implant use. Otol Neurotol 26:1152–1160.

Badde S, Ley P, Rajendran SS, Shareef I, Kekunnaya R, Röder B (2019) Cross-modal temporal biases emerge during early sensitive periods. bioRxiv.

Bagherzadeh Y, Baldauf D, Pantazis D, Desimone R (2020) Alpha Synchrony and the Neurofeedback Control of Spatial Attention. Neuron 105:577-587.e5 1.

Balz J, Keil J, Roa Romero Y, Mekle R, Schubert F, Aydin S, Ittermann B, Gallinat J, Senkowski D (2016) GABA concentration in superior temporal sulcus predicts gamma power and perception in the sound-induced

flash illusion. Neuroimage 125:724–730.

Batardière A, Barone P, Knoblauch K, Giroud P, Berland M, Dumas AM, Kennedy H (2002) Early Specification of the Hierarchical Organization of Visual Cortical Areas in the Macaque Monkey. Cereb Cortex 12:453–465.

Bavelier D, Neville HJ (2002) Cross-modal plasticity: Where and how? Nat Rev Neurosci 3:443–452.

Bednaya E, Mirkovic B, Berto M, Ricciardi E, Martinelli A, Federici A, Debener S, Bottari D (2022) Early visual cortex tracks speech envelope in the absence of visual input. bioRxiv:2022.06.28.497713.

Bednaya E, Pavani F, Ricciardi E, Pietrini P, Bottari D (2021) Oscillatory signatures of Repetition Suppression and Novelty Detection reveal altered induced visual responses in early deafness. Cortex.

Bell AJ, Sejnowski TJ (1995) An information-maximization approach to blind separation and blind deconvolution. Neural Comput 7:1129–1159.

Bennett CR, Bailin ES, Gottlieb TK, Bauer CM, Bex PJ, Merabet LB (2018) Assessing visual search performance in ocular compared to cerebral visual impairment using a virtual reality simulation of human dynamic movement. ACM Int Conf Proceeding Ser.

Bennett CR, Bauer CM, Bailin ES, Merabet LB (2020) Neuroplasticity in cerebral visual impairment (CVI): Assessing functional vision and the neurophysiological correlates of dorsal stream dysfunction. Neurosci Biobehav Rev 108:171–181.

Bennett CR, Bauer CM, Bex PJ, Bottari D, Merabet LB (2021) Visual search performance in cerebral visual impairment is associated with altered alpha band oscillations. Neuropsychologia 161:108011 Available at: https://doi.org/10.1016/j.neuropsychologia.2021.108011.

Benetti S, Van Ackeren MJ, Rabini G, Zonca J, Foa V, Baruffaldi F, Rezk M, Pavani F, Rossion B, Collignon O (2017) Functional selectivity for face processing in the temporal voice area of early deaf individuals. Proc Natl Acad Sci U S A 114:E6437–E6446.

Berto M, Ricciardi E, Pietrini P, Bottari D (2021) Interactions between auditory statistics processing and visual experience emerge only in late development. iScience 24:103383 Available at: https://doi.org/10.1016/j.isci.2021.103383.

Bhattacharya J, Shams L, Shimojo S (2002) Sound-induced illusory flash perception: Role of gamma band responses. Neuroreport 13:1727–1730.

Billings CJ, Bennett KO, Molis, M. R. &, Leek MR (2011) cortical encoding of signals in noise: effects of stimulus type and recording paradigm. Ear Hear 32(1):53–60.

Binda P, Kurzawski JW, Lunghi C, Biagi L, Tosetti M, Morrone MC (2018) Response to short-term deprivation of the human adult visual cortex measured with 7T bold. Elife 7:1–25.

Boot FH, Pel JJM, van der Steen J, Evenhuis HM (2010) Cerebral visual impairment: Which perceptive visual dysfunctions can be expected in children with brain damage? A systematic review. Res Dev Disabil 31:1149–1159.

Bottari D, Bednaya E, Dormal G, Villwock A, Dzhelyova M, Grin K, Pietrini P, Ricciardi E, Rossion B, Röder B (2020) EEG frequency-tagging demonstrates increased left hemispheric involvement and crossmodal plasticity for face processing in congenitally deaf signers. Neuroimage 223:117315.

Bottari D, Berto M (2021) Three factors to characterize plastic potential transitions in the visual system. Neurosci Biobehav Rev 126:444–446.

Bottari D, Troje NF, Ley P, Hense M, Kekunnaya R, Röder B (2015) The

neural development of the biological motion processing system does not rely on early visual input. Cortex 71:359–367.

Bottari D, Troje NF, Ley P, Hense M, Kekunnaya R, Röder B (2016) Sight restoration after congenital blindness does not reinstate alpha oscillatory activity in humans. Sci Rep 6.

Bottari D, Kekunnaya R, Hense M, Troje NF, Sourav S, Röder B (2018) Motion processing after sight restoration: No competition between visual recovery and auditory compensation. Neuroimage 167:284–296.

Buzsáki G, Draguhn A. Neuronal oscillations in cortical networks. Science. 2004 Jun 25;304(5679):1926-9.

Cardin V, Grin K, Vinogradova V, Manini B (2020) Crossmodal reorganisation in deafness: Mechanisms for functional preservation and functional change. Neurosci Biobehav Rev 113:227–237 Available at: https://doi.org/10.1016/j.neubiorev.2020.03.019.

Castaldi E, Lunghi C, Morrone MC (2020) Neuroplasticity in adult human visual cortex. Neurosci Biobehav Rev 112:542–552.

Chandna, A., Nichiporuk, N., Nicholas, S., Kumar, R., & Norcia, A. M. (2021). Motion Processing Deficits in Children With Cerebral Visual Impairment and Good Visual Acuity. Investigative Ophthalmology & Visual Science, 62(14), 12-12.

Chang EF, Merzenich MM (2003) Environmental noise retards auditory cortical development. Science (80-) 300:498–502.

Chang, M. Y., & Borchert, M. S. (2020). Advances in the evaluation and management of cortical/cerebral visual impairment in children. Survey of ophthalmology, 65(6), 708-724.

Chen CC, Kiebel SJ, Kilner JM, Ward NS, Stephan KE, Wang WJ, Friston KJ (2012) A dynamic causal model for evoked and induced responses.

Neuroimage 59:340–348.

Chen YC, Lewis TL, Shore DI, Maurer D (2017) Early Binocular Input Is Critical for Development of Audiovisual but Not Visuotactile Simultaneity Perception. Curr Biol 27:583–589.

Chen Y, Schmidt F, Keitel A, Rösch S, Hauswald A, Chen Y (2022) Speech intelligibility changes the temporal evolution of neural speech tracking.

Chokron S, Dutton GN (2016) Impact of cerebral visual impairments on motor skills: Implications for developmental coordination disorders. Front Psychol 7:1–15.

Chokron S, Kovarski K, Dutton GN (2021) Cortical Visual Impairments and Learning Disabilities. Front Hum Neurosci 15 Available at: https://pubmed.ncbi.nlm.nih.gov/34720906/ [Accessed July 24, 2022].

Chokron S, Kovarski K, Zalla T, Dutton GN (2020) The inter-relationships between cerebral visual impairment, autism and intellectual disability. Neurosci Biobehav Rev 114:201–210 Available at: https://doi.org/10.1016/j.neubiorev.2020.04.008.

Clayton MS, Yeung N, Cohen Kadosh R (2018) The many characters of visual alpha oscillations. Eur J Neurosci 48:2498–2508 Available at: https://onlinelibrary.wiley.com/doi/full/10.1111/ejn.13747 [Accessed July 24, 2022].

Colgin LL (2013) Mechanisms and functions of theta rhythms. Annu Rev Neurosci 36:295–312.

Collignon O, Dormal G, De Heering A, Lepore F, Lewis TL, Maurer D (2015) Long-Lasting Crossmodal Cortical Reorganization Triggered by Brief Postnatal Visual Deprivation. Curr Biol 25:2379–2383 Available at: http://dx.doi.org/10.1016/j.cub.2015.07.036.

Combrisson E, Jerbi K (2015) Exceeding chance level by chance: The caveat of theoretical chance levels in brain signal classification and statistical assessment of decoding accuracy. J Neurosci Methods 250:126–136.

Cooke J, Poch C, Gillmeister H, Costantini M, Romei V (2019) Oscillatory properties of functional connections between sensory areas mediate cross-modal illusory perception. J Neurosci 39:5711–5718.

Crosse MJ, Di Liberto GM, Bednar A, Lalor EC (2016) The multivariate temporal response function (mTRF) toolbox: A MATLAB toolbox for relating neural signals to continuous stimuli. Front Hum Neurosci 10:1–14.

Crosse MJ, Zuk NJ, Liberto GM Di, Nidiffer A, Molholm S, Lalor EC (2021) Linear Modeling of Neurophysiological Responses to Naturalistic Stimuli: Methodological Considerations for Applied Research. bioRxiv.

Dale AM, Liu AK, Fischl BR, Buckner RL, Belliveau JW, Lewine JD, Halgren E (2000) Dynamic statistical parametric mapping: combining fMRI and MEG for high-resolution imaging of cortical activity. Neuron 26:55–67.

de Heering A, Dormal G, Pelland M, Lewis T, Maurer D, Collignon O (2016) A Brief Period of Postnatal Visual Deprivation Alters the Balance between Auditory and Visual Attention. Curr Biol:1–5.

Dehaene-Lambertz G, Spelke ES (2015) The Infancy of the Human Brain. Neuron 88:93–109.

Delorme A, Makeig S (2004) EEGLAB: An open source toolbox for analysis of single-trial EEG dynamics including independent component analysis. J Neurosci Methods 134:9–21.

Delorme A, Sejnowski T, Makeig S (2007) Enhanced detection of artifacts

in EEG data using higher-order statistics and independent component analysis. Neuroimage 34:1443–1449.

Di Liberto GM, O'Sullivan JA, Lalor EC (2015) Low-frequency cortical entrainment to speech reflects phoneme-level processing. Curr Biol 25:2457–2465.

Dugué L, Marque P, VanRullen R (2015) Theta Oscillations Modulate Attentional Search Performance Periodically. J Cogn Neurosci 27:945–958 Available at: https://direct.mit.edu/jocn/article/27/5/945/28348/Theta-Oscillations-Modulate-Attentional-Search [Accessed July 24, 2022].

Dutton GN (2003) Cognitive vision, its disorders and differential diagnosis in adults and children: knowing where and what things are. Eye (Lond) 17:289–304.

Dutton GN (2013) The spectrum of cerebral visual impairment as a sequel to premature birth: An overview. Doc Ophthalmol 127:69–78.

Dutton GN, Jacobson LK (2001) Cerebral visual impairment in children. Semin Neonatol 6:477–485.

Dutton, G. N., & Lueck, A. H. (2015). Impairment of vision due to damage to the brain. Vision and the brain: Understanding cerebral visual impairment in children, 3-20.

Edgar JC, Khan SY, Blaskey L, Chow VY, Rey M, Gaetz W, Cannon KM, Monroe JF, Cornew L, Qasmieh S, Liu S, Welsh JP, Levy SE, Roberts TPL (2015) Neuromagnetic Oscillations Predict Evoked-Response Latency Delays and Core Language Deficits in Autism Spectrum Disorders. J Autism Dev Disord 45:395–405.

Eggermont JJ, Ponton CW (2003) Auditory-evoked potential studies of cortical maturation in normal hearing and implanted children:

Correlations with changes in structure and speech perception. Acta Otolaryngol 123:249–252.

Espinosa JS, Stryker MP (2012) Development and Plasticity of the Primary Visual Cortex. Neuron 75:230–249.

Farahani ED, Wouters J, van Wieringen A (2019). Contributions of non-primary cortical sources to auditory temporal processing. NeuroImage, 191: 303-314.

Fazzi E et al. (2021) Early visual training and environmental adaptation for infants with visual impairment. Dev Med Child Neurol 63:1180–1193.

Fazzi E, Signorini SG, Bova SM, La Piana R, Ondei P, Bertone C, Misefari W, Bianchi PE (2007) Spectrum of visual disorders in children with cerebral visual impairment. J Child Neurol 22:294–301.

Fieger A, Röder B, Teder-Sälejärvi W, Hillyard SA, Neville HJ (2006) Auditory spatial tuning in late-onset blindness in humans. J Cogn Neurosci 18:149–157.

Fiori, S., et al., Reliability of a novel, semi-quantitative scale for classification of structural brain magnetic resonance imaging in children with cerebral palsy. Dev Med Child Neurol, 2014. 56(9): p. 839-45.

Froesel M, Cappe C, Ben Hamed S (2021) A multisensory perspective onto primate pulvinar functions. Neurosci Biobehav Rev 125:231–243.

Fujisaki W, Shimojo S, Kashino M, Nishida S (2004) Recalibration of audiovisual simultaneity. Nat Neurosci 2004 77 7:773–778.

Galambos, R. (1992). A comparison of certain gamma band (40-Hz) brain rhythms in cat and man. In Induced rhythms in the brain (pp. 201-216). Birkhäuser, Boston, MA.

Gandal MJ, Edgar JC, Ehrlichman RS, Mehta M, Roberts TPL, Siegel SJ (2010) Validating γ Oscillations and Delayed Auditory Responses as Translational Biomarkers of Autism. Biol Psychiatry 68:1100–1106.

Geers A, Tobey E, Moog J, Brenner C (2008) Long-term outcomes of cochlear implantation in the preschool years: From elementary grades to high school. Int J Audiol 47.

Giard MH, Peronnet F (1999). Auditory-visual integration during multimodal object recognition in humans: a behavioral and electrophysiological study. Journal of cognitive neuroscience, 11:473-490.

Gillis M, Decruy L, Vanthornhout J, Francart T (2021) Hearing loss is associated with delayed neural responses to continuous speech Running title : Hearing loss delays neural responses to speech : KU Leuven , Department of Neurosciences , ExpORL , 3000 Leuven , Belgium : Institute for Systems Research , Univ.

Giraud AL, Poeppel D (2012) Cortical oscillations and speech processing: Emerging computational principles and operations. Nat Neurosci 15:511–517.

Good W V., Jan JE, Burden SK, Skoczenski A, Candy R (2001) Recent advances in cortical visual impairment. Dev Med Child Neurol 43:56–60.

Goswami U (2011) A temporal sampling framework for developmental dyslexia. Trends Cogn Sci 15:3–10.

Goswami U (2014) Cognition In Children. Cogn Child.

Guerreiro MJS, Putzar L, Röder B (2015) The effect of early visual deprivation on the neural bases of multisensory processing. Brain 138:1499–1504.

Gustafson SJ, Billings CJ, Hornsby BWY, Key AP (2019) Effect of competing noise on cortical auditory evoked potentials elicited by speech sounds in 7- to 25-year-old listeners. Hear Res 373:103–112.

Gutteling TP, Sillekens L, Lavie N, Jensen O (2022) Alpha oscillations reflect suppression of distractors with increased perceptual load. Prog Neurobiol 214:102285.

Guzzetta A, D'acunto G, Rose S, Tinelli F, Boyd R, Cioni G (2010) Plasticity of the visual system after early brain damage. Dev Med Child Neurol 52:891–900.

Hadad B-S, Maurer D, Lewis TL (2012) Sparing of sensitivity to biological motion but not of global motion after early visual deprivation. Dev Sci 15:474–481.

Hansen P, Kringelbach M, Salmelin R (2010) MEG: An Introduction to Methods. Oxford University Press (OUP).

Heim S, Friedman JT, Keil A, Benasich AA (2011) Reduced sensory oscillatory activity during rapid auditory processing as a correlate of language-learning impairment. J Neurolinguistics 24:538–555.

Hensch TK (2004) Critical period regulation. Annu Rev Neurosci 27:549–579.

Hensch TK (2005) Critical period plasticity in local cortical circuits. Nat Rev Neurosci 6:877–888.

Hensch TK, Quinlan EM (2018) Critical periods in amblyopia. Vis Neurosci 35:E014.

Hirst RJ, McGovern DP, Setti A, Shams L, Newell FN (2020) What you see is what you hear: Twenty years of research using the Sound-Induced Flash Illusion. Neurosci Biobehav Rev 118:759–774.

Hong, F., Badde, S., & Landy, M. S. (2021). Causal inference regulates audiovisual spatial recalibration via its influence on audiovisual perception. PLoS computational biology, 17(11), e1008877.

Holt RF, Svirsky MA (2008) An exploratory look at pediatric cochlear implantation: Is earliest always best? Ear Hear 29:492–511.

Houston DM, Stewart J, Moberly A, Hollich G, Miyamoto RT (2012) Word learning in deaf children with cochlear implants: Effects of early auditory experience. Dev Sci 15:448–461.

Hubel DH, Wiesel TN (1970) The period of susceptibility to the physiological effects of unilateral eye closure in kittens. J Physiol 206:419–436.

Huo R, Burden SK, Hoyt CS, Good W V. (1999) Chronic cortical visual impairment in children: Aetiology, prognosis, and associated neurological deficits. Br J Ophthalmol 83:670–675.

Jacobson, L., Ek, V., Fernell, E., Flodmark, O., & Broberger, U. (1996). Visual impairment in preterm children with periventricular leukomalacia--visual, cognitive and neuropaediatric characteristics related to cerebral imaging. Dev Med Child Neurol, 1996. 38(8): p. 724-35.

Jensen O, Bonnefond M, VanRullen R (2012) An oscillatory mechanism for prioritizing salient unattended stimuli. Trends Cogn Sci 16:200–206.

Jensen O, Gips B, Bergmann TO, Bonnefond M (2014) Temporal coding organized by coupled alpha and gamma oscillations prioritize visual processing. Trends Neurosci 37:357–369.

Jensen O, Mazaheri A (2010). Shaping functional architecture by oscillatory alpha activity: gating by inhibition. Frontiers in human neuroscience, 186.

Jessen S, Fiedler L, Münte TF, Obleser J (2019) Quantifying the individual auditory and visual brain response in 7-month-old infants watching a brief cartoon movie. Neuroimage 202:116060.

Jung T-P, Makeig S, Humphries C, Lee T-W, McKeown MJ, Iragui V, Sejnowski TJ (2000a) Removing electroencephalographic artifacts by blind source separation. Psychophysiology 37:163–178.

Jung TP, Makeig S, Westerfield M, Townsend J, Courchesne E, Sejnowski TJ (2000b) Removal of eye activity artifacts from visual event-related potentials in normal and clinical subjects. Clin Neurophysiol 111:1745–1758.

Kalashnikova M, Peter V, Di Liberto GM, Lalor EC, Burnham D (2018) Infant-directed speech facilitates seven-month-old infants' cortical tracking of speech. Sci Rep 8:1–8.

Karmarkar UR, Dan Y (2006) Experience-dependent plasticity in adult visual cortex. Neuron 52:577–585.

Keil J (2020) Double Flash Illusions: Current Findings and Future Directions. Front Neurosci 14:1–8.

Keil A, Bernat EM, Cohen MX, Ding M, Fabiani M, Gratton G, Kappenman ES, Maris E, Mathewson KE, Ward RT, Weisz N (2022) Recommendations and publication guidelines for studies using frequency domain and time-frequency domain analyses of neural time series. Psychophysiology 59:1–37.

Keshavarzi M, Mandke K, Macfarlane A, Parvez L, Gabrielczyk F, Wilson A, Flanagan S, Goswami U (2022) Decoding of Speech Information using EEG in Children with Dyslexia: Less Accurate Low-Frequency Representations of Speech, Not "Noisy" Representations. bioRxiv:2022.05.02.490279.

Klimesch W (2012) Alpha-band oscillations, attention, and controlled access to stored information. Trends Cogn Sci 16:606–617.

Klimesch W, Russegger H, Doppelmayr M, Pachinger T (1998) A method for the calculation of induced band power: Implications for the significance of brain oscillations. Electroencephalogr Clin Neurophysiol 108:123–130.

Klimesch W, Sauseng P, Hanslmayr S (2007) EEG alpha oscillations: The inhibition-timing hypothesis. Brain Res Rev 53:63–88.

Knudsen EI (2004) Sensitive periods in the development of the brain and behavior. J Cogn Neurosci 16:1412–1425.

Kral A, Dorman MF, Wilson BS (2019) Neuronal Development of Hearing and Language: Cochlear Implants and Critical Periods. Annu Rev Neurosci 42:47–65.

Kral A, O'Donoghue GM (2010) Profound Deafness in Childhood. N Engl J Med 363:1438–1450.

Kral A, Sharma A (2012) Developmental neuroplasticity after cochlear implantation. Trends Neurosci 35:111–122.

Kral A, Yusuf PA, Land R (2017) Higher-order auditory areas in congenital deafness: Top-down interactions and corticocortical decoupling. Hear Res 343:50–63.

Kuhl PK (2004) Early language acquisition: Cracking the speech code. Nat Rev Neurosci 5:831–843.

Lakatos P, Gross J, Thut G (2019) A New Unifying Account of the Roles of Neuronal Entrainment. Curr Biol 29:R890–R905.

Lalor EC, Power AJ, Reilly RB, Foxe JJ (2009) Resolving precise temporal

processing properties of the auditory system using continuous stimuli. J Neurophysiol 102:349–359.

Lam FC, Lovett F, Dutton GN (2010) Cerebral visual impairment in children: A longitudinal case study of functional outcomes beyond the visual acuities. J Vis Impair Blind 104:625–635.

Lange J, Oostenveld R, Fries P (2011) Perception of the touch-induced visual double-flash illusion correlates with changes of rhythmic neuronal activity in human visual and somatosensory areas. Neuroimage 54:1395–1405.

Lange J, Oostenveld R, Fries P (2013) Reduced Occipital Alpha Power Indexes Enhanced Excitability Rather than Improved Visual Perception. J Neurosci 33:3212–3220.

Lehmann D, Skrandies W (1980) Reference-free identification of components of checkerboard-evoked multichannel potential fields. Electroencephalogr Clin Neurophysiol 48:609–621.

Lennert T, Samiee S, Baillet S (2021) Coupled oscillations enable rapid temporal recalibration to audiovisual asynchrony. Commun Bio, 4:1-12.

Levelt CN, Ḧubener M (2012) Critical-period plasticity in the visual cortex. Annu Rev Neurosci 35:309–330.

Lo Verde L, Morrone MC, Lunghi C (2017) Early Cross-modal Plasticity in Adults. J Cogn Neurosci 29:520–529.

Lueck AH, Dutton GN, Chokron S (2019) Profiling Children With Cerebral Visual Impairment Using Multiple Methods of Assessment to Aid in Differential Diagnosis. Semin Pediatr Neurol 31:5–14.

Lunghi C, Berchicci M, Morrone MC, Di Russo F (2015a) Short-term monocular deprivation alters early components of visual evoked

potentials. J Physiol 593:4361–4372.

Lunghi C, Burr DC, Morrone C (2011) Brief periods of monocular deprivation disrupt ocular balance in human adult visual cortex. Curr Biol 21:538–539.

Lunghi C, Emir UE, Morrone MC, Bridge H (2015b) Short-Term monocular deprivation alters GABA in the adult human visual cortex. Curr Biol 25:1496–1501.

Lunghi C, Sale A (2015) A cycling lane for brain rewiring. Curr Biol 25:R1122–R1123.

Lunghi C, Sframeli AT, Lepri A, Lepri M, Lisi D, Sale A, Morrone MC (2019) A new counterintuitive training for adult amblyopia. Ann Clin Transl Neurol 6:274–284.

Luo H, Poeppel D (2007) Phase Patterns of Neuronal Responses Reliably Discriminate Speech in Human Auditory Cortex. Neuron 54:1001–1010.

Magrou L, Barone P, Markov NT, Killackey HP, Giroud P, Berland M, Knoblauch K, Dehay C, Kennedy H (2018) How Areal Specification Shapes the Local and Interareal Circuits in a Macaque Model of Congenital Blindness. Cereb Cortex 28:3017–3034.

Manrique M, Cervera-Paz FJ, Huarte A, Perez N, Molina M, García-Tapia R (1999) Cerebral auditory plasticity and cochlear implants. Int J Pediatr Otorhinolaryngol 49:S193–S197.

Maris E, Oostenveld R (2007) Nonparametric statistical testing of EEG- and MEG-data. J Neurosci Methods 164:177–190.

Matsuba CA, Jan JE (2006) Long-term outcome of children with cortical visual impairment. Dev Med Child Neurol 48:508–512.

Matusz PJ, Dikker S, Huth AG, Perrodin C (2019) Are We Ready for Real-world Neuroscience? J Cogn Neurosci 31:327–338.

Maurer D, Werker JF (2014) Perceptual narrowing during infancy: A comparison of language and faces. Dev Psychobiol 56:154–178.

McConnell EL, Saunders KJ, Little JA (2021) What assessments are currently used to investigate and diagnose cerebral visual impairment (CVI) in children? A systematic review. Ophthalmic Physiol Opt 41:224–244.

McCulloch, D. L., Mackie, R. T., Dutton, G. N., Bradnam, M. S., Day, R. E., McDaid, G. J., ... & Shepherd, A. J. (2007). A visual skills inventory for children with neurological impairments. Developmental Medicine & Child Neurology, 49(10), 757-763.

McDowell, N., & Dutton, G. N. (2019). Hemianopia and features of balint syndrome following occipital lobe hemorrhage: identification and patient understanding have aided functional improvement years after onset. Case reports in ophthalmological medicine, 2019.

McKillop E, Dutton GN (2008) Impairment of vision in children due to damage to the brain: a practical approach. Br Ir Orthopt J 5:8.

Merabet LB, Hamilton R, Schlaug G, Swisher JD, Kiriakopoulos ET, Pitskel NB, Kauffman T, Pascual-Leone A (2008). Rapid and reversible recruitment of early visual cortex for touch. PLoS one, 3:e3046.

Mirkovic B, Debener S, Jaeger M, De Vos M (2015) Decoding the attended speech stream with multi-channel EEG: Implications for online, daily-life applications. J Neural Eng 12.

Mishra J, Martinez A, Sejnowski TJ, Hillyard SA (2007) Early cross-modal interactions in auditory and visual cortex underlie a sound-induced visual illusion. J Neurosci 27:4120–4131.

Moro SS, Steeves JKE (2018a) Normal temporal binding window but no sound-induced flash illusion in people with one eye. Exp Brain Res 236:1825–1834.

Moro SS, Steeves JKE (2018b) Audiovisual plasticity following early abnormal visual experience: Reduced McGurk effect in people with one eye. Neurosci Lett 672:103–107.

Mower GD (1991) The effect of dark rearing on the time course of the critical period in cat visual cortex. Dev Brain Res 58:151–158.

Murphy E, Benítez-Burraco A (2017) Language deficits in schizophrenia and autism as related oscillatory connectomopathies: An evolutionary account. Neurosci Biobehav Rev 83:742–764.

Mushtaq F, Wiggins IM, Kitterick PT, Anderson CA, Hartley DEH (2020) The Benefit of Cross-Modal Reorganization on Speech Perception in Pediatric Cochlear Implant Recipients Revealed Using Functional Near-Infrared Spectroscopy. Front Hum Neurosci 14:1–18.

Narinesingh C, Goltz HC, Raashid RA rha., Wong AMF (2015) Developmental Trajectory of McGurk Effect Susceptibility in Children and Adults With Amblyopia. Invest Ophthalmol Vis Sci 56:2107–2113.

Narinesingh C, Goltz HC, Wong AMF (2017) Temporal binding window of the sound-induced flash illusion in amblyopia. Investig Ophthalmol Vis Sci 58:1442–1448.

Nelson CA (1999) Human Development. 8:42–45.

Niparko JK, Tobey EA, Thal DJ, Eisenberg LS, Wang NY, Quittner AL, Fink NE (2010) Spoken language development in children following cochlear implantation. Jama 303:1498–1506.

Nogueira W, Cosatti G, Schierholz I, Egger M, Mirkovic B, Büchner A

(2020) Toward Decoding Selective Attention from Single-Trial EEG Data in Cochlear Implant Users. IEEE Trans Biomed Eng 67:38–49.

O'Sullivan JA, Power AJ, Mesgarani N, Rajaram S, Foxe JJ, Shinn-Cunningham BG, Slaney M, Shamma SA, Lalor EC (2015) Attentional Selection in a Cocktail Party Environment Can Be Decoded from Single-Trial EEG. Cereb Cortex 25:1697–1706.

Obleser J, Kayser C (2019) Neural Entrainment and Attentional Selection in the Listening Brain. Trends Cogn Sci 23:913–926.

Osberger MJ, Zimmerman-Phillips S, Koch DB (2002) Cochlear implant candidacy and performance trends in children. Ann Otol Rhinol Laryngol 111:62–65.

Oostenveld R, Fries P, Maris E, Schoffelen JM (2011) FieldTrip: Open source software for advanced analysis of MEG, EEG, and invasive electrophysiological data. Comput Intell Neurosci 2011.

Opoku-Baah C, Wallace MT (2020) Brief period of monocular deprivation drives changes in audiovisual temporal perception. J Vis 20:1–13.

Ortibus, E., Laenen, A., Verhoeven, J., De Cock, P., Casteels, I., Schoolmeesters, B., ... & Lagae, L. (2011). Screening for cerebral visual impairment: value of a CVI questionnaire. Neuropediatrics, 42(04), 138-147.

Osberger MJ, Zimmerman-Phillips S, Koch DB (2002) Cochlear implant candidacy and performance trends in children. Ann Otol Rhinol Laryngol 111:62–65.

Pascual-Leone A, Amedi A, Fregni F, Merabet LB (2005) The plastic human brain cortex. Annu Rev Neurosci 28:377–401.

Paul BT, Uzelac M, Chan E, Dimitrijevic A (2020) Poor early cortical differentiation of speech predicts perceptual difficulties of severely hearing-impaired listeners in multi-talker environments. Sci Rep 10:1–12.

Pavlova M (2003) Perception and production of biological movement in patients with early periventricular brain lesions. Brain 126:692–701.

Peelle JE, Davis MH (2012) Neural oscillations carry speech rhythm through to comprehension. Front Psychol 3:1–17.

Peylo C, Hilla Y, Sauseng P (2021) Cause or consequence? Alpha oscillations in visuospatial attention. Trends Neurosci 44:705–713.

Pérez-Bellido A, Ernst MO, Soto-Faraco S, López-Moliner J (2015) Visual limitations shape audio-visual integration. J Vis 15:1–15.

Pernet CR, Wilcox RR, Rousselet GA (2013). Robust correlation analyses: false positive and power validation using a new open source matlab toolbox. Frontiers in psychology, 606.

Philip SS, Dutton GN (2014) Identifying and characterising cerebral visual impairment in children: A review. Clin Exp Optom 97:196–208.

Polley DB, Steinberg EE, Merzenich MM (2006). Perceptual learning directs auditory cortical map reorganization through top-down influences. Journal of neuroscience, 26:4970-4982.

Putzar, L., Goerendt, I., Lange, K., Rösler, F., & Röder, B. (2007). Early visual deprivation impairs multisensory interactions in humans. Nature neuroscience, 10(10), 1243-1245.

Reh RK, Dias BG, Nelson CA, Kaufer D, Werker JF, Kolbh B, Levine JD, Hensch TK (2020) Critical period regulation acrossmultiple timescales. Proc Natl Acad Sci U S A 117:23242–23251.

Ricciardi E, Bottari D, Ptito M, Röder B, Pietrini P (2020) The sensory-deprived brain as a unique tool to understand brain development and function. Neurosci Biobehav Rev 108:78–82.

Richards MD, Goltz HC, Wong AMF (2017) Alterations in audiovisual simultaneity perception in amblyopia. PLoS One 12:1–20.

Robertson CE, Baron-Cohen S (2017) Sensory perception in autism. Nat Rev Neurosci 18:671–684 Available at: http://dx.doi.org/10.1038/nrn.2017.112.

Röder B, Ley P, Shenoy BH, Kekunnaya R, Bottari D (2013) Sensitive periods for the functional specialization of the neural system for human face processing. Proc Natl Acad Sci U S A 110:16760–16765.

Röder B, Rösler F, Spence C (2004) Early Vision Impairs Tactile Perception in the Blind. Curr Biol 14:121–124.

Röder B, Kekunnaya R (2021) Visual experience dependent plasticity in humans. Curr Opin Neurobiol 67:155–162.

Röder B, Kekunnaya R, Guerreiro MJS (2021) Neural mechanisms of visual sensitive periods in humans. Neurosci Biobehav Rev 120:86–99.

Rohe T, Ehlis AC, Noppeney U. (2019). The neural dynamics of hierarchical Bayesian causal inference in multisensory perception. Nature Communications, 10:1-17.

Romei V, Gross J, Thut G (2010) On the role of prestimulus alpha rhythms over occipito-parietal areas in visual input regulation: Correlation or causation? J Neurosci 30:8692–8697.

Ruben RJ (1997) A time frame of critical/sensitive periods of language development. Indian J Otolaryngol Head Neck Surg 51:85–89.

Sakki HEA, Dale NJ, Sargent J, Perez-Roche T, Bowman R (2018) Is there consensus in defining childhood cerebral visual impairment? A systematic review of terminology and definitions. Br J Ophthalmol 102:424–432 Available at: https://bjo.bmj.com/content/102/4/424 [Accessed July 24, 2022].

Sandmann P, Dillier N, Eichele T, Meyer M, Kegel A, Pascual-Marqui RD, Marcar VL, Ja¨ncke L&, Debener S (2012) Visual activation of auditory cortex reflects maladaptive plasticity in cochlear implant users. :555–568.

Sanes DH, Woolley SMN (2011) A behavioral framework to guide research on central auditory development and plasticity. Neuron 72:912–929.

Schwenk JCB, VanRullen R, Bremmer F (2020) Dynamics of Visual Perceptual Echoes Following Short-Term Visual Deprivation. Cereb Cortex Commun 1:1–11.

Shams L, Kamitani Y, Shimojo S (2000) What You See Is What You Hear. Nature 408:2000.

Sharma A, Campbell J, Cardon G (2015) Developmental and cross-modal plasticity in deafness: evidence from the P1 and N1 event related potentials in cochlear implanted children. Int J Psychophysiol 95:135–144.

Sharma A, Dorman MF, Kral A (2005) The influence of a sensitive period on central auditory development in children with unilateral and bilateral cochlear implants. Hear Res 203:134–143.

Sharma A, Dorman MF, Spahr A (2002a) A sensitive period for the development of the central auditory system in children with cochlear implants: Implications for age of implantation. Ear Hear 23:532–539.

Sharma A, Dorman M, Spahr A, Todd NW (2002b) Early cochlear implantation in children allows normal development of central auditory pathways. Ann Otol Rhinol Laryngol 111:38–41.

Siegel M, Donner TH, Engel AK (2012) Spectral fingerprints of large-scale neuronal interactions. Nat Rev Neurosci 13:121–134.

Skoczenski, A. M., & Norcia, A. M. (1999). Development of VEP Vernier acuity and grating acuity in human infants. Investigative Ophthalmology & Visual Science, 40(10), 2411-2417.

Somers B, Verschueren E, Francart T (2019) Neural tracking of the speech envelope in cochlear implant users. J Neural Eng 16:1–23.

Spence C (2011). Crossmodal correspondences: A tutorial review. Attention, Perception, & Psychophysics, 73(4): 971-995.Wang C, Zhang Q (2021). Word frequency effect in written production: Evidence from ERPs and neural oscillations. Psychophysiology, 58:e13775.

Spolidoro M, Sale A, Berardi N, Maffei L (2009) Plasticity in the adult brain: Lessons from the visual system. Exp Brain Res 192:335–341.

Steinschneider M, Liégeois-Chauvel C, Brugge JF (2011) Auditory Evoked Potentials and Their Utility in the Assessment of Complex Sound Processing. In: The Auditory Cortex (Springer, Boston M, ed), pp 535–559.

Stropahl M, Plotz K, Schönfeld R, Lenarz T, Sandmann P, Yovel G, De Vos M, Debener S (2015) Cross-modal reorganization in cochlear implant users: Auditory cortex contributes to visual face processing. Neuroimage 121:159–170.

Stropahl M, Bauer AKR, Debener S, Bleichner MG (2018) Source-Modeling auditory processes of EEG data using EEGLAB and brainstorm. Front Neurosci 12:309.

Tadel F, Baillet S, Mosher JC, Pantazis D, Leahy RM (2011) Brainstorm: A user-friendly application for MEG/EEG analysis. Comput Intell Neurosci 2011.

Takesian AE, Hensch TK (2013) Balancing plasticity/stability across brain development, 1st ed. Elsevier B.V. Available at: http://dx.doi.org/10.1016/B978-0-444-63327-9.00001-1.

Tallon-Baudry C, Bertrand O (1999) Oscillatory gamma activity in humans and its role in object representation. Trends Cogn Sci 3:151–162.

Turrigiano G (2012) Homeostatic synaptic plasticity: Local and global mechanisms for stabilizing neuronal function. Cold Spring Harb Perspect Biol 4.

Turrigiano GG, Nelson SB (2004). Homeostatic plasticity in the developing nervous system. Nature reviews neuroscience, 5:97-107.

Tyll S, Budinger E, Noesselt T (2011) Thalamic influences on multisensory integration. Commun Integr Biol 4:378–381.

Uziel AS, Sillon M, Vieu A, Artieres F, Piron JP, Daures JP, Mondain M (2007) Ten-year follow-up of a consecutive series of children with multichannel cochlear implants. Otol Neurotol 28:615–628.

Van Atteveldt N, Murray MM, Thut G, Schroeder CE (2014) Multisensory integration: Flexible use of general operations. Neuron 81:1240–1253.

Vanes LD, White TP, Wigton RL, Joyce D, Collier T, Shergill SS (2016) Reduced susceptibility to the sound-induced flash fusion illusion in schizophrenia. Psychiatry Res 245:58–65.

VanRullen R (2016) Perceptual Cycles. Trends Cogn Sci 20:723–735.

Vanthrnhout J, Decruy L, Wouters J, Simon JZ, Francart T (2018) Vanthrnhout et al., 2017_Speech Intelligibility Predicted from Neural Entrainment of the Speech Envelope.pdf. :181–191.

Vetter P, Bola Ł, Reich L, Bennett M, Muckli L, Amedi A (2020) Decoding Natural Sounds in Early "Visual" Cortex of Congenitally Blind Individuals. Curr Biol 30:3039-3044.e2.

Viola FC, Thorne J, Edmonds B, Schneider T, Eichele T, Debener S (2009) Semi-automatic identification of independent components representing EEG artifact. Clin Neurophysiol 120:868–877.

Watkins S, Shams L, Tanaka S, Haynes JD, Rees G (2006) Sound alters activity in human V1 in association with illusory visual perception. Neuroimage 31:1247–1256.

Watson, T., Orel-Bixler, D., & Haegerstrom-Portnoy, G. (2010). Early visual evoked potential acuity and future behavioral acuity in cortical visual impairment. Optometry and vision science: official publication of the American Academy of Optometry, 87(2), 80.

Weinstein JM, Gilmore RO, Shaikh SM, Kunselman AR, Trescher W V., Tashima LM, Boltz ME, McAuliffe MB, Cheung A, Fesi JD (2012) Defective motion processing in children with cerebral visual impairment due to periventricular white matter damage. Dev Med Child Neurol 54.

Werker JF, Hensch TK (2015) Critical Periods in Speech Perception: New Directions. Annu Rev Psychol 66:173–196.

Whittingham KM, McDonald JS, Clifford CWG (2014) Synesthetes show normal sound-induced flash fission and fusion illusions. Vision Res 105:1–9.

Winkler I, Debener S, Muller KR, Tangermann M (2015) On the influence of high-pass filtering on ICA-based artifact reduction in EEG-ERP. Proc

Annu Int Conf IEEE Eng Med Biol Soc EMBS 2015-November:4101–4105.

Winn MB, Nelson PB (2022) 2 . What a Cochlear Implant Is. :1–18.

Wiesel TN, Hubel DH (1963) Responses in Striate Deprived of Vision Cortex of One Eye. J Neurophysiol 26:1003–1017.

Yusuf PA, Hubka P, Tillein J, Kral A (2017) Induced cortical responses require developmental sensory experience. Brain 140:3153–3165.

Yuval-Greenberg S, Tomer O, Keren AS, Nelken I, Deouell LY (2008) Transient Induced Gamma-Band Response in EEG as a Manifestation of Miniature Saccades. Neuron 58:429–441.

Zhou J, Baker DH, Simard M, Saint-Amour D, Hess RF (2015) Short-term monocular patching boosts the patched eye's response in visual cortex. Restor Neurol Neurosci 33:381–387.

Unless otherwise expressly stated, all original material of whatever nature created by Albert Einstein and included in this thesis, is li¬censed under a Creative Commons Attribution Noncommercial Share Alike 3.0 Italy License.

Check on Creative Commons site:

https://creativecommons.org/licenses/by-nc-sa/3.0/it/legalcode

https://creativecommons.org/licenses/by-nc-sa/3.0/it/deed.en

Ask the author about other uses.